UNIVERSIDADE DE SÃO PAULO
ESCOLA DE ENGENHARIA DE SÃO CARLOS
DEPARTAMENTO DE ENGENHARIA DE ESTRUTURAS

IGOR FREDERICO STOIANOV COTTA

SPLITTING METHOD IN MULTISITE DAMAGE SOLIDS: Mixed Mode Fracturing and Fatigue Problems

CORRECTED VERSION

(Original version is available at EESC-USP)

SÃO CARLOS - SP
2016

IGOR FREDERICO STOIANOV COTTA

SPLITTING METHOD IN MULTISITE DAMAGE SOLIDS: Mixed Mode Fracturing and Fatigue Problems

CORRECTED VERSION

(Original version is available at EESC-USP)

Text presented to the São Carlos School of Engineering of the University of São Paulo as one of the requisites for obtaining the Doctor in Science degree.

Advisor: Prof. Sergio Persival Baroncini Proença

SÃO CARLOS

2016

Stoianov Cotta, Igor Frederico
SPLITTING METHOD IN MULTISITE DAMAGE SOLIDS: Mixed Mode Fracturing and Fatigue Problems / Igor Frederico Stoianov Cotta; orientador Sergio Persival Baroncini Proença. São Carlos, 2015.

S843Co
ts

Tese (Doutorado) - Programa de Pós-Graduação em Engenharia de Estruturas -- Escola de Engenharia de São Carlos da Universidade de São Paulo, 2015.

1. Splitting Method. 2. Generalized Finite Element Method. 3. Fracture Mechanics. 4. Computational framework. I. Título.

FOLHA DE JULGAMENTO

Candidato: Engenheiro **IGOR FREDERICO STOIANOV COTTA**.

Título da dissertação: "O método da partição em sólidos multi-fraturados: fraturas em modos mistos e problemas de fadiga".

Data da defesa: 29/01/2016

Comissão Julgadora:	**Resultado:**
Prof. Titular **Sergio Persival Baroncini Proença (Orientador)** (Escola de Engenharia de São Carlos/EESC)	APROVADO
Prof. Dr. **Edson Denner Leonel** (Escola de Engenharia de São Carlos/EESC)	APROVADO
Prof. Dr. **Leandro Palermo Junior** (Universidade Estadual de Campinas/UNICAMP)	APROVADO
Prof. Dr. **João Augusto de Lima Rocha** (Universidade Federal da Bahia/UFBA)	APROVADO participação por videoconferência
Dr. **Carlos Eduardo Chaves** (Empresa Brasileira de Aeronáutica S.A./EMBRAER)	Aprovado

Coordenador do Programa de Pós-Graduação em Engenheira Civil (Engenharia de Estruturas):
Prof. Titular **Humberto Breves Coda**

Presidente da Comissão de Pós-Graduação:
Prof. Associado **Paulo Sergio Lima Segantine**

This work is dedicated to my beautiful wife Andreza Marques de Castro Leão and my dear mother Olga Stoianov.

Acknowledgment

I'd like to thank the Prof. Sergio Persival Baroncini Proença for the friendship and for sharing his knowledge with me.

To my beautiful and special wife Andreza Marques de Castro Leão, for the comprehension and love.

To my mother Olga Stoianov for all love given to me in my whole life.

To aunt Maria for the support.

I am also grateful to the colleagues Ayrton, David Amorim, Dorival Piedade Neto, Manoel Denis da Costa Ferreira and Rafael Marques Lins for theirs friendship.

Finally, I am grateful to CAPES, for financial support.

“If I have seen further it is by standing on the shoulders of giants.”

Isaac Newton

Abstract

COTTA, I.F.S. **Splitting Method in Multisite Damage Solids: Mixed Mode Fracturing and Fatigue Problems**. 2015. 157p. PhD Thesis (Doctor in Structure Engineering) - School of Engineering of São Carlos, University of São Paulo, São Carlos, 2015.

The design of complex structures demands the prediction of possible fracture-dominant failure processes, due to the existence of unavoidable preexistent flaws and other defects, as well as sharps and cracks. On one hand, the complexity of the structure and the presence of many defects to be accounted for in the modeling can become the computational effort impracticable. On the other hand, it is important to seek the development of a computational framework based on some numerical method to study these problems. A way to overcome the difficulties mentioned, therefore making feasible the analysis of complex structures with many cracks, flaws and other defects, consists of combining a representative mechanical modeling with an efficient numerical method. This is precisely the fundamental aim of this work. Firstly, the Splitting Method is used aiming to build a representative modeling. Secondly, the Generalized Finite Element Method (GFEM) is chosen as an efficient numerical method, in which enrichment strategies of the approximated solution using stress functions in particular can be explored. The GFEM framework also allows avoiding the excessive refinement of the mesh, which increases the computational effort in conventional finite element analysis. In the Splitting Method, a kind of decomposition method, the original problem is subdivided in local and global problems which are then combined by imposing null traction at the crack surfaces. In this work, the Splitting Method was completely programmed in Python language and its use extended to analyze crack propagation including fatigue crack growth. The generated code presents in addition to several features related to Fracture Mechanics concepts, as the computation of the stress intensity factor (mode I and II) trough *J Integral*. Some examples are presented to depict the propagation of the cracks in multisite damage structures. It is shown that for this kind of problems the enrichment strategy provided by GFEM is essential. Moreover, the final example demonstrates that the computational tool allows for investigation of different possible crack scenarios with a low cost analysis. One concludes about the representativeness and efficiency of the methodology hereby proposed.

Keywords: Splitting Method. Fracture Mechanic. Generalized Finite Element Method. Stress Intensity Factors. Fatigue Crack Growth.

Resumo

COTTA, I.F.S. **O Método da Partição em Sólidos Multi-Fraturados: Fraturas em modos mistos e problemas de fadiga.** 2015. 157p. Tese de doutoramento (Doutorado em Engenharia de Estruturas) - Escola de Engenharia de São Carlos, Universidade de São Paulo, São Carlos, 2015.

O projeto de estruturas complexas demanda a previsão de possíveis processos de ruptura governados por fraturamento, devido à existência de inevitáveis defeitos pré-existentes, como entalhes e fissuras. Por um lado, a complexidade da estrutura e a presença de muitos defeitos a serem considerados no modelo podem tornar a análise inviável devido ao esforço computacional necessário. Por outro lado, é importante procurar desenvolver uma estrutura computacional baseada em métodos numéricos para estudar estes problemas. Um modo de superar as dificuldades mencionadas, portanto tornando possível a análise de estruturas complexas com muitas fissuras e outros defeitos, consiste em combinar um modelo mecânico que seja representativo com um método numérico eficiente. Este é precisamente o objetivo fundamental deste trabalho. Primeiramente, o Método da Partição é utilizado para a construção de um modelo representativo. Em segundo lugar, o Método dos Elementos Finitos Generalizados (GFEM) é empregado por ser um método numérico eficiente, no qual as estratégias de enriquecimento da solução aproximada usando funções de tensão, em particular, podem ser exploradas. A estrutura do GFEM também permite evitar o excessivo refinamento da malha, que aumenta o esforço computacional em análises convencionais nas quais se utiliza o método dos elementos finitos. No Método da Partição, um tipo de método de decomposição, o problema original é subdividido em problemas locais e globais que são então combinados impondo-se a nulidade do vetor de tensões na superfície da fissura. Neste trabalho, o Método da Partição foi completamente programado em linguagem Python® e sua utilização estendida para analisar a propagação de fissuras, incluindo-se a associação do crescimento com a resposta em fadiga. Além disso, o código gerado apresenta diversas características relacionadas aos conceitos da Mecânica da Fratura, como o cálculo do fator de intensidade de tensão (modos I e II) mediante a *Integral J*. Alguns exemplos são apresentados para ilustrar a propagação de fissuras em estruturas multi-fraturadas. Mostra-se que para este tipo de problemas a estratégia de enriquecimento fornecida pelo GFEM é essencial. Além disso, o exemplo final comprova que a ferramenta computacional permite a investigação de diferentes possíveis cenários de fissuras com uma análise de baixo custo. Conclui-se sobre a representatividade e eficiência da metodologia proposta.

Palavras-chave: Método da Partição. Mecânica da Fratura. Método dos Elementos Finitos Generalizados. Fatores de Intensidade de Tensão. Crescimento da Fissura à Fadiga.

List of Figures

List of symbols

$\{\alpha\}$:	Vector containing the "α" parameters
a_i:	Length of the crack *i*
β:	Number of the element
C:	Constant depending on the material in the fatigue analysis
$C_0^\infty(\omega_i)$:	Space of functions that, together with all theirs partial derivatives, are continuous and have compact support on ω_i
da/dn:	Fatigue Crack Growth Rate
$\underline{\underline{T}}$:	Second order stress tensor
$\left[\frac{\partial u_G^{(k)}}{\partial n_{\Gamma^{(i)}}}\right]$:	Jump in the traction vector applied in $\Gamma^{(i)}$ contour
$u_G^{(k)}$:	Jump in the displacement vector applied in $\Gamma^{(i)}$ contour
ΔK:	Variation of the Stress Intensity Factor
$\phi_i(x)$:	Real shape function defined in $C_0^\infty(\omega_i)$
$\Im_j$:	Set of linearly function that generates the enrichment space
$\Im_N^{k,p}$:	Set of functions that provides the HP-Clouds
E:	Young's modulus
EPFM:	Elastic-Plastic Fracture Mechanics
$\Gamma^{(i)}$:	Rectangular contour of the local sub-problem
G:	Energy release rate
$[GI]$:	General Influence Matrix
GFEM:	Generalized Finite Element Method
J:	*J Integral*
κ:	Kolosov constant
L_{ji}:	Function in $\Im_j$
L_α:	Enrichment functions space
m:	Constant depending on the material in the fatigue analysis
n:	Number of cycles in fatigue analysis
$N_j(x)$:	Shape function
ω_j:	Open regions called "clouds"
Ω:	Open bounded subset of R^n
ngp:	Number of sampling points of the Gauss quadrature

ν:	Poisson's ratio
K_I, K_{II}, K_{III}:	Stress Intensity Factor, referred to Modes I, II and III, respectively
P_K:	Basis of the approximation function
$\boldsymbol{P_G^{(0)}}$:	Global sub-problem, similar to the original problem, but without the cracks
$\boldsymbol{P_G^{(k)}}$:	Global sub-problem of the Splitting Method
$\boldsymbol{P_L^{(k)}}$:	Local sub-problem of the Splitting Method
(ξ_i,η_i):	Coordinate system used to analyze cracks
$\{r\}$:	Vector containing the weighted tractions in the crack lines in the global problem $\boldsymbol{P_G^{(0)}}$
R:	Energy required per increment of crack extension
R^n:	Euclidean vector space of dimension n
$r(\theta)_{plane\ stress}$:	Radius of the plastic zone in the plane stress state
S:	Contour line of the domain V
$S_0^{(i)}$:	Contour of the local domain in the local sub-problem
S_{ci}:	Contour line of the crack i
S_{ci}^+:	"Positive" crack surface of the crack i
S_{ci}^-:	"Negative" crack surface of the crack i
S_j:	Contour line of the hole j
SIF:	Stress Intensity Factor
S_β:	Obtained functions by the multiply of the $\Im_j$ by the PU in the element β
S_u:	Contour where the displacements are imposed
S_t:	Contour where the tractions are imposed
T:	Traction vector
$\underline{t}$:	Total traction vector
$\underline{t}^+$:	Traction vector applied in S_{ci}^+
$\underline{t}^-$:	Traction vector applied in S_{ci}^-
$\underline{t}_G^{(0)}$:	Traction vector in the global problem $\boldsymbol{P_G^{(0)}}$ in the crack lines
$\underline{t}_L^{(k)}$:	Traction vector in the local problem $\boldsymbol{P_L^{(k)}}$ in the crack lines
$\underline{t}_G^{(k)}$:	Traction vector in the local problem $\boldsymbol{P_G^{(k)}}$in the crack lines
$t^{(i)}$:	Traction vector in the $\Gamma^{(i)}$ contour

$\underline{u}$:	Imposed displacement field
$\tilde{u}(x)$:	Approximation function
$u_j^{(i)}$:	Displacement field in the $\Gamma^{(i)}$ contour
u_x, u_y :	Displacement fields in the *x* and *y* directions, respectively
u_1^I, u_2^I:	Decomposition of the displacements fields in directions 1 and 2, respectively, referred to Mode I
u_1^{II}, u_2^{II}:	Decomposition of the displacements fields in directions 1 and 2, respectively, referred to Mode II
V:	Domain of the sub-problems
$V_L^{(i)}$:	Local domain containing the crack *i*
W:	Strain energy density
$We(x_i)$:	Weight function evaluated in x_i
XFEM:	Extended Finite Element Method
x_j:	Point in Ω
$Z(z)$:	Complex function

List of Tables

Nomenclature

COD:	Crack Opening Displacement
CSD:	Crack Sliding Displacement
CST:	Constant Strain Triangle
FEM:	Finite Element Method
GFEM:	Generalized Finite Element Method
LSM:	Least Square Method
LST:	Linear Strain Triangle
PUM:	Partition of Unit Method
SGBEM:	Symmetric Galerkin Boundary Element Method
XFEM:	Extended Finite Element Method

Index

Chapter 1: Introduction

It is well known that strength failures can be either of the yielding-dominant or fracture-dominant types. Defects are important for both types of failure, but those of primary importance to fracture differ remarkably from those influencing yielding.

For fracture-dominant failures, *i.e.* fracture before complete yielding of the net section, the size scale of the defects which are of major significance is essentially macroscopic. In other words, the defects can be visualized and, in some circumstances, can be measured. Therefore, it is of great interest to model the effects of cracks on the behavior of solids to more precisely simulate the failure.

The commonly accepted first successful analysis of a fracture-dominant problem was that of Griffith in 1920. Quoting the words of Janssen *et al* (2006):

> "Griffith formulated the now well-known concept that an existing crack will propagate if thereby the total energy of the system is lowered, and he assumed that there is a simple energy balance, consisting of a decrease in elastic strain energy within the stressed body as the crack extends, counteracted by the energy needed to create the new surfaces."

In the middle of 1950 decade Irwin contributed with another major advance by showing that the energy approach is equivalent to a stress intensity factor (K) approach, according to which fracture occurs when a critical stress distribution ahead of the crack tip is reached. Since then, several methods have been developed to allow evaluating the stress intensity factors in order to offer a description of the crack growth.

Further confirming the importance of fracture mechanics, back to the nineteenth century, the Industrial Revolution led to an enormous increase in the use of metals (mainly irons and steels). Unfortunately, many accidents owing to failure of these structures started to occur. Some of these accidents were due to poor design, but it was also gradually discovered that material deficiencies in the form of pre-existing flaws could initiate cracks and fracture.

Furthermore, a new era of accident-prone structures was ushered in by the advent of all-welded designs. For example, out of 2500 Liberty ships built during the World War II, 145 broke in two and almost 700 experienced serious failures. See Figure 1.1.

Figure 1.1 Liberty ship

(Source: http://inspecaoequipto.blogspost.com.br/2013_11_01_archive.html Researched in 05/01/2015)

The aircraft accident of the Boeing 737-200, which occurred near Maui, Hawaii, in April 28, 1988, is another important example, closer to the field of interest of this work. According to the Official Accident Report, the Failure of the Aloha Airlines maintenance program detected the presence of significant disbanding and fatigue damage which led to failure of the lap joint and the separation of the fuselage upper lobe.

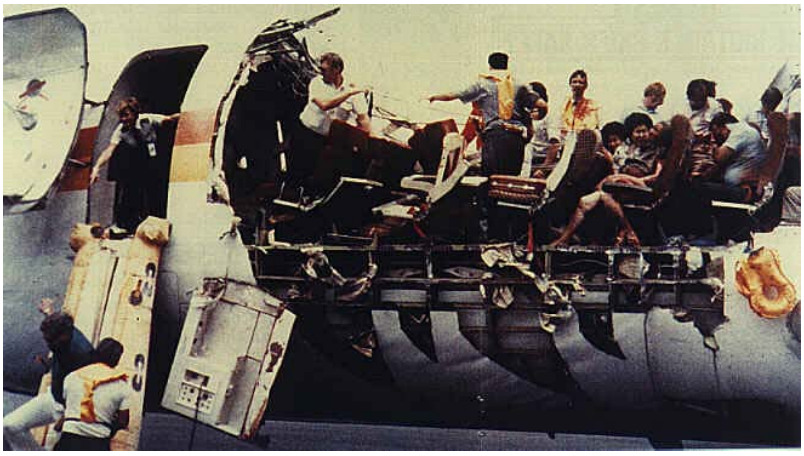

Figure 1.2 Aircraft accident of the Aloha Boeing 737

(Source: http://www.aloha.net/~icarus/ Researched in 04/02/2016)

On the other hand, the analysis of structures of complex geometry, for example, demands the development and employment of robust numerical methods. Moreover, achieve accurate estimates to the stress fields close to the crack tips can be a challenging task, often requiring high cost computational work. In this study, the Generalized Finite Element Method (GFEM) (Duarte *et al*, 2000; Duarte; Kim, 2008) is explored in face of its known efficacy in the analysis of the linear elastic fracture mechanics problems. In short, GFEM consists of a Partition of Unity Method (PUM) "enriched" with a special class of functions, in which the partition of unity is provided by the shape functions of conventional finite element method.

Even if a good numerical tool is available for the analysis of a cracked solid, in many engineering problems there is a need to analyze the effect of different local crack scenarios in the same structure. For example, recent aircraft accidents have strongly appointed to the need for considering combined effects of multiple growing cracks where each individual crack can be harmless, but the combined effect caused by several cracks can be disastrous. Hence, often it is necessary to consider many possible damage locations and damage sizes in the structures. Obviously, find out the worst scenario can demand an excessive computational effort.

In order to reach this goal, the so called decomposition methods started to be developed. Quoting Alves (2010), Lachenbruch (1961) was pioneered in the use of the Schwartz-Newmann Alternating Method to analyze Fracture Mechanics problems. Such method deals with the Superposition Principle, and the final result is obtained by summation of the solution of two different problems. The first one presents an infinite body containing a crack and aims to capture the local singularity of the problem. The second one refers to a finite domain without cracks. The regular parcel of the solution is obtained of this last problem.

In the sequel, in the work of Nishioka and Atluri (1983), the Finite Element Method was used with analytical solutions of the Alternating Method. However, the calculus of the Stress Intensity Factors was done by an iterative process. As an alternative, Babuška and Andersson (2005) developed the Splitting Method, which consists of a direct method to solve problems containing multiple cracks, therefore avoiding iterative procedures.

In this work, due to its favorable features, the Splitting Method (Babuška & Andersson, 2005) is explored for solving problems of this type, *i. e.*, looking for the worst scenario solutions, or performing fatigue crack growth analyses where numerous

solutions for different crack sizes and crack patterns are needed. Aiming a further contribution to the original formulation of the method, a new improved version including mixed mode crack opening effects and aiming the analysis of fatigue by a propagation method is hereby proposed. In this manner, it is possible to realize a deterministic rupture analysis including fatigue and multi-site damage not considered in the early works on the method.

The Splitting Method was implemented in a pre-existent toolkit for the Generalized Finite Element Method program. The *SCIEnCE* (São Carlos Integrity Environment Computational Engineer) explores the object oriented programming methodology, being its class structure originally conceived by the research group of the Structural Engineering Department of the School of Engineering of São Carlos. More details about the code can be found in Piedade Neto (2013).

Structure of the thesis

As an overall comment, it was the intention of the author to provide a text as concise as possible about the new proposed developments and applications of the Splitting Method, also emphasizing the main features of the developed computational framework.

In Chapter 2, the Stress Functions are presented, since they constitute the basis of the enrichment strategy used in GFEM. In addition, concepts like *COD*, *CSD* and *J Integral* are explained because they were implemented in the computational code. Finally, some comments about fatigue crack growth are presented.

Chapter 3 is devoted to the description of the Splitting Method. The mathematical aspects are omitted; however related references are indicated to fulfill this gap.

In Chapter 4, some computational aspects related to the implementation of the Splitting Method are commented either to evidence the difficulties in programming the Splitting Method or to make clear the possibilities for future improvements.

In Chapter 5, a brief review about GFEM is presented, since this strategy was used to reach better accuracy in the numerical results.

Finally, in Chapter 6 some examples are presented. It is expected that the examples may have elucidated and cover all the aspects cited in the text and implemented computationally.

In Chapter 7, the main achievements, contributions and conclusions are presented, as well as some suggestions for future studies. To the sake of better understanding, some key concepts of the Fracture Mechanics are presented in the Appendix Section.

When modeling multi-cracked solids it is important to have in mind the necessity for answering the following questions, proposed by Broek (1986):

1. What is the residual strength as a function of crack size?
2. What is the maximum size of a crack than can be tolerated at the expected service load; *i.e.* what is the critical crack size?
3. How long does it take for a crack to grow from a certain initial size to the critical size?

Moreover, the approach hereby adopted also allows addressing the following question:

4. Given many patterns of possible cracks, is it possible to detect the most critical one?

In order to answer properly these questions, firstly some of the main concepts of the Fracture Mechanics of interest must be reviewed. Next, an explanation of how those concepts are used in this research is presented.

2.1 Opening modes.

The "opening modes" are concepts of major significance in Fracture Mechanics and, from now on, they will be claimed along all the work. It is important to mention that there are three independent movements between the crack surfaces, shown in Figure 2.1.

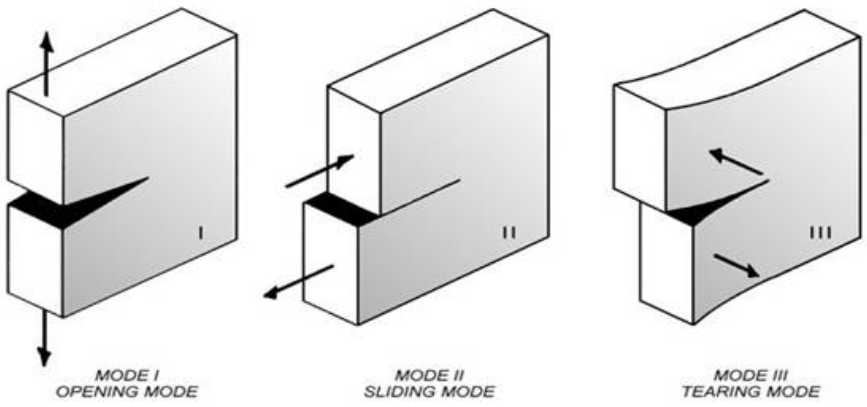

Figure 2.1 Modes of crack surface displacements (Figure extracted of JANSEEN, 2002)

Mode I or "Opening Mode": the relative movement between the crack surfaces occurs in the perpendicular direction to the plane of the crack;

Mode II or "Sliding Mode": the displacement of the crack surfaces is in the plane of the crack and in direction perpendicular to the leading edge of the crack;

Mode III or "Tearing Mode": relative sliding between the crack surfaces caused by out-of-plane shear.

In this work, as the modeling is restricted to two-dimensional analysis, only the Modes I and II are considered.

2.2 Stress Functions.

The Elastic Fracture Mechanics encompasses problems consisting of elastic solids with cracks. An important feature is that, at the crack tips, a singular stress concentration occurs.

The Westergaard (1939) complex stress functions provide the analytical solutions to the fracture mechanics problems. In order to present a brief review of these functions, let be considered an infinite two-dimensional domain containing a crack of length equal to *2a,* as shown in Figure 2.2-a. The plate is bi-axially loaded in tension by a stress σ_∞. According to Janssen *et al* (2006), the boundary conditions for this problem are:

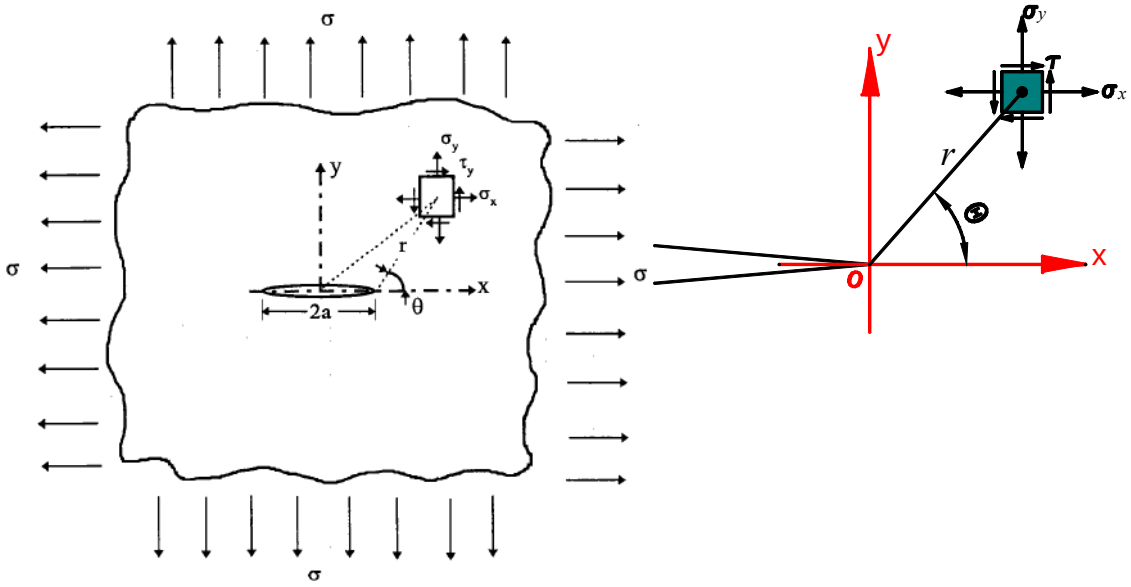

a. Bi-axially loaded plate (repeated in Appendix A)

b. Local coordinate system

Figure 2.2 Stress element close to the crack tip and local coordinate system

i. $\sigma_y = 0$, for $-a < x < +a$ and $y = 0$;

ii. $\sigma_x \rightarrow \sigma_\infty$ and $\sigma_y \rightarrow \sigma_\infty$ for $x \rightarrow \pm\infty$ and/or $y \rightarrow \pm\infty$;

iii. $\sigma_y \rightarrow \infty$ for $x = \pm a$ and $y = 0$.

Actually, the condition (iii) is a characteristic of the fracture mechanics problems and is obtained from the analysis. However, since it is necessary to find out a complex function that encompasses this condition, it can be stated as a boundary condition.

As detailed in Appendix A, a complex Airy stress function that fulfills the above boundary conditions is:

$$\phi(z) = \frac{\sigma z}{\sqrt{z^2 - a^2}} \tag{2.1}$$

where $z = x + iy$. The Cartesian axes are placed with origin at the crack tip as shown in Figure 2.2-b.

To the purpose of this section, it is sufficient to know the solutions to the displacements and stress fields in the neighborhood of the crack tip with respect to each fracture opening mode. As already mentioned, more details are given in Appendix A.

Related to Mode I, the components of the solution to the displacements fields are given by:

$$u_x = \frac{K_I}{\mu}\sqrt{\frac{r}{2\pi}}\cos\frac{\theta}{2}\left[\frac{1}{2}(\kappa - 1) + sen^2\frac{\theta}{2}\right] \tag{2.2}$$

$$u_y = \frac{K_I}{\mu}\sqrt{\frac{r}{2\pi}}sen\frac{\theta}{2}\left[\frac{1}{2}(\kappa + 1) - \cos^2\frac{\theta}{2}\right] \tag{2.3}$$

And, for stress fields:

$$\sigma_{xx} = \frac{K_I}{\sqrt{2\pi r}}\cos\frac{\theta}{2}\left(1 - sen\frac{\theta}{2}sen\frac{3\theta}{2}\right) \tag{2.4}$$

$$\sigma_{yy} = \frac{K_I}{\sqrt{2\pi r}}\cos\frac{\theta}{2}\left(1 + sen\frac{\theta}{2}sen\frac{3\theta}{2}\right) \tag{2.5}$$

$$\sigma_{xy} = \frac{K_I}{\sqrt{2\pi r}}\cos\frac{\theta}{2}\cos\frac{\theta}{2}sen\frac{3\theta}{2} \tag{2.6}$$

The Stress Intensity Factor (*SIF*), in equations (2.2)-(2.6), is given by:

$$K_I = \lim_{r\to\infty} \sqrt{2\pi r}\ \sigma_{yy}(r, \theta = 0) \qquad (2.7)$$

The variables *r* and θ are the polar coordinates, presented in Figure 2.2-b.

In addition, in correspondence to the Mode II, the components are given by:

$$u_x = \frac{K_{II}}{\mu}\sqrt{\frac{r}{2\pi}}\, sen\frac{\theta}{2}\left[\frac{1}{2}(\kappa + 1) + cos^2\frac{\theta}{2}\right] \qquad (2.8)$$

$$u_y = \frac{K_{II}}{\mu}\sqrt{\frac{r}{2\pi}}\, cos\frac{\theta}{2}\left[\frac{1}{2}(1 - \kappa) + sen^2\frac{\theta}{2}\right] \qquad (2.9)$$

And for stress fields:

$$\sigma_{xx} = -\frac{K_{II}}{\sqrt{2\pi r}}\, sen\frac{\theta}{2}\left(2 + cos\frac{\theta}{2}cos\frac{3\theta}{2}\right) \qquad (2.10)$$

$$\sigma_{yy} = \frac{K_{II}}{\sqrt{2\pi r}}\, sen\frac{\theta}{2}cos\frac{\theta}{2}cos\frac{3\theta}{2} \qquad (2.11)$$

$$\sigma_{xy} = \frac{K_{II}}{\sqrt{2\pi r}}\, cos\frac{\theta}{2}\left(1 - sen\frac{\theta}{2}sen\frac{3\theta}{2}\right) \qquad (2.12)$$

The Stress Intensity Factor (SIF), in equations (2.8)-(2.12), is given by:

$$K_{II} = \lim_{r\to\infty} \sqrt{2\pi r}\ \sigma_{xy}(r, \theta = 0) \qquad (2.13)$$

The constant κ appearing in the previous relations for the displacement fields is the Kolosov constant and it can assume the following values:

$\kappa = (3 - 4\nu)$, for Plane Strain;

$\kappa = (3 - \nu)/(1 + \nu)$, for Plane Stress.

It is immediate to verify that the stress components tend to infinity at the crack tip (*r=0*), i.e.:

$$\lim_{r\to 0}\sigma_{xx} = \infty; \quad \lim_{r\to 0}\sigma_{yy} = \infty\ ; \lim_{r\to 0}\sigma_{xy} = \infty \qquad (2.14)$$

2.3 On the use of the Generalized Finite Element Method.

At this point, it is enough to address directly to the use of Generalized Finite Element Method, from now on called GFEM. More details about GFEM, not necessary to the aim of this section, are given in Chapter 5.

The main feature of the GFEM consists of the "enrichment" of the nodes of the elements that are completely or partially cut by a crack. The enrichment is advantageous when using appropriate functions to capture the displacement fields and the high stress gradients. Taking this into account, the stress functions provided from classical analysis of Fracture Mechanics are adequate to be used as enrichments.

The enriched element shape functions space can be spanned from the following enrichment basis functions:

$$L_\alpha = \{1, \sqrt{r}\cdot\cos\frac{\theta}{2}, \sqrt{r}\cdot\sin\frac{\theta}{2}, \sqrt{r}\cdot\sin\frac{\theta}{2}\cdot\sin\theta, \sqrt{r}\cdot\cos\frac{\theta}{2}\cdot\sin\theta\}$$

To elucidate the enrichment effects, the example depicted in Figure 2.3 is presented. This example consists of a plate subjected to a constant traction load, containing a crack on the right edge.

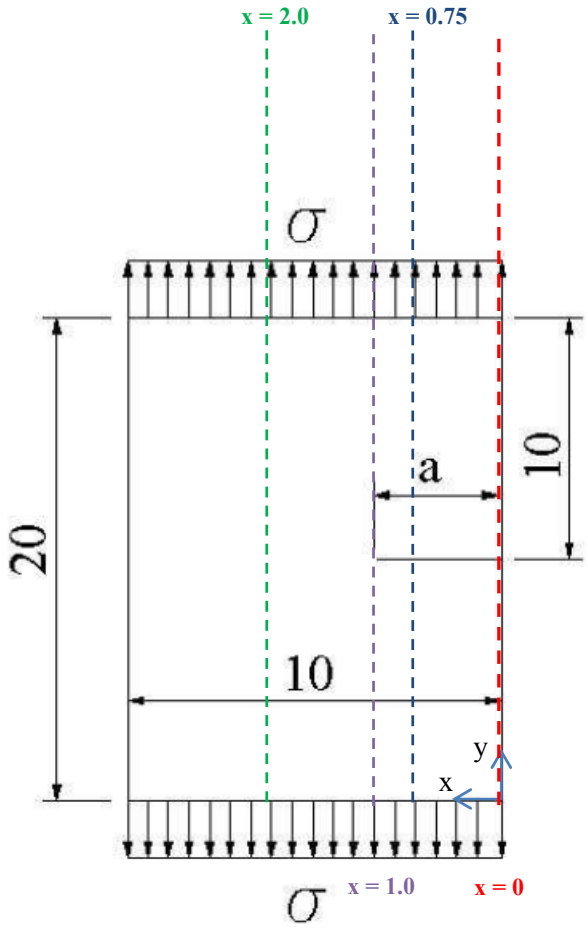

Figure 2.3 **Rectangular plate subjected to a constant load**

Data of the problem, adopted without units for convenience:

i. Young's modulus (E) = 1.0;
ii. Poisson's ratio (ν) = 0.3;
iii. Traction load (σ) = 1.0;
iv. Length of the crack (a) = 1.0.

The plate was discretized using a single quadrilateral finite element. Figures 2.4 and 2.5 depict the enrichment effects, considering several lines positioned along the *x-axis*.

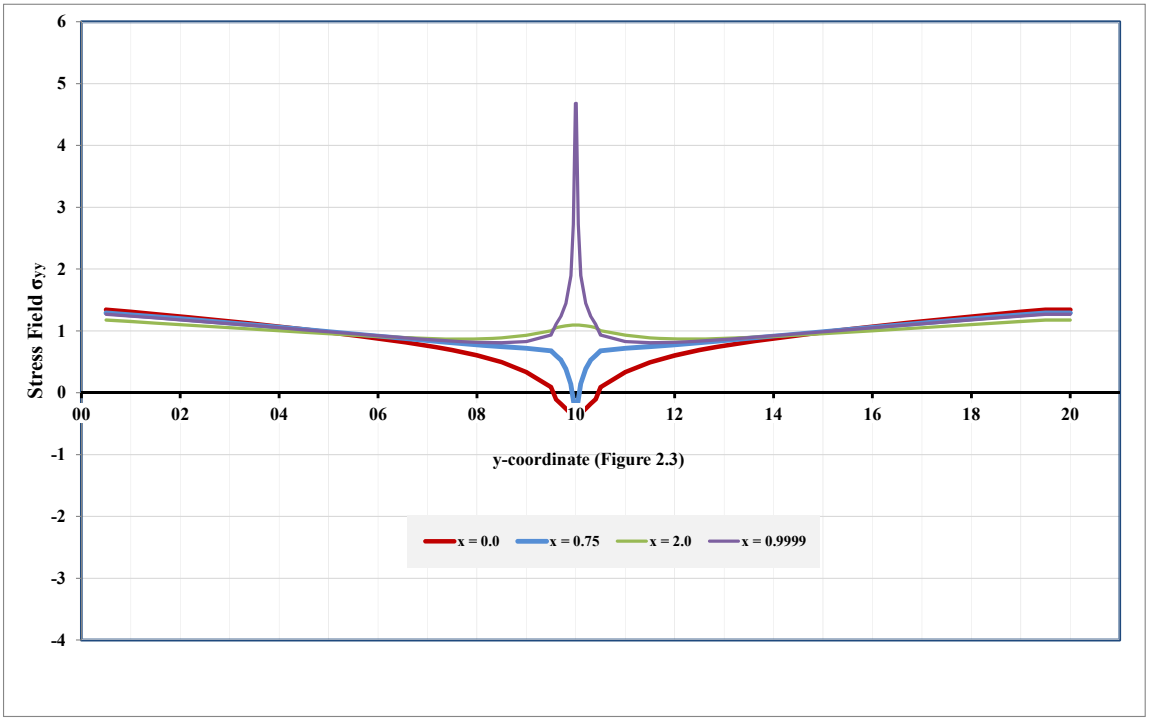

Figure 2.4 Stress field σ_{yy}

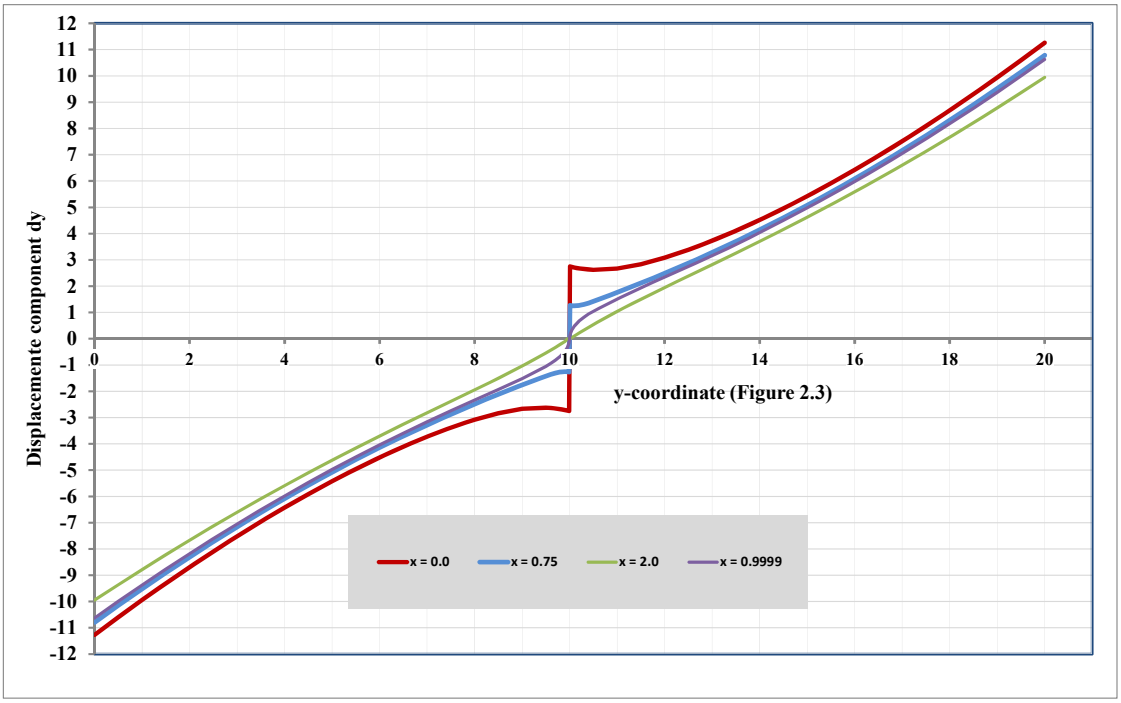

Figure 2.5 Displacement field u_y

It is possible to note in Figure 2.4 that the stress component σ_{yy} tends to infinity at crack tip ($x = 0.9999...$) and there was a discontinuity in the displacement component u_y for $x < 1.0$.

This example is very simple but shows the effectiveness of the enrichment in the modeling of the phenomenon that occurs in the neighborhood of the crack tip. Use of the GFEM combined with the refinement of the mesh must provide better results.

2.4 *J Integral*

Aiming to evaluate the Stress Intensity Factors (*SIFs*), Rice (1968) formulated the *J Integral* concept. It addresses a path-independent line integral which value has correspondence to the decreasing in potential energy when an increment of crack extension occurs. The *J Integral* applies either in linear or nonlinear elastic materials.

Moreover, an important advantage of the *J Integral*, quoting Broek (1986) is that "within certain limitations, the *J Integral* provides a means to determine an energy release rate for cases where plasticity effects are not negligible". This characteristic of the *J Integral* is important in order to guarantee that the Splitting Method can be extended do analyze problems involving ductile materials. However, this aspect was not considered in this work.

The *J Integral* can be represented by:

$$J = \int_{\Gamma} \left(W dy - T \cdot \frac{\partial \vec{u}}{\partial x} ds \right) \tag{2.22}$$

or, in an alternative expression, conveniently using indicial notation, as:

$$J = \int_{\Gamma} \left(W \mathrm{n}_1 - T_i \cdot \frac{\partial \mathrm{u}_i}{\partial x_1} \right) ds \tag{2.23}$$

where:

i. W is the strain energy density:

$$W = W(x, y) = \frac{1}{2}\left(\sigma_x \varepsilon_x + \sigma_y \varepsilon_y + \tau_{xy} \gamma_{xy}\right) \tag{2.24}$$

ii. The traction vector T is a force per unit area acting at a point with respect to a plane defined by a normal versor n, as shown in Figure 2.6.

$$T = \begin{Bmatrix} T_x \\ T_y \end{Bmatrix} = \begin{bmatrix} \sigma_x & \tau_{xy} \\ \tau_{xy} & \sigma_y \end{bmatrix} \begin{Bmatrix} n_x \\ n_y \end{Bmatrix} \tag{2.25}$$

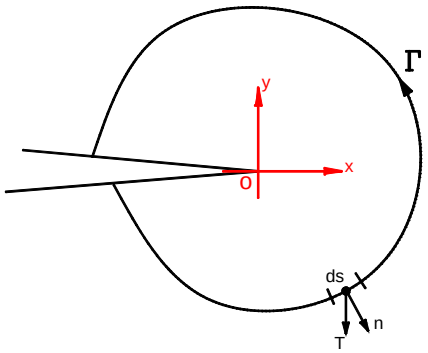

Figure 2.6 **Arbitrary path *Γ* enclosing a crack tip. Traction vector *T* and normal vector *n* to the segment *ds***

It is important to verify in Figure 2.6 that the path of integration Γ is not, necessarily, circular. However, in this work a circular path was adopted in order to take advantage of some favorable features of the polar coordinates. Therefore:

$$J = \int_{-\pi}^{\pi} \left(W \cos(\theta) - T_x \frac{\partial u_x}{\partial x} - T_y \frac{\partial u_y}{\partial x} \right) \rho d\theta \qquad (2.26)$$

The *J Integral* can be viewed as an energy parameter, comparable to the energy release rate *G*, or else, *G=J,* in the elasticity limit. Finally, it is important to remind the relations between *J Integral* and the Stress Intensity Factors:

$$K_I^2 + K_{II}^2 = EJ \qquad \text{(Plane Stress)} \qquad (2.27a)$$

$$K_I^2 + K_{II}^2 = \frac{EJ}{(1-\nu^2)} \qquad \text{(Plane Strain)} \qquad (2.27b)$$

To evaluate the *J Integral* numerically, a particular procedure is hereby proposed. First of all, let be a circular path of integration around the crack tip. This path is divided into 4 segments. Next, each segment is further subdivided into 3 segments. Therefore, there are 4 segments, each one with 2 intermediate points. The reason is due to the option of mapping an arc of circumference through a polynomial of order 3. In Figure 2.7a, the referred segments can be observed: i) 0-1-2-3; ii) 3-4-5-6; iii) 6-7-8-9; iv) 9-10-11-12.

Remark: The finite element mesh adopted to discretize the neighborhood of the crack tip is omitted to focus only the integration path. The axes depicted in the figure are local axes.

Next, each segment is mapped onto a dimensionless straight line segment, as shown in Figure 2.7b. It is important to follow the integration direction, according to the adopted numbering of the points belonging to the segments, as depicted in Figure 2.7. Thus, for the first segment (0-1-2-3), the point labeled "0" is attached to coordinate ξ = -1.0, the point labeled "1" is attached to coordinate ξ = -1/3, the point labeled "2" is attached to coordinate ξ = +1/3, and the point labeled "3" is attached to coordinate ξ = +1.0, and so on for the other segments.

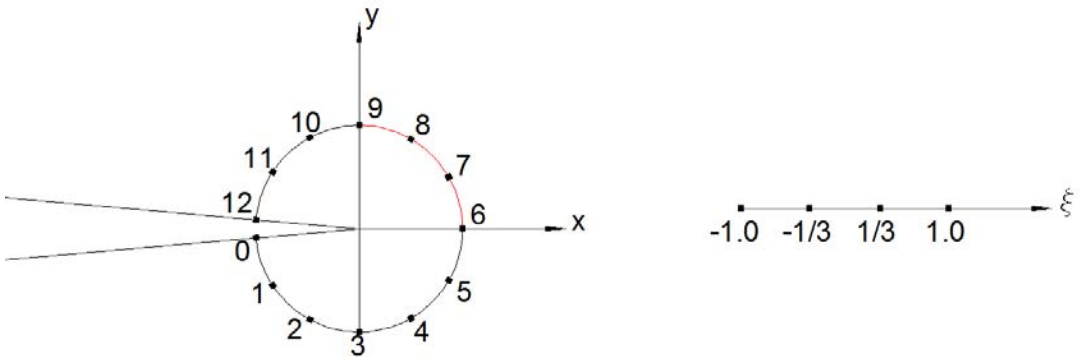

a. Circular path subdivided into segments b. Natural coordinates

Figure 2.7 Path of integration

In the next step, the integration along the path Γ must be done using each discretized segment. In other words, the integration along Γ is substituted by a sum of integrals along each segment, as shown in Equation 2.28:

$$J = \int_{\Gamma} \left(W \cdot \mathrm{n}_1 - T_i \cdot \frac{\partial \mathrm{u}_i}{\partial x_1} \right) ds = \sum_{j=1}^{nseg} \int_{\Gamma_j} \left(W \cdot \mathrm{n}_1 - T_i \cdot \frac{\partial \mathrm{u}_i}{\partial x_1} \right) ds \qquad (2.28)$$

where *nseg* is the number of segments in which the path Γ is divided. In the example shown in Figure 2.7a, *nseg* is equal to 4.

Afterwards, each integral on the right hand side of Equation (2.28) is made using the natural coordinate system defined above and shown in Figure 2.7-b:

$$\int_{\Gamma_j} \left(W \cdot \mathrm{n}_1 - T_i \cdot \frac{\partial \mathrm{u}_i}{\partial x_1} \right) ds = \int_{-1.0}^{1.0} \left(W \cdot \mathrm{n}_1 - T_i \cdot \frac{\partial \mathrm{u}_i}{\partial x_1} \right) Jac.\, d\xi \quad , j = 1..4 \qquad (2.29)$$

where *Jac* is the Jacobian operator relating the natural coordinates to the local coordinates.

The relation between natural coordinates and local coordinates is well known and given by:

$$x = x_1\phi_1 + x_2\phi_2 + x_3\phi_3 + x_4\phi_4 \qquad (2.30a)$$

$$y = y_1\phi_1 + y_2\phi_2 + y_3\phi_3 + x_4\phi_4 \qquad (2.30b)$$

where:

$$\phi_1(\xi) = -(9\xi^3 - 9\xi^2 - \xi + 1)/16 \qquad (2.31a)$$

$$\phi_2(\xi) = (27\xi^3 - 9\xi^2 - 27\xi + 9)/16 \qquad (2.31b)$$

$$\phi_3(\xi) = -(27\xi^3 + 9\xi^2 - 27\xi - 9)/16 \qquad (2.31c)$$

$$\phi_4(\xi) = (9\xi^3 + 9\xi^2 - \xi - 1)/16 \qquad (2.31d)$$

Finally:

$$Jac = \left(\left(\frac{dx}{d\xi} \right)^2 + \left(\frac{dy}{d\xi} \right)^2 \right)^{1/2} \qquad (2.32)$$

Finally, the right hand side of Equation (2.28) can be substituted by a numerical integration:

$$\int_{-1.0}^{1.0}\left(W\cdot \mathrm{n}_1 - T_i\cdot\frac{\partial \mathrm{u}_i}{\partial x_1}\right)Jac.d\xi = \sum_{i=1}^{ngp}\left(W(x_i)\cdot n_1(x_i) - T_1(x_i)\frac{\partial \mathrm{u}_1}{\partial x_1}\Big|_{x_i} - T_2(x_i)\frac{\partial \mathrm{u}_2}{\partial x_1}\Big|_{x_i}\right)Jac.We(x_i) \tag{2.33}$$

where:

1. *ngp* is the number of sampling points of the Gauss quadrature;
2. x_i is the i^{th} sampling point;
3. $We(x_i)$ is the weight function evaluated in x_i.

The sampling points of the Gauss quadrature *ngp* coincide with the points shown in Figure 2.7-b. In order to calculate Equation (2.33), the required displacements and stress fields must be obtained only at the points shown in Figure 2.7-a, owing to the correspondence between them and the points of the mapping shown in Figure 2.7-b. Both fields can be obtained by using the procedures described in Section 4.1 and Appendix B.

However, instead of computing Equation (2.33) directly, it is necessary to divide *J* in order to obtain K_I and K_{II} separately. This procedure was presented by Ishikawa et al (1980) and used by Kzam (2009). According to Equation (2.34), the *J Integral* can be separated into two parts:

$$J = J_I + J_{II} \tag{2.34}$$

where:

1. J_I refers to Mode I of opening;
2. J_{II} refers to Mode II of sliding.

To calculate J_I, the displacements and stress fields are replaced by auxiliary fields u^I and σ^I, respectively, according to Equations (2.35) and (2.36):

$$\begin{Bmatrix} u_1^I \\ u_2^I \end{Bmatrix} = \frac{1}{2}\begin{Bmatrix} u_1 + u_1' \\ u_2 - u_2' \end{Bmatrix} \tag{2.35}$$

$$\begin{Bmatrix} \sigma_{11}^{I} \\ \sigma_{22}^{I} \\ \sigma_{12}^{I} \end{Bmatrix} = \frac{1}{2} \begin{Bmatrix} \sigma_{11} + \sigma_{11}' \\ \sigma_{22} + \sigma_{22}' \\ \sigma_{12} - \sigma_{12}' \end{Bmatrix} \tag{2.36}$$

In Equation (2.35), $u' = (u_1', u_2')$ is the displacement field at a symmetric point of the point that is been analyzed in relation to the local *x-axis*. Similarly, in Equation (2.36) $\sigma^1 = (\sigma_1', \sigma_2')$ is the stress field at the same point. For example, in Figure 2.7a, the point "12" is the symmetric of point "0", point "11" is the symmetric of point "1" and so on. Obviously, the reciprocal is also true.

Furthermore, to evaluate J_{II}, the auxiliary fields are given by:

$$\begin{Bmatrix} u_1^{II} \\ u_2^{II} \end{Bmatrix} = \frac{1}{2} \begin{Bmatrix} u_1 - u_1' \\ u_2 + u_2' \end{Bmatrix} \tag{2.37}$$

$$\begin{Bmatrix} \sigma_{11}^{II} \\ \sigma_{22}^{II} \\ \sigma_{12}^{II} \end{Bmatrix} = \frac{1}{2} \begin{Bmatrix} \sigma_{11} - \sigma_{11}' \\ \sigma_{22} - \sigma_{22}' \\ \sigma_{12} + \sigma_{12}' \end{Bmatrix} \tag{2.38}$$

In Figure 2.8, the results of the operations correspondent to Equations (2.35)-(2.38) are presented for an arbitrary point *P* and its symmetrical point *P*'.

Mode I

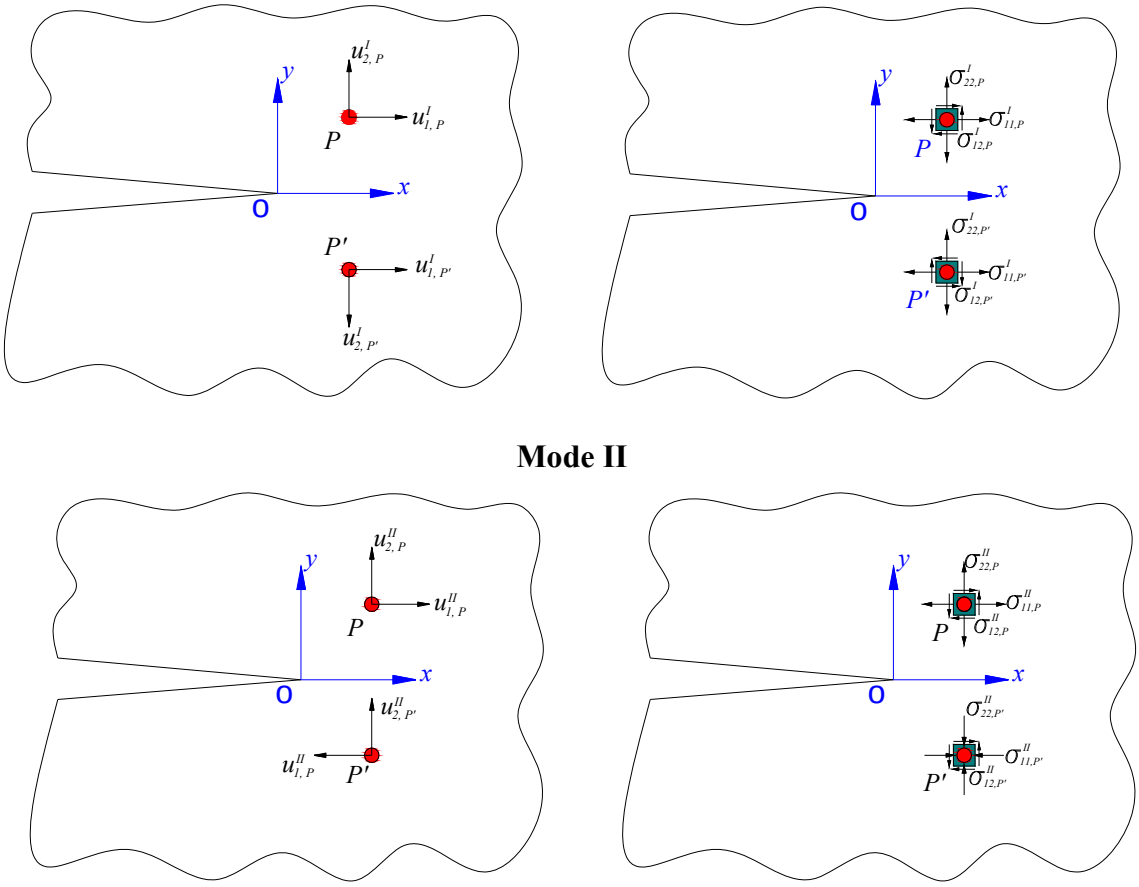

Figure 2.8 **Symmetric and anti-symmetric components of the displacement field for Modes I and II**

Analyzing Equations (2.35)-(2.38), and by observing Figure 2.8, it can be calculated that for Mode I:

i. $u^I_{1,P} = u^I_{1,P'}$

ii. $u^I_{2,P} = -u^I_{2,P'}$

iii. $\sigma^I_{11,P} = \sigma^I_{11,P'}$

iv. $\sigma^I_{22,P} = \sigma^I_{22,P'}$

v. $\sigma^I_{12,P} = -\sigma^I_{12,P'}$

And, for Mode II:

vi. $u^{II}_{1,P} = -u^{II}_{1,P'}$

vii. $u^{II}_{2,P} = u^{II}_{2,P'}$

viii. $\sigma^{II}_{11,P} = -\sigma^{II}_{11,P'}$

ix. $\sigma^{II}_{22,P} = -\sigma^{II}_{22,P'}$

x. $\sigma^{II}_{12,P} = \sigma^{II}_{12,P'}$

An important aspect that must be mentioned is that loads are applied to the crack surfaces and their contributions must be considered in the calculus of the *J Integral*. To address this issue, the solution proposed by Karlsson and Bäcklund (1978), was hereby adopted. Accordingly, a decomposition of the *J integral* is assumed as:

$$J = J_{cp} + J_{scs} + J_{ics} \tag{2.39}$$

where J_{cp} is the contribution of the circular path to the *J Integral* and J_{scs} , J_{ics} are the contributions of the superior and inferior crack surfaces, respectively.

The procedure to compute the values of J_{scs} and J_{ics} is identical to that described above for the calculus of the *J Integral* in the circular path, and each crack surface is analogously divided into 3 segments and then mapped into a linear segment. See Figure 2.9.

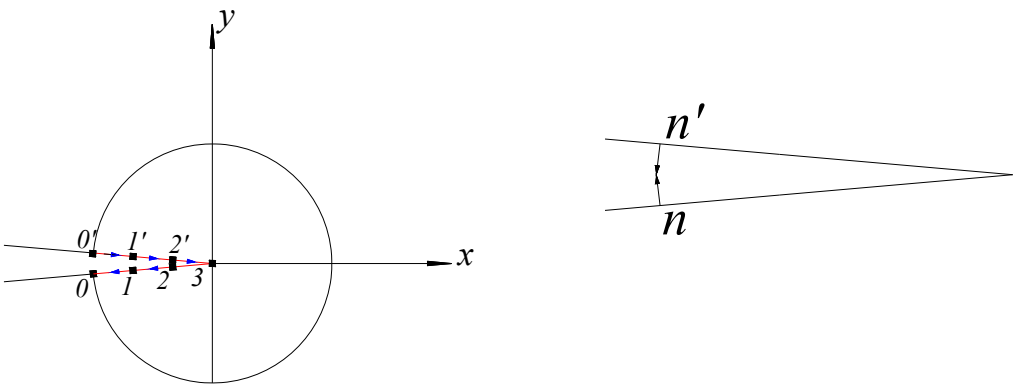

Figure 2.9 ***J Integral* at the crack surfaces**

It is important to observe the direction of the integration indicated by the arrows in the Figure 2.9. The positive outward normal vector *n* to each crack surface is also indicated.

The procedure to evaluate the contribution of the crack surfaces for the *J Integral* is identical to that described for the contributions in the circular path. However, it was treated separately in this paper in order to emphasize some important features:

1. Most of the programs containing routines for calculating *J* require a specification of an integration path around the crack tip from the user, assuming that the crack surface is traction free. This is not an assumption in the developed code;
2. The error in the calculus of the *J Integral* including the crack surfaces can be strongly affected by the accuracy of the stress field very close to the crack tip. Therefore, special care must be taken aiming to improve the accuracy in that region, for example, by refining the mesh or, as hereby adopted, by using enrichment strategies.

2.5 *"Crack Open Displacement" (COD) and "Crack Sliding Displacement" (CSD)*

The *COD* method was hereby considered in order to provide an alternative respecting the *J Integral.* The extraction of *SIFs* by means of displacement correlation technics is done using the displacements at the crack surface resulting from the analysis.

$$K_I = \sqrt{\frac{2\pi}{r}} \cdot \frac{\mu}{(\kappa+1)} \cdot COD \tag{2.40a}$$

$$K_{II} = \sqrt{\frac{2\pi}{r}} \cdot \frac{\mu}{(\kappa+1)} \cdot CSD \tag{2.40b}$$

where:

1. *COD* ("Crack Opening Displacement") is the difference between the normal displacements in correlated points placed at the crack surfaces. It is recommended, or better, it is usual to place the referred points at a distance between 15% up to 50% of the half-length of the crack;
2. *CSD* ("Crack Sliding Displacement") is the difference between the tangential displacements in correlated points placed at the crack surfaces (See Figure 2.10).

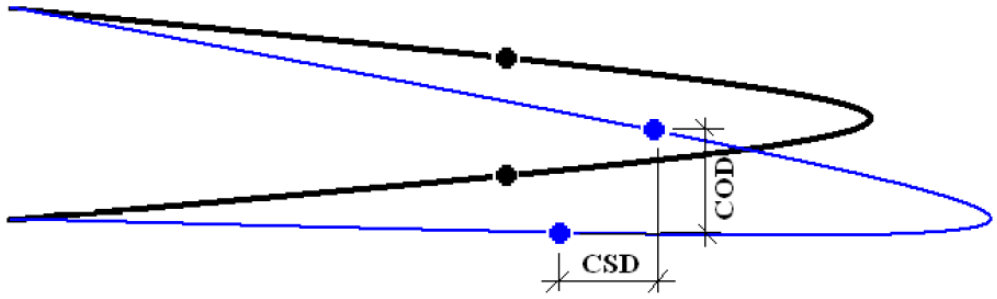

Figure 2.10 COD and CSD (Source: Leonel, 2010)

2.6 The maximum principal stress criterion.

The main purpose of this section is to establish a criterion to evaluate the angle in which the crack growth will occur. This topic is worth to addressing, once the computational program developed in this work treats of the fatigue crack growth under mixed mode loading.

The maximum principal stress criterion postulates that crack growth will take place in the direction perpendicular to the maximum principal stress. If a cracked solid is loaded in combined mode I and II, the σ_θ and $\tau_{r\theta}$ at the crack tip (i.e., when dr tends to zero, see Figure 2.11) are given by the following expressions:

$$\sigma_\theta = \frac{1}{\sqrt{2\pi r}}\cos\left(\frac{\theta}{2}\right)\left[K_I cos^2\left(\frac{\theta}{2}\right) - \frac{3}{2}K_{II}\sin\theta\right] \tag{2.41}$$

$$\tau_{r\theta} = \frac{1}{2\sqrt{2\pi r}}\cos\left(\frac{\theta}{2}\right)[K_I \sin\theta + K_{II}(3\cos\theta - 1)] \tag{2.42}$$

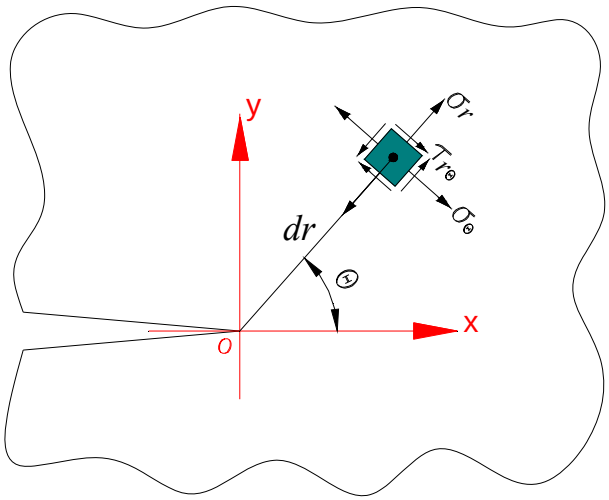

Figure 2.11 Stress element rotated in relation to a local system

The stress σ_θ will be the principal stress if $\tau_{r\theta} = 0$. This is the case for $\theta = \theta_c$ where θ_c is found from equating the Equation (2.42) to zero:

$$K_I \sin\theta_c + K_{II}(3\cos\theta_c - 1) = 0 \tag{2.43}$$

The Equation (2.43) can be solved by writing:

$$2K_I \sin\frac{\theta_c}{2}\cos\frac{\theta_c}{2} + 3K_{II}\left(cos^2\frac{\theta_c}{2} - sin^2\frac{\theta_c}{2}\right) - K_{II}\left(sin^2\frac{\theta_c}{2} + cos^2\frac{\theta_c}{2}\right) = 0 \tag{2.44}$$

which yields:

$$2K_{II}tan^2\frac{\theta_c}{2} - K_I tan\frac{\theta_c}{2} - K_{II} = 0 \tag{2.45}$$

so that:

$$\left(tan\frac{\theta_c}{2}\right)_{1,2} = \frac{1}{4}\frac{K_I}{K_{II}} \pm \frac{1}{4}\sqrt{\left(\frac{K_I}{K_{II}}\right)^2 + 8} \tag{2.46}$$

and finally:

$$\theta_{c,1} = 2\,\mathrm{atan}\left(\frac{1}{4}\frac{K_I}{K_{II}} + \frac{1}{4}\sqrt{\left(\frac{K_I}{K_{II}}\right)^2 + 8}\right) \tag{2.47a}$$

$$\theta_{c,2} = 2\,\mathrm{atan}\left(\frac{1}{4}\frac{K_I}{K_{II}} - \frac{1}{4}\sqrt{\left(\frac{K_I}{K_{II}}\right)^2 + 8}\right) \tag{2.47b}$$

The principal stresses are then given as:

$$\sigma_1 = \sigma_\theta\left(\theta = \theta_{c,1}\right) = \frac{1}{\sqrt{2\pi r}} cos^2\frac{\theta_{c,1}}{2}\left(K_I cos\frac{\theta_{c,1}}{2} - 3K_{II} sin\frac{\theta_{c,1}}{2}\right) \tag{2.48a}$$

$$\sigma_2 = \sigma_\theta\left(\theta = \theta_{c,2}\right) = \frac{1}{\sqrt{2\pi r}} cos^2\frac{\theta_{c,2}}{2}\left(K_I cos\frac{\theta_{c,2}}{2} - 3K_{II} sin\frac{\theta_{c,2}}{2}\right) \tag{2.48b}$$

If $|\sigma_1| \geq |\sigma_2|$, then $\theta_{c,1}$ is used as the propagation angle. In the other hand, if $|\sigma_1| < |\sigma_2|$, then $\theta_{c,2}$ is used as the propagation angle.

2.7 Fatigue Crack Growth.

In this section, the description of the Fatigue Crack Growth using the Splitting Method is presented. The possibility of taking into account several patterns of cracks and their respective paths of propagation is indeed an important advancement achieved by this work.

The main aim of this analysis is to determine the so-called Fatigue Crack Growth Rate Curve (*da/dn x ΔK)* and construct the crack length versus the number of cycles curve (*a x n)*. It is important to stress that:

1. *da/dn* is the crack length growth with respect to the number of cycles;

2. *ΔK* is the amplitude of the Stress Intensity Factor. In fact, *ΔK* is a function of *a* and σ, or else, $\Delta K = f(a, \sigma)$.

The strategy proposed in this work consists of finding an approximation function that relates the amplitude of the Stress Intensity Factor (*ΔK)* and the half-length of the cracks (*a*), for each crack present in the solid. After that, by using the referred function

and a crack growth law, the aim is to determine the so-called Fatigue Crack Growth Rate Curve by means of an analytic integration.

In order to elucidate these concepts, let's consider the cracked plate of the Figure 2.12.

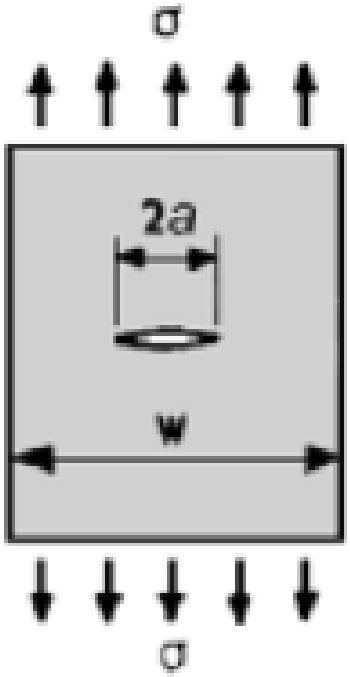

Figure 2.12 Cracked plate (Extracted of JANSEEN, 2002)

In this case, the Stress Intensity Factor related to the Mode I is given by the Equation (2.49):

$$K_I = C_g \cdot \sigma\sqrt{\pi a} \tag{2.49}$$

where a is the half-length of the crack. According to Feddersen (1967), C_g is given by Equation (2.50):

$$C_g = \sqrt{\sec(\frac{\pi a}{W})} \tag{2.50}$$

It is clear that, for a given crack length, the Stress Intensity Factor depends upon of the level of the applied load. It follows that the amplitude of the Stress Intensity Factor is directly related to the amplitude of the applied load. Thus, the Equation (2.49) becomes:

$$\Delta K_I = C_g \cdot \Delta\sigma\sqrt{\pi a} \tag{2.51}$$

In Figure 2.13 a possible variation of an applied cyclic load is exemplified.

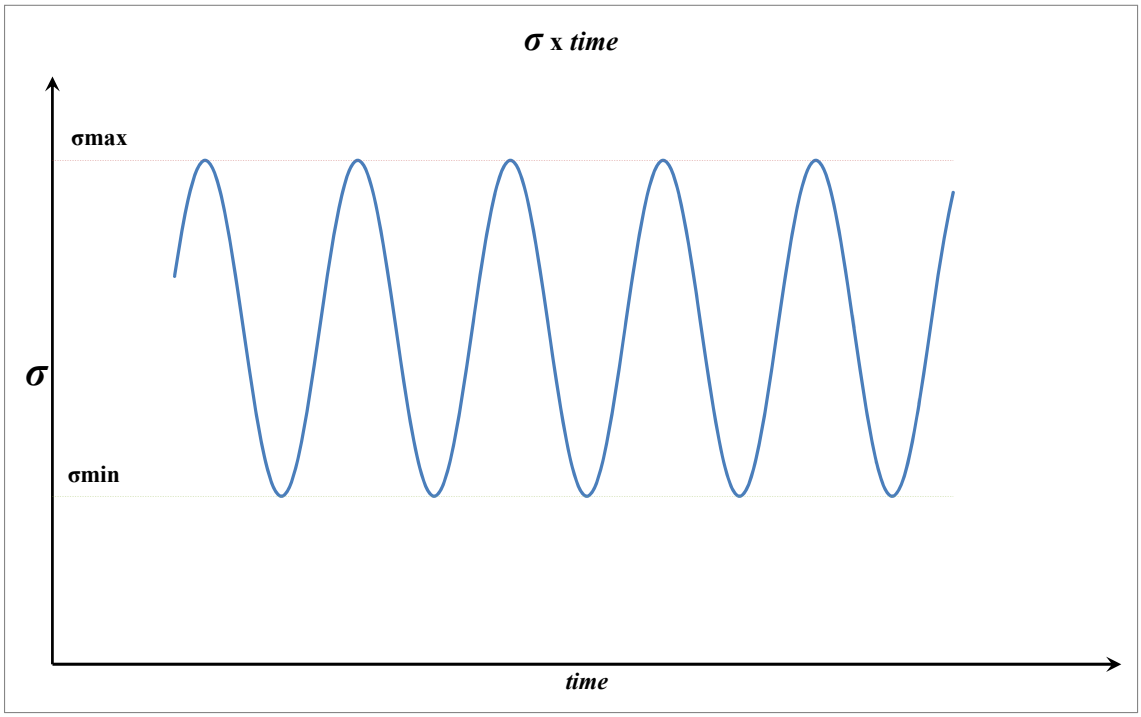

Figure 2.13 Level of the tensile load x time

For an arbitrary, but fixed, crack length *2a*, there is a maximum Stress Intensity Factor $K_{I,max}$ associated to σ_{max} and a minimum Stress Intensity Factor $K_{I,min}$ associated to σ_{min}. Therefore, the amplitude of the Stress Intensity Factor is calculated as follows:

$$\Delta K_I = K_{I,max} - K_{I,min} \tag{2.52}$$

For the Fatigue Crack Growth Rate Curve *da/dn x ΔK*, in this work it is adopted the most widely known crack growth law, the Paris equation:

$$\frac{da}{dn} = C(\Delta K_I)^m \tag{2.53}$$

where *C* and *m* are constants depending on the material.

Once integrating the Equation (2.53), it is possible to construct a crack length versus number of cycles relation. In the case of the solid depicted in Figure 2.13, substituting the Equation (2.51) into Equation (2.53), the following differential equation results:

$$\frac{da}{dn} = C\left(C_g \cdot \Delta\sigma\sqrt{\pi a}\right)^m \tag{2.54}$$

Integrating the Equation (2.54), the crack length versus the number of cycles curve (*a x n)* arises. However, many structures are not only subjected to pure tension but they can be subjected to shear and torsional loading. Cracks may therefore be exposed to tension and shear, which leads to mixed-mode crack opening, *i.e.*, a mixture of modes I and II. In order to taking in account the mixed mode fracture, ΔK_I must be replace by $\Delta K_{I,eq}$ in Equation (2.53), which is determined as follows:

$$K_{I,eq} = K_I \cdot \left(\cos\left(\frac{\theta_c}{2}\right)\right)^3 - 3 \cdot K_{II} \cdot \left(\cos\left(\frac{\theta_c}{2}\right)\right)^2 \cdot \sin\left(\frac{\theta_c}{2}\right) \tag{2.55a}$$

and, consequently:

$$\Delta K_{I,eq} = \Delta K_I \cdot \left(\cos\left(\frac{\theta_c}{2}\right)\right)^3 - 3 \cdot \Delta K_{II} \cdot \left(\cos\left(\frac{\theta_c}{2}\right)\right)^2 \cdot \sin\left(\frac{\theta_c}{2}\right) \tag{2.55b}$$

where θ_c is the direction of crack growth, defined in Section 2.6. For more details about Equations (2.55a) and (2.55b), see Broek (1986).

For a few problems it is possible to find relations such as (2.49) and (2.51), which are closed forms that can be integrated analytically. Nevertheless, for more complex problems, presenting complex geometry, loading and patterns of cracks, such relations are not available. A possible manner to solve this problem is to determine the amplitude of the Stress Intensity Factors versus the crack length curve using discrete values of the crack lengths and calculating theirs respective *SIFs* using the Splitting Method, which has provide good numerical estimates for the Stress Intensity Factors.

A simple methodology based on the Splitting Method is hereby proposed for solving problems with many cracks in order to determine each singular crack growth law and evaluate the fatigue crack growth rate.

The main steps of the conceived procedure are described in the sequel:

1. Choose a suitable increment of crack growth Δa_{max}, which must be small enough to obtain sufficient accuracy, but not too small to demand excessive calculation effort;

2. By using the Splitting Method, calculate the Stress Intensity Factors K_I and K_{II} for each crack tip, considering theirs original lengths. By using the Equations (2.55a) and (2.55b), calculate $\Delta K_{I,eq}$. Comparing the whole set of values, determine the maximum value of $\Delta K_{I,eq}$, from now on indicated as $\Delta K_{I,eq.\,max}$. Therefore;

$$\Delta K_{I,eq.max} = max\left(\Delta K_{I,eq,j} \middle| j = 1..number\ of\ cracks\ tips\right) \tag{2.56}$$

Remark: for internal cracks, there will be more than one tip for each crack.

3. The crack length increments are defined as suggested by Sing *et al* (2012), "for multiple crack problems, first a principal crack tip is decided on the basis of maximum value of $\Delta K_{I,eq}$, then a constant value of maximum crack (Δa_{max}) can be taken for this principal crack tip". Then, the remaining crack increments are obtained as:

$$\Delta a_j = \Delta a_{max} \cdot \left(\frac{\Delta K_{I,eq,j}}{\Delta K_{I,eq.max}}\right)^m \qquad j = 1...number\ of\ crack\ tips \tag{2.57}$$

where m is the exponent of the Paris Law, see Equation (2.53).

4. The previous steps must be repeated over the required number of steps, previously established in the analysis. Each crack must be increased according to Equation (2.57). For example, in the first iteration, for an arbitrary crack tip j, the length will be:

$$a_{j,1} = a_{j,0} + \Delta a_j \tag{2.58}$$

where:

i. $a_{j,1}$ is the half-length of the crack tip j in the first iteration;

ii. $a_{j,0}$ is the half-length of the crack tip j in the original configuration;

iii. Δa_j is the increment calculated using the Equation (2.57).

In Figure 2.14, a graph relating $K_{I,eq}$ and the half-length a of an arbitrary crack is illustrated. There are two curves relating $K_{I,eq}$ and a: the first one correspond to the maximum value of σ (σ_{max}) and the second one correspond to the minimum value of σ

(σ_{min}). It is possible to verify from the graph that discrete values are presented and each pair of values is related to a fixed crack length. An example is shown in Figure 2.15.

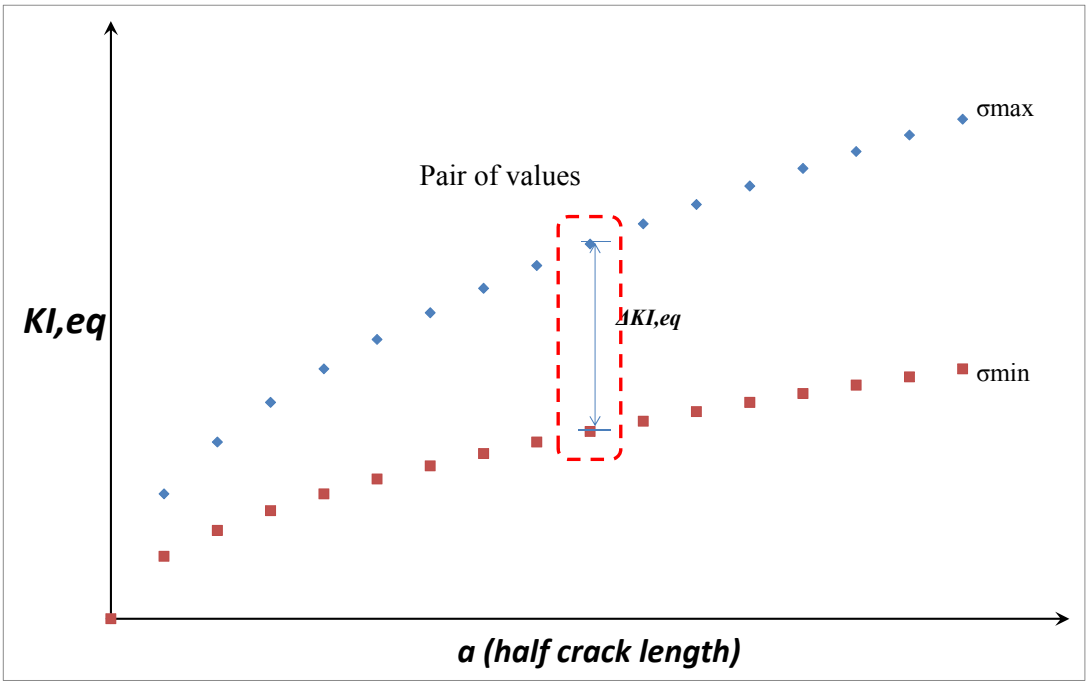

Figure 2.14 $K_{I,eq}$ **x** a **for an arbitrary crack**

Using the values of $K_{I,eq}$ related to σ_{max} and σ_{min}, it is possible to evaluate $\Delta K_{I,eq}$:

$$\Delta K_{I,eq}\big|_a = K_{I,eq,max}\big|_a - K_{I,eq,min}\big|_a \tag{2.59a}$$

Obviously:

$$K_{I,eq,max} = K_{I,max} \cdot \left(\cos\left(\frac{\theta_c}{2}\right)\right)^3 - 3 \cdot K_{II,max} \cdot \left(\cos\left(\frac{\theta_c}{2}\right)\right)^2 \cdot \sin\left(\frac{\theta_c}{2}\right)$$

$$K_{I,eq,min} = K_{I,min} \cdot \left(\cos\left(\frac{\theta_c}{2}\right)\right)^3 - 3 \cdot K_{II,min} \cdot \left(\cos\left(\frac{\theta_c}{2}\right)\right)^2 \cdot \sin\left(\frac{\theta_c}{2}\right)$$

(2.55a – repeated)

After solving the problem using this procedure for a considerable number of steps, it is possible to construct a table relating $\Delta K_{I,eq}$ and a for each crack, by using Equation (2.55b):

Table 2.1 $\Delta K_{I,eq}$ **x** a **(for a fixed crack)**

a	a_0 (original crack)	a_1	a_2	…	a_{nstep}
$\Delta K_{I,eq}$	$\Delta K_{I,eq,\ 0}$	$\Delta K_{I,eq,\ 1}$	$\Delta K_{I,eq,\ 2}$	…	$\Delta K_{I,eq,\ nstep}$

Next, a polynomial approximation function of degree p can be constructed from the obtained values by means of the *LSM*.

$$\Delta K_{I,eq} = f(a) \cong p(a) = \beta_0 + \beta_1 \cdot a + \beta_2 \cdot a^2 + \cdots + \beta_p \cdot a^p \qquad (2.60)$$

Remark: in fact, the Equation (2.60) is a function that depends only on the crack length a for an arbitrary, but fixed, $\Delta\sigma$. However, it is feasible to construct an approximation function in which $\Delta\sigma$ be a function of a or the number of cycles n.

The polynomial approximation function of $\Delta K_{I,eq}$ is shown in Figure 2.15.

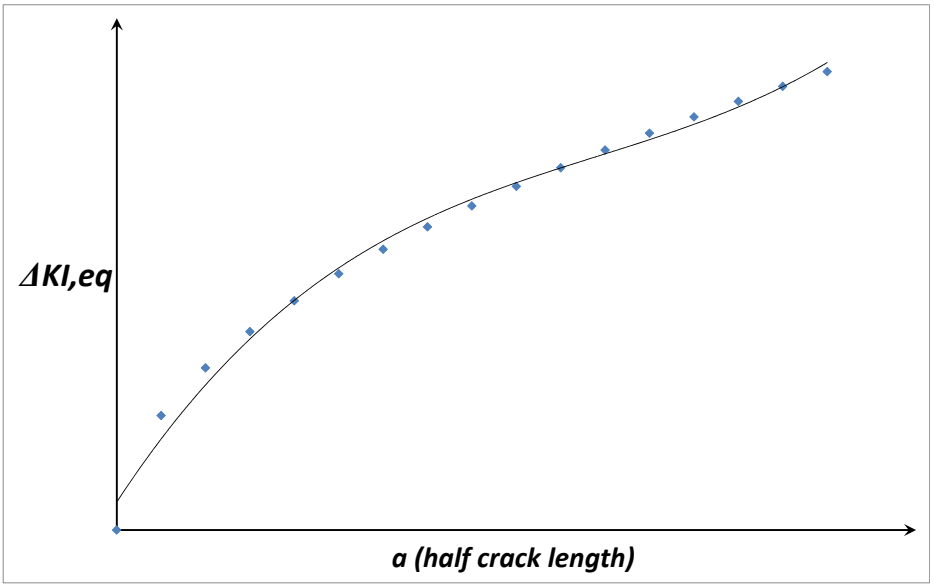

Figure 2.15 $\Delta K_{I,eq}$ **x** a **for an arbitrary crack**

Substituting (2.60) in (2.53) and integrating, it is possible to recover the relation between the length of the crack (a) and the number of cycles of alternating stress (n).

The presented method is especially useful when the relation between ΔK and a is unknown. In this work, the analysis of a problem containing a closed expression relating ΔK and a was performed aiming to validate the procedure and is presented further on in the Example 6.1, Section 6.1.6 of the Chapter 6.

2.8 Slow Stable Crack Growth and the *R*-Curve

To conclude the review of the Fracture Mechanics topics, the author deems be necessary to establish a criterion to assess the crack resistance and consequent failure of the analyzed solid. Accomplished with that criterion the proposed method becomes feasible for performing a complete study of a given problem, including the verification of some possibilities of failure.

It is possible to state that there are at least two main reasons that endorse the necessity for establishing a criterion to stop the incremental process used in this work:

1. The proposed method will model the real phenomenon with better accuracy of an engineer view point, since the limit to the crack growth from which the failure follows could be determined;
2. If a criterion to stop the incremental process is established, it is possible to avoid an excessive number of increments and, consequently, saving computational effort. The time saved in the process could be used to analyze other patterns in other problems with many cracks, for example.

It was already mentioned that, for each crack tip, and for each step of the analysis described in the Section 2.7, the method will provide the Stress Intensity Factors K_I and K_{II}. To assess if the crack growth will be unstable, one can to apply the Equation (2.61) using the referred *SIFs* (BROEK, 1986):

$$\left(\frac{K_I}{K_{Ic}}\right)^2 + \left(\frac{K_{II}}{K_{IIc}}\right)^2 \leq 1 \tag{2.61}$$

where K_{Ic} and K_{IIc} is the critical Stress Intensity Factor referred to the opening Modes I and II, respectively, and are material properties.

In many cases, $K_{Ic} = K_{IIc}$. In these cases, it is possible to apply the Equation (2.62):

$$K_{I,eq} \leq K_{Ic} \tag{2.62}$$

Chapter 3: The splitting method as a tool for analysis of problems of the Linear-Elastic Fracture Mechanics

3.1 Introduction

The superposition technic is probably the most common technic for obtaining the *SIFs*. In this chapter it is shown how such technic is explored in the Splitting Method in order to solve two-dimensional problems of solids presenting internal and external cracks, as well as cracks linked to the borders of holes.

3.2 The Bueckner principle and superposition models

Bueckner (1958) stated that "[a]ny crack or notch problem can be reduced to one where the external load appears in the form of tractions distributed over the faces of the crack." This is called the Bueckner's principle, illustrated in Figure 3.1.

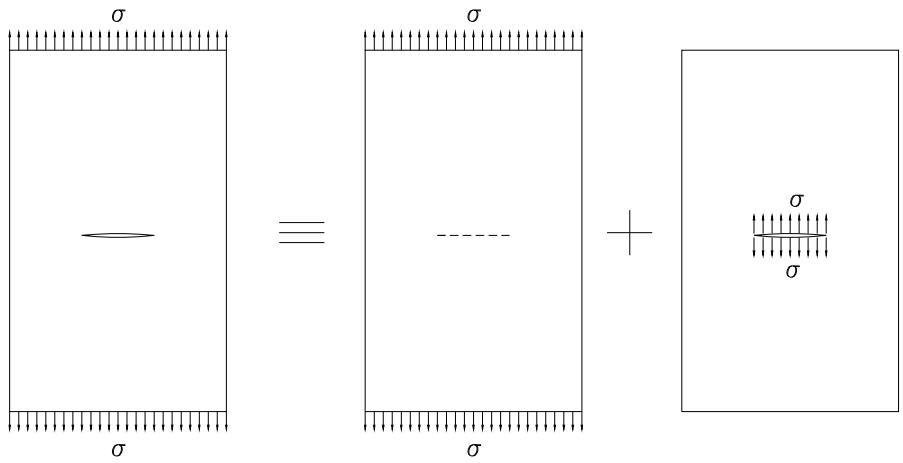

Figure 3.1 Bueckner principle

In addition, according to Janssen (2006), "in the vicinity of the crack tip the total stress field due to two or more different mode I loading systems can be obtained by an algebraic summation of the respective stress intensity factors." This is the superposition principle.

Both principles play a fundamental role in the development of the Splitting Method.

3.3 The Splitting Method

The Splitting Method belongs to the class of decomposition methods and was originally proposed by Andersson & Babuska (2005). In this section, the main concepts of the method are addressed. Complementary aspects can be found in Alves (2010).

Figure 3.2 illustrates the problem to be analyzed using the Splitting Method. The two-dimensional linear elastic domain V_c has a boundary S divided into two non-intersecting complementary parts S_u and S_t ($S = S_t \cup S_u$ and $S_t \cap S_u = \emptyset$) on which restrictions over displacements and loading can be prescribed, respectively. The domain contains holes with cracks, an internal crack and a border crack and is submitted in its boundary S_t to a tensile load.

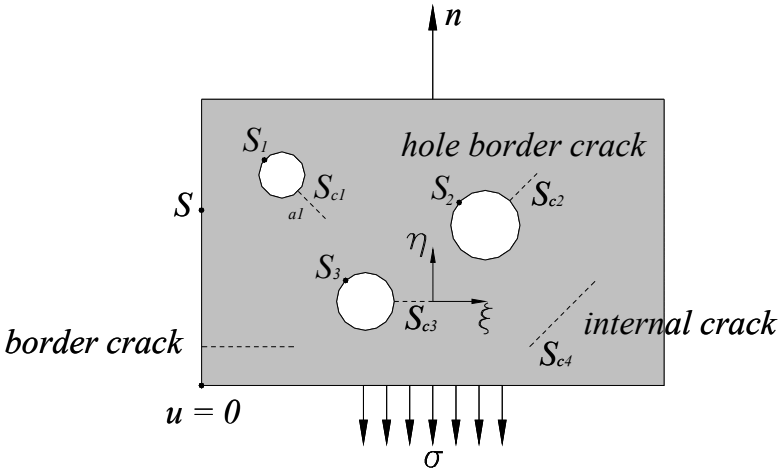

Figure 3.2 Two-dimensional domain containing holes and cracks.

Assuming that in S_u the displacement vector u is prescribed, the equations governing the equilibrium conditions and the static boundary conditions of the problem are:

$$\Delta u = 0 \qquad \text{on } V_c \tag{3.1a}$$

$$\partial u/\partial n = \underline{\underline{T}}\,\underline{n} = \sigma \qquad \text{on } S_t \tag{3.1b}$$

$$\partial u/\partial n = \underline{\underline{T}}\,\underline{n} = 0 \qquad \text{on } S_{ci},\ i = 1\ldots4 \tag{3.1c}$$

where $\Delta(.)$ is the 'generalized' Laplacian operator. In fact, the first condition is a condensed form of representing Lamé's equations, in which also the geometrical characteristics of deformations and the elastic properties of the material are implicit. Equation (3.1b) is a boundary condition making the stress tensor T and the applied loading compatible. In particular, Equation (3.1c) means that the crack surfaces are traction free.

In the Splitting Method the above problem is divided into sub-problems. The basic aim is to find a stress vector solution $\underline{t}$ at the crack faces such that:

$$\underline{t} = \underline{t}_G^{(0)} + \underline{t}_L^{(k)} + \underline{t}_G^{(k)} = \underline{0} \tag{3.2}$$

where $\underline{t}_G^{(0)}$ and $\underline{t}_G^{(k)}$ are stress vector solutions at the crack lines obtained from the sub-problems $P_G^{(0)}$ and $P_G^{(k)}$, respectively, and $\underline{t}_L^{(k)}$ is the stress vector prescribed at the crack faces in the local sub-problem $P_L^{(k)}$.

In Alves (2010), the numerical performance of the Splitting Method was improved by combining it with enrichment strategies of the approximation functions.

The main aim of the present research is to extend the scope of the Splitting Method to assess fatigue problems, by incorporating a step-by-step crack propagation procedure. An additional important improvement included in the extended scope is the possibility of evaluating *SIFs* for I-II mixed mode.

According to the theoretical conception of the method, it is possible to consider border cracks, holes with cracks and internal cracks. However, in the computational code developed in this work, only holes with cracks and internal cracks were considered.

This chapter is mostly devoted to describe the sub-problems composing the method. Each sub-problem will be described in detail in the sequel.

3.4 The global sub-problem $\boldsymbol{P_G^{(0)}}$

The global sub-problem $\boldsymbol{P_G^{(0)}}$ is basically the original problem without the cracks. However, identification lines are placed where should be the center lines of the original cracks. From the analysis of the $\boldsymbol{P_G^{(0)}}$, traction vectors will be identified in those lines.

Thus, the governing equations of this type of sub-problem are:

$$\Delta u_G^{(0)} = 0 \qquad \text{on } V \tag{3.3}$$

$$\partial u_G^{(0)} / \partial n = \sigma \quad \text{on } S_t \tag{3.4}$$

where V is the domain of the un-cracked domain and $u_G^{(0)}$ is the displacement field related to it.

Therefore, it is also important to highlight the following geometric features and variables:

1. As already cited, V is the domain of the plate, without the cracks;
2. Boundary line S, of the domain V and a normal vector n attached to it;

3. Identification line S_{ci} of the crack i. In fact, this line is not modeled, but it must be considered in order to evaluate the traction vector;
4. Boundary line S_j of the hole j. It is possible to solve problems with different numbers of cracks and holes (see Figure 3.2);
5. Local coordinate system (ξ_i,η_i). The ξ_i-axis must be aligned with the crack a_i. The origin of the local system must be placed at crack tip, as depicted in Figure 3.2;
6. Length of the crack: a_i.

It is also important to mention:

i. Segment S_u of the boundary line S where displacement components are prescribed:

$$u_G^{(0)} = \overline{u_G^{(0)}} = \begin{Bmatrix} u_x \\ u_y \end{Bmatrix} \quad \text{on } S_u; \tag{3.5}$$

ii. Complementary segment S_t of the boundary line where traction vector is imposed:

$$\partial u_G^{(0)}/\partial n = \sigma = \begin{Bmatrix} t_x \\ t_y \end{Bmatrix} = \underline{\underline{T}}.\underline{n} = \underline{\bar{t}} \text{ on } S_t; \tag{3.6}$$

Obviously, $S = S_t \cup S_u$ and $S_t \cap S_u = \emptyset$.

iii. Null traction vector along the internal hole boundary S_i:

$$\underline{\underline{T}}.\underline{n} = \underline{0} \text{ on } S_i. \tag{3.7}$$

Due to the simplicity of this sub-problem, it is possible to use a coarse mesh in the discretization can be defined. In fact, it is adequate to adopt a refinement in the mesh only to ensure some accuracy around the holes and identification lines corresponding to the original cracks. Therefore, local enrichment of the approximation may be exempt, by setting up a situation in which GFEM/ XFEM coincides with FEM.

Since the length, position and direction of the cracks are known, the traction vector can be computed in the identification lines using the numerical solution of this global sub-

problem. In fact, as the numerical solution provides components of the traction vector at some arbitrary points along the line S_{ci}, a continuous approximation of these components can be recovered by means of the Least Square Method (*LSM*). More specifically, the continuous approximation is written as a linear combination of an adopted polynomial basis function.

3.5 Local Sub-problem $P_L^{(k)}$

The basic aim of this sub-problem is to compute the *SIFs* using GFEM/XFEM. By using fracture functions as local enrichments it becomes feasible to consider the effects of the singularities without demanding an excessive mesh refinement.

In each local sub-problem, only one crack is considered. This crack may be an internal crack or a hole with a crack, as depicted in Figure 3.3. Surrounding the crack or the crack and hole, an arbitrary rectangular contour should be made, hereafter represented as $\Gamma^{(i)}$. It is important to mention that $\Gamma^{(i)}$ cannot intercept other cracks.

In each sub-problem, a set of internal pressure loads is applied to the crack faces, using the same normalized polynomial basis (it means, each component has a maximum unitary value) employed in the global sub-problem $P_G^{(0)}$ to identify the continuous traction vectors along the crack lines. Finally, as well as the *SIFs*, for each component of the polynomial basis, the displacement field $u_j^{(i)}$ and the traction vector $t^{(i)}$ along $\Gamma^{(i)}$are also computed.

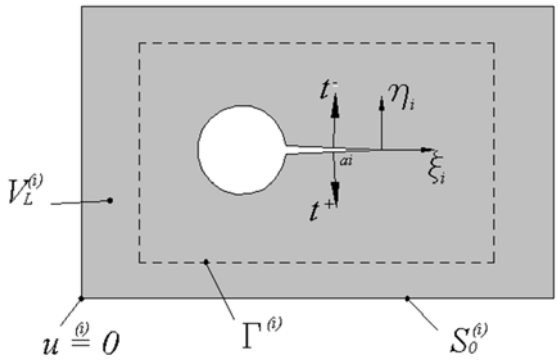

Figure 3.3 Local Sub-Problem $P_L^{(k)}$

The governing equations of this type of sub-problem are:

$$\Delta u_L^{(i)} = 0 \text{ on } V_L^{(i)} \tag{3.8}$$

The variables of this problem are (see Figure 3.3):

1. Local domain containing the crack: $V_L^{(i)}$;
2. Boundary line of the local domain: $S_0^{(i)}$;
3. Line S_{ci} of the crack i;
4. Local coordinate system (ξ_i,η_i). The origin of the system must be placed at the crack tip;
5. Length of the crack i: a_i;
6. Arbitrary rectangular contour enclosing the hole and the crack i: $\Gamma^{(i)}$.

Moreover, the main features of this type of sub-problem are:

i. Prescribed displacement field in $S_0^{(i)}$, aiming to avoid rigid body movement of $V_L^{(i)}$:

$$u_L^{(i)} = \overline{u_L^{(i)}} \text{ on } S_0^{(i)}; \tag{3.9}$$

Remark: The boundary conditions are arbitrary. The only restriction is that they must avoid the rigid body movement.

ii. Null traction vector at the hole border:

$$\partial u_L^{(i)}/\partial n = \begin{Bmatrix} t_x \\ t_y \end{Bmatrix} = \underline{\underline{T}}.\underline{n} = \underline{0} \text{ on } S_i; \tag{3.10}$$

iii. Traction vector applied at the crack surface: the components of this vector are polynomial functions of the natural coordinate ξ_i:

$$\underline{t}^+ = \underline{Q}_j(\xi_i/a_i) \text{ on } S_{ci}^+, \tag{3.11a}$$

$$\underline{t}^- = \underline{Q}_j(\xi_i/a_i) \text{ on } S_{ci}^-. \tag{3.11b}$$

Where:

$$\underline{Q}_j(\xi_i/a_i) = (\xi_i/a_i)^j, j = 0,1,2 \tag{3.12}$$

In the present work, polynomial basis with components of order 0, 1 or 2 were adopted.

It is clear that any approximation function will be represented as a linear combination using elements that belongs to this set.

3.6 The Global Sub-problem $P_G^{(k)}$

The Global Sub-problem $P_G^{(k)}$ is geometrically similar to $P_G^{(0)}$. Therefore, geometry is described without cracks as well and the same boundary conditions of the $P_G^{(0)}$ are considered. However, only the displacement field and traction vectors identified in $\Gamma^{(i)}$ of the correspondent local sub-problem $P_L^{(k)}$ are imposed as "jumps" on $P_G^{(k)}$. It is important to note that the number of global sub-problems coincides with the number of local sub-problems.

It is important to state in this point that $u_G^{(i)}$ represents the solution of the sub-problem $P_G^{(k)}$ and consists of the displacement field in the domain *V* of the plate.

The governing equations of this type of sub-problem are:

$$\Delta u_G^{(i)} = 0 \text{ on } V \tag{3.13}$$

$$\partial u_G^{(i)}/\partial n = 0 \quad \text{on } S_t \tag{3.14}$$

The main imposed restrictions to this sub-problem are:

1. Dirichlet boundary conditions, which are the same ones as the sub-problem $P_G^{(0)}$:

   $$u_G^{(i)} = \overline{u_G^{(i)}} = \overline{u_G^{(0)}} \text{ on } S_u \text{ (See also Equation 3.5);} \tag{3.15}$$

2. Newman boundary conditions consisting of null traction vector in S_t and in the hole borders:

   $$\partial u_G^{(i)}/\partial n = \underline{\underline{T}}\,\underline{n} = \underline{0} \quad \text{on } S_t, \tag{3.16}$$

   $$\partial u_G^{(i)}/\partial n = \underline{\underline{T}}\,\underline{n} = \underline{0} \quad \text{on } S_i. \tag{3.17}$$

Finally, it is very important to highlight the "jumps" that must be prescribed:

3. "Jump" in the traction vector on the $\Gamma^{(i)}$:

$$\left[\frac{\partial u_G^{(i)}}{\partial n_{\Gamma^{(i)}}}\right] = \partial u_L^{(i)}/\partial n = t_L^{(i)} \quad \text{on } \Gamma^{(i)} \tag{3.18a}$$

4. "Jump" in the displacement field on the $\Gamma^{(i)}$:

$$\left[u_G^{(i)}\right] = u_L^{(i)} \quad \text{on } \Gamma^{(i)} \tag{3.18b}$$

where $u_L^{(i)}$ and $t_L^{(i)}$ are obtained from the solutions of the local problems $P_L^{(k)}$. The jumps in the $n_{\Gamma^{(i)}}$-directions defined in the Equations (3.18-a) and (3.18-b) are denoted by [•]. See Figure 3.4.

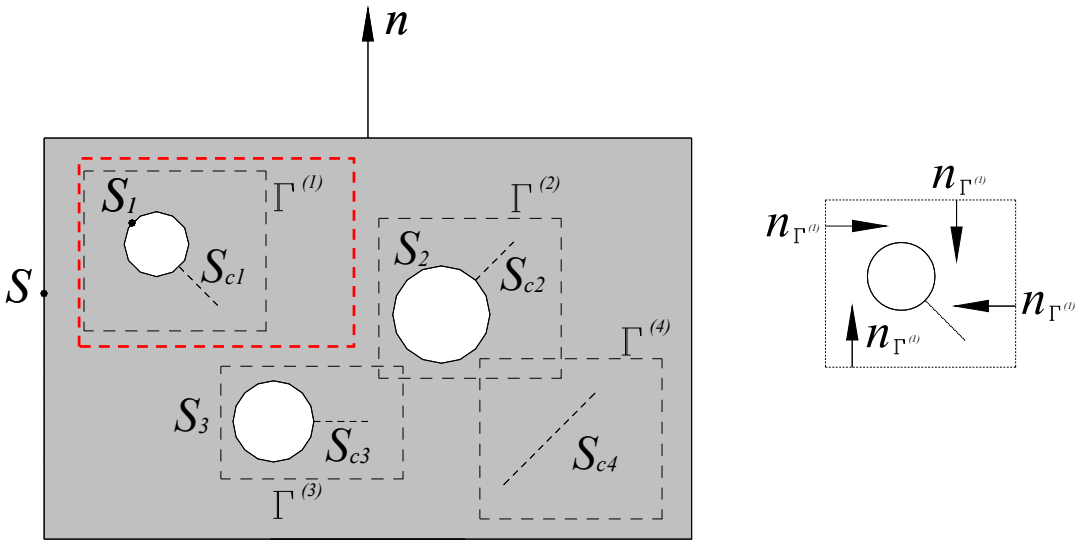

a. Geometry and $\Gamma^{(i)}$ b. $n_{\Gamma^{(i)}}$-directions

Figure 3.4 Global Sub-Problem $P_G^{(k)}$

It is important to state that the most important aim of this type of sub-problem is to evaluate corrections in the solution of the global problem $P_G^{(0)}$, since the local problems $P_L^{(k)}$ are quite different of the original problem and, therefore, the Bueckener's principle cannot be directly applied. It is clear that these corrections must be found as solutions of a global domain without cracks. Considering the referred aim of this sub-problem, one concludes that the Splitting Method can be used to solve problems with just one crack in the domain. Furthermore, it is possible to note that the application of the Bueckner's principle is a particular case of the Splitting Method, when the geometry of the local sub-problems is identical to the original problem.

Finally, another important result of this sub-problem that must be cited is the traction vector on the S_{ci} lines, evaluated as in the global sub-problem $P_G^{(0)}$.

3.7 Assemblage of the problems. Coefficients provided by $P_G^{(0)}$ and $P_G^{(k)}$

In the given problem P_G, the traction vector must be null in the crack surfaces. This can be expressed through a weighted residual form, using each component of the approximation basis according to the following relations:

$$\int_0^{a_i} \underline{t}.\underline{Q}_{j2}(\xi_i/a_i)d\xi = 0 \qquad \text{with } j_2 = 1,\ldots,J \qquad (3.19\text{-a})$$

$$\text{and} \qquad \underline{t} = \underline{t}_G^{(0)} + \underline{t}_L^{(k)} + \underline{t}_G^{(k)} \qquad (3.19\text{-b})$$

where $\underline{t}_G^{(0)}$, $\underline{t}_L^{(k)}$ and $\underline{t}_G^{(k)}$ are the traction vectors in the S_{ci} provided by $P_G^{(0)}$, $P_L^{(k)}$ and $P_G^{(k)}$, respectively. $\underline{Q}_{j2}(\xi_i/a_i)$ is the weight function, taken as one of the components of the polynomial basis functions (see Equations 3.7 and 3.8).

The traction vector contributions can be represented using $\underline{Q}_j\left(\frac{\xi_i}{a_i}\right)$ as follows:

1. Global sub-problem $P_G^{(0)}$:

   a. $\underline{t}_G^{(0)} \approx \sum_{j=1}^{J} b_{i,j}.\underline{Q}_j(\xi_i/a_i)$, with $0 \le \xi_i \le a_i$ (3.20)

2. Local sub-problem $P_L^{(k)}$:

   b. $\underline{t}_L^{(k)} = -\sum_{j=1}^{J} \alpha_{j+(i-1)J}.\underline{Q}_j(\xi_i/a_i)$, with $0 \le \xi_i \le a_i$ (3.21)

3. Global sub-problem $P_G^{(k)}$:

   c. $\underline{t}_G^{(k)} = \sum_{j=1}^{J}\sum_{k=1}^{M} \alpha_k.c_{i,j}^{(k)}.\underline{Q}_j(\xi_i/a_i)$, with $0 \le \xi_i \le a_i$ (3.22)

where M = number of local (or global) problems and J = number of terms of the approximation basis.

The "α" coefficients must be organized as a vector composing the unknown vector solution of the linear system (Figure 3.7 below). The "*b*" and "c" coefficients can be

previously identified using the results of the global sub-problems $P_G^{(0)}$ and $P_G^{(k)}$, respectively, by means of the *LSM*.

Remark: so far, in order to make it easier to understand the text, only the Mode I has been considered.

By substituting equations (3.20), (3.21) and (3.22) in equations (3.19a) and (3.19b), the result is:

$$\int_0^{a_i}\left[\sum_{j=1}^{J} b_{i,j}.\underline{Q}_j(\xi_i/a_i) - \sum_{j=1}^{J}\alpha_{j+(i-1)J}.\underline{Q}_j(\xi_i/a_i) + \sum_{j=1}^{J}\sum_{k=1}^{M}\alpha_k.c_{i,j}^{(k)}.\underline{Q}_j(\xi_i/a_i)\right].\underline{Q}_{j2}(\xi_i/a_i)d\xi = 0$$

$$\Rightarrow \int_0^{a_i}\sum_{j=1}^{J}\left[b_{i,j} - \alpha_{j+(i-1)J} + \sum_{k=1}^{M}\alpha_k.c_{i,j}^{(k)}\right].\underline{Q}_j(\xi_i/a_i).\underline{Q}_{j2}(\xi_i/a_i)d\xi = 0 \qquad (3.23)$$

Finally, it is possible to assemble a system as a function of the *"α"* coefficients:

$$[GI].\{\alpha\} = \{r\} \qquad (3.24)$$

where $[GI]$ is the General Influence matrix.

3.8 Additional features of $P_L^{(k)}$ sub-problems.

The main purpose of this section is to detail some hereby proposed additional features of the local sub-problems $P_L^{(k)}$ not considered in the publication of Andersson & Babuska (2005). Such features are modifications to taking in account internal cracks and opening modes I and II occurring simultaneously.

Firstly, it is important to focus on how to apply internal pressure to the internal crack surfaces. Depending on its geometry, each internal crack can be divided into several line segments, which is even more convenient in particular if the crack is not straight, therefore presenting a more complex geometry. For instance, in Figure 3.5, the crack is optionally composed by two segments of length a_i. As already cited, these segments may be not aligned in the case of a more complex geometry. In addition, the user can subdivide a straight segment into other segments, if necessary.

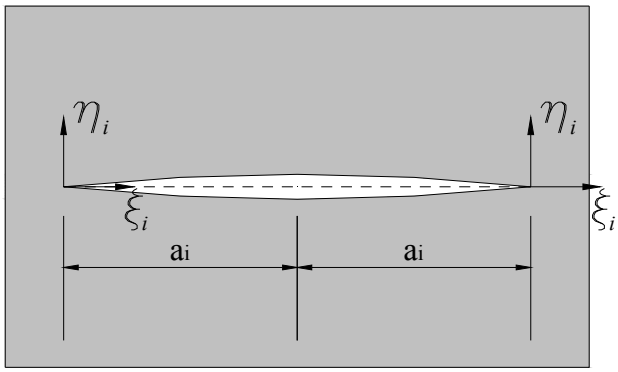

Figure 3.5 Segments of the crack *i*

Once the subdivision of the crack line is made, when defining the local sub-problems, each segment is treated as a crack line, and hereafter will be indicated as S_{ci}.

As shown in Figure 3.6, an internal load must be applied to each S_{ci}. Note that in addition to conventional Mode I, cases of loading associated to the mixed mode crack opening can also be considered.

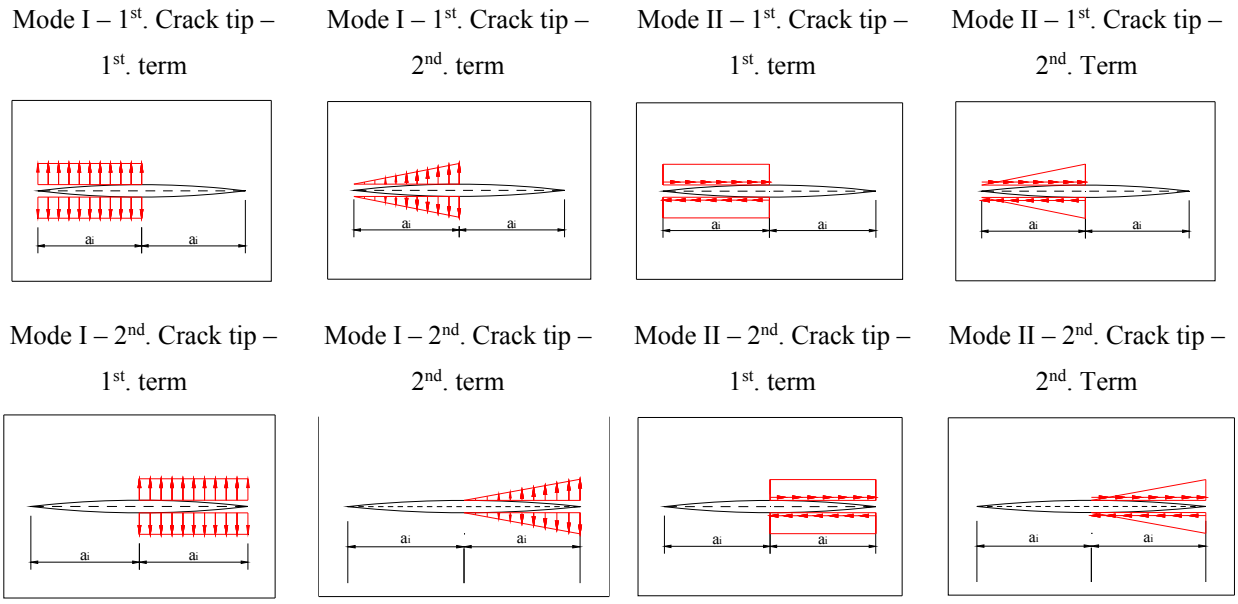

Figure 3.6 Applied loads on the S_{ci}

It is worth mentioning that there must be set a *"α"* coefficient to each local problem and the correspondent global problem (see Equation 3.23).

To assemble the vector $\{\alpha\}$ a hierarchy was conceived, as indicated in Figure 3.7.

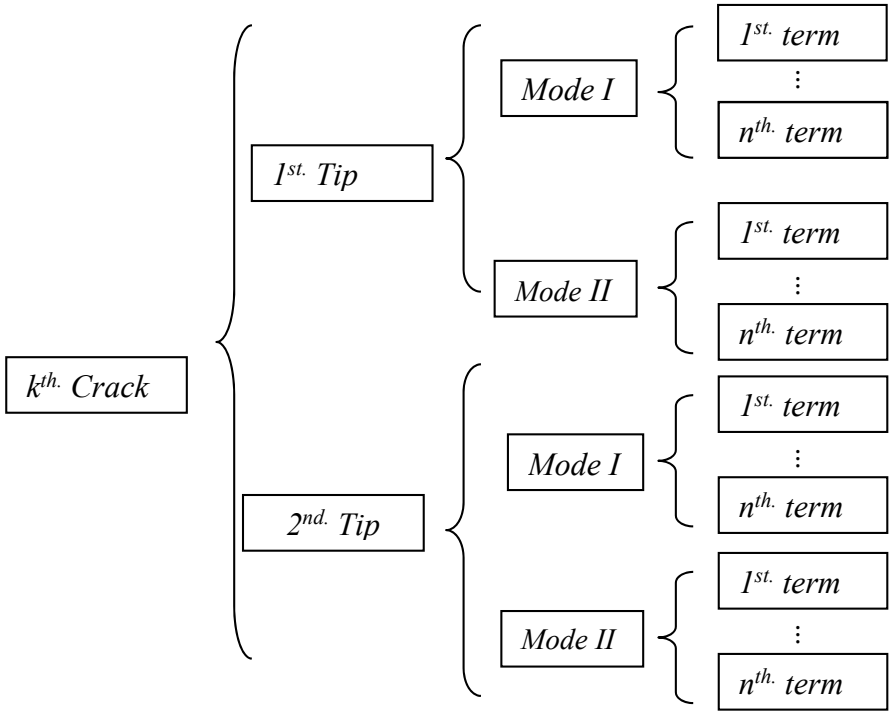

Figure 3.7 Hierarchy of the vector {α}

3.9 Assemblage of the Γ contour

The Γ contour is a rectangular polygon completely enclosing the crack. For each local sub-problem $P_L^{(k)}$, the displacements and stress fields must be obtained at each node of this contour. However, an excessive number should be avoided in order to reduce the costs in terms of mesh refinement in the correspondent sub-problem $P_G^{(k)}$.

According to condition (3.18-b), the displacement field is then imposed in the correspondent sub-problem $P_G^{(k)}$ as a local "jump" in displacements. Analogously, as indicated by Equation (3.18-a), the stress field is imposed as a "jump" in forces in the same sub-problem $P_G^{(k)}$. It is clear that correspondent nodes must be positioned in sub-problems $P_G^{(k)}$ to allow for the application of both results.

3.10 On the inner product character of the weak form of traction vector nullity condition.

As already mentioned before, the traction vector must be null in the crack surfaces:

$$\underline{t} = \underline{t}_G^{(0)} + \underline{t}_L^{(k)} + \underline{t}_G^{(k)} = \underline{0} \qquad \text{(3.19 – Repeated)}$$

In order to give an interpretation to this nullity condition in a weak form, the inner product is claimed here.

Let $\underline{t}$ be the traction vector on the first segment S_{ci} of a crack. We define, for 2D-problems:

$$\underline{t} \in P_n(\xi) X\, P_n(\xi) = V \Longrightarrow \underline{t} = \big(Q_y(\xi), Q_x(\xi)\big) \qquad (3.25)$$
$$Q_x(\xi), Q_y(\xi) \in P_n(\xi)$$

where:

1. $\underline{t}$ is the ordered pair whose components are vectors in $P_n(\xi)$.
2. The first component ($Q_y(\xi)$) of $\underline{t}$ is referred to Mode I, while the second component ($Q_x(\xi)$) is referred to Mode II (see Figure 3.7).
3. $P_n(\xi)$ is the linear space that consists of complete polynomials of *n* degrees $p(\xi) = b_0 + b_1 \cdot \xi + \cdots + b_n \cdot \xi^n\ ,\ 0 \le \xi \le a_i$.

On the other hand, let *q* and *p* be vectors in $P_n(\xi)$. The inner product is defined as:

$$\langle q, p\rangle = \int_0^{a_i} q(\tfrac{\xi_i}{a_i}) p(\tfrac{\xi_i}{a_i}) d\xi \qquad (3.26)$$

Using this definition of inner product, it is possible to define an inner product in *V*. Let then *q* and *p* be vectors in *V*. The inner product of this space can be defined as:

$$\langle q, p\rangle = \int_0^{a_i} q_x(\tfrac{\xi_i}{a_i}) \cdot p_x(\tfrac{\xi_i}{a_i}) d\xi + \int_0^{a_i} q_y(\tfrac{\xi_i}{a_i}) \cdot p_y(\tfrac{\xi_i}{a_i}) d\xi \qquad (3.27)$$

where q_x, q_y, p_x and p_y are vectors in $P_n(\xi)$.

A basis for *V* can be defined as:

$$\beta = \{(1,0), (\xi, 0), (\xi^2, 0), \dots, (\xi^n, 0), (0,1), (0, \xi), (0, \xi^2), \dots, (0, \xi^n)\}.$$

In fact, the vector components are linearly independent and therefore, any vector in V can be represented as a linear combination of the basis vectors.

Finally, if $\underline{t}$ is the null vector, then it is orthogonal to each vector in β. Thus:

$$\left.\begin{array}{l} \int_0^{a_i} Q_{y(\xi)} \cdot 1 d\xi = 0 \\ \int_0^{a_i} Q_{y(\xi)} \cdot \xi d\xi = 0 \\ \vdots \\ \int_0^{a_i} Q_{y(\xi)} \cdot \xi^n d\xi = 0 \\ \int_0^{a_i} Q_{x(\xi)} \cdot 1 d\xi = 0 \\ \int_0^{a_i} Q_{x(\xi)} \cdot \xi d\xi = 0 \\ \vdots \\ \int_0^{a_i} Q_{x(\xi)} \cdot \xi^n d\xi = 0 \end{array}\right\} \Rightarrow System\ with\ 2(n+1)\ equations \tag{3.28}$$

The above condition must be imposed to the segments of each crack.

The system of equations above provides the "α" coefficients of the Splitting Method.

3.11 Assemblage of the linear system on the "α" coefficients considering multiple cracks.

In this section the assemblage of the linear system for many internal cracks is described.

The variables and constants used in this section are:

1. Number of cracks: I;
2. Number of components in the approximation basis: J;
3. Number of segments of each crack: 2;
4. Number of local sub-problems (and global sub-problems): $2 \cdot 2 \cdot I \cdot J = 4 \cdot I \cdot J$

Remark: the number of local sub-problems must be multiplied by 2 to consider the two opening modes. Although two segments are considered above, the extension for more than two segments for each crack is straightforward.

By using Equation (3.12-a), the following is obtained:

1. First tip, mode I:

$$\int_0^{a_i} \sum_{j=1}^{J} \left[b^I_{2i-1,j} - \alpha_{4J(i-1)+j} + \sum_{k=1}^{4IJ} \alpha_k . c^{I\,(k)}_{2i-1,j} \right] . \underline{Q}_{y,j}\left(\xi_{i,1st\ tip}/a_i\right) . \underline{Q}_{y,j2}\left(\xi_{i,1st\ tip}/a_i\right) d\xi = 0 \tag{3.29}$$

2. First tip, mode II:

$$\int_0^{a_i} \sum_{j=1}^{J} \left[b^{II}_{2i-1,j} - \alpha_{4J(i-1)+j+J} + \sum_{k=1}^{4IJ} \alpha_k . c^{II\,(k)}_{2i-1,j} \right] . \underline{Q}_{x,j}\left(\xi_{i,1st\ tip}/a_i\right) . \underline{Q}_{x,j2}\left(\xi_{i,1st\ tip}/a_i\right) d\xi = 0 \tag{3.30}$$

3. Second tip, mode I:

$$\int_0^{a_i} \sum_{j=1}^{J} \left[b^I_{2i,j} - \alpha_{4J(i-1)+j+2J} + \sum_{k=1}^{4IJ} \alpha_k . c^{I\,(k)}_{2i,j} \right] . \underline{Q}_{y,j}\left(\xi_{i,2nd\ tip}/a_i\right) . \underline{Q}_{y,j2}\left(\xi_{i,2nd\ tip}/a_i\right) d\xi = 0 \tag{3.31}$$

4. Second tip, mode II:

$$\int_0^{a_i} \sum_{j=1}^{J} \left[b^{II}_{2i,j} - \alpha_{4J(i-1)+j+3J} + \sum_{k=1}^{4IJ} \alpha_k . c^{II\,(k)}_{2i,j} \right] . \underline{Q}_{x,j}\left(\xi_{i,2nd\ tip}/a_i\right) . \underline{Q}_{x,j2}\left(\xi_{i,2nd\ tip}/a_i\right) d\xi = 0 \tag{3.32}$$

with $j_2 = 1 \ldots J$ in all equations.

For example, if we consider the first segment of the first crack, Equations (3.29)-(3.32) become:

$$\begin{aligned}
&\int_0^{a_1} \sum_{j=1}^{J} \left[b^I_{1,j} - \alpha_j + \sum_{k=1}^{4IJ} \alpha_k . c^{I\,(k)}_{1,j} \right] . \underline{Q}_{y,j}\left(\xi_{1,1st\ tip}/a_1\right) . \underline{Q}_{y,1}\left(\xi_{1,1st\ tip}/a_1\right) d\xi = 0 \\
&\int_0^{a_1} \sum_{j=1}^{J} \left[b^I_{1,j} - \alpha_j + \sum_{k=1}^{4IJ} \alpha_k . c^{I\,(k)}_{1,j} \right] . \underline{Q}_{y,j}\left(\xi_{1,1st\ tip}/a_1\right) . \underline{Q}_{y,2}\left(\xi_{1,1st\ tip}/a_1\right) d\xi = 0 \\
&\qquad\qquad \vdots \\
&\int_0^{a_1} \sum_{j=1}^{J} \left[b^I_{1,j} - \alpha_j + \sum_{k=1}^{4IJ} \alpha_k . c^{I\,(k)}_{1,j} \right] . \underline{Q}_{y,j}\left(\xi_{1,1st\ tip}/a_1\right) . \underline{Q}_{y,J}\left(\xi_{1,1st\ tip}/a_1\right) d\xi = 0
\end{aligned} \tag{3.33a}$$

$$\int_0^{a_1} \sum_{j=1}^{J} \left[b_{1,j}^{II} - \alpha_{j+J} + \sum_{k=1}^{4IJ} \alpha_k . c_{1,j}^{II\,(k)} \right] . \underline{Q}_{x,j}\left(\xi_{1,1st\ tip}/a_1\right) . \underline{Q}_{x,1}\left(\xi_{1,1st\ tip}/a_1\right) d\xi = 0$$

$$\int_0^{a_1} \sum_{j=1}^{J} \left[b_{1,j}^{II} - \alpha_{j+J} + \sum_{k=1}^{4IJ} \alpha_k . c_{1,j}^{II\,(k)} \right] . \underline{Q}_{x,j}\left(\xi_{1,1st\ tip}/a_1\right) . \underline{Q}_{x,2}\left(\xi_{1,1st\ tip}/a_1\right) d\xi = 0$$

$$\vdots$$

$$\int_0^{a_1} \sum_{j=1}^{J} \left[b_{1,j}^{II} - \alpha_{j+J} + \sum_{k=1}^{4IJ} \alpha_k . c_{1,j}^{II\,(k)} \right] . \underline{Q}_{x,j}\left(\xi_{1,1st\ tip}/a_1\right) . \underline{Q}_{x,J}\left(\xi_{1,1st\ tip}/a_1\right) d\xi = 0$$

(3.33b)

The following system can be found by considering the second tip. The procedure must be repeated for all cracks:

$$\begin{gathered} \left[GI_{1st.tip,\ \ Mode\ I}\right] \cdot \left\{\alpha_{1st.tip,\ \ Mode\ I}\right\} = \left\{r_{1st.tip,\ \ Mode\ I}\right\} \\ +\left[GI_{1st.tip,\ \ Mode\ II}\right] \cdot \left\{\alpha_{1st.tip,\ \ Mode\ II}\right\} = \left\{r_{1st.tip,\ \ Mode\ II}\right\} \\ +\left[GI_{2nd.tip,\ \ Mode\ I}\right] \cdot \left\{\alpha_{2nd.tip,\ \ Mode\ I}\right\} = \left\{r_{2nd.tip,\ \ Mode\ I}\right\} \\ +\left[GI_{2nd.tip,\ \ Mode\ II}\right] \cdot \left\{\alpha_{2nd.tip,\ \ Mode\ II}\right\} = \left\{r_{2nd.tip,\ \ Mode\ II}\right\} \\ \hline [GI] \cdot \{\alpha\} = \{r\} \end{gathered}$$

(3.34)

The *General Influence* matrix [GI] can be divided into two sub-matrices:

$$[GI] = [GI]_L + [GI]_G \tag{3.35}$$

Where:

1. $[GI]_L$ contains the terms related to the local sub-problems;
2. $[GI]_G$ contains the terms related to the global sub-problems.

The $[GI]_L$ matrix, considering all cracks, is presented in the sequel:

$$[GI]_L = \begin{bmatrix} \left[Q_{I,1t}^{(1)}\right] & [0] & [0] & [0] & [0] & [0] & \cdots & [0] \\ [0] & \left[Q_{II,1t}^{(1)}\right] & [0] & [0] & [0] & [0] & \cdots & [0] \\ [0] & [0] & \left[Q_{I,2t}^{(1)}\right] & [0] & [0] & [0] & \cdots & [0] \\ [0] & [0] & [0] & \left[Q_{II,2t}^{(1)}\right] & [0] & [0] & \cdots & [0] \\ [0] & [0] & [0] & [0] & \ddots & [0] & \cdots & [0] \\ [0] & [0] & [0] & [0] & [0] & \left[Q_{II,1t}^{(I)}\right] & \cdots & [0] \\ \vdots & \vdots & \vdots & \vdots & \vdots & \vdots & \left[Q_{I,2t}^{(I)}\right] & \vdots \\ [0] & [0] & [0] & [0] & [0] & [0] & \cdots & \left[Q_{II,2t}^{(I)}\right] \end{bmatrix}_{4IJx4IJ} \tag{3.36}$$

where:

1. $[0]$ is a null matrix of order $J\,x\,J$;
2. $\left[Q_{I,1t}^{(i)}\right]$ is the matrix of order $J\,x\,J$, related to Mode I, crack i and first crack tip.

The $\left[Q_{I,1t}^{(i)}\right]$ and $\left[Q_{II,1t}^{(i)}\right]$ component matrices are described in detail in the sequel:

$$\left[Q_{I,1t}^{(i)}\right] = \begin{bmatrix} \int_0^{a_i} Q_{y,1}Q_{y,1}\partial\xi & \int_0^{a_i} Q_{y,2}Q_{y,1}\partial\xi & \cdots & \int_0^{a_i} Q_{y,J}Q_{y,1}\partial\xi \\ \int_0^{a_i} Q_{y,1}Q_{y,2}\partial\xi & \int_0^{a_i} Q_{y,2}Q_{y,2}\partial\xi & \cdots & \int_0^{a_i} Q_{y,J}Q_{y,2}\partial\xi \\ \vdots & \vdots & \ddots & \vdots \\ \int_0^{a_i} Q_{y,1}Q_{y,J}\partial\xi & \int_0^{a_i} Q_{y,2}Q_{y,J}\partial\xi & \cdots & \int_0^{a_i} Q_{y,J}Q_{y,J}\partial\xi \end{bmatrix} \tag{3.37}$$

$$\left[Q_{II,1t}^{(i)}\right] = \begin{bmatrix} \int_0^{a_i} Q_{x,1}Q_{x,1}\partial\xi & \int_0^{a_i} Q_{x,2}Q_{x,1}\partial\xi & \cdots & \int_0^{a_i} Q_{x,J}Q_{x,1}\partial\xi \\ \int_0^{a_i} Q_{x,1}Q_{x,2}\partial\xi & \int_0^{a_i} Q_{x,2}Q_{x,2}\partial\xi & \cdots & \int_0^{a_i} Q_{x,J}Q_{x,2}\partial\xi \\ \vdots & \vdots & \ddots & \vdots \\ \int_0^{a_i} Q_{x,1}Q_{x,J}\partial\xi & \int_0^{a_i} Q_{x,2}Q_{x,J}\partial\xi & \cdots & \int_0^{a_i} Q_{x,J}Q_{x,J}\partial\xi \end{bmatrix} \tag{3.38}$$

The matrix $[GI]_G$ provides the effects of each crack over the other cracks. For example, $\left[cQ_{I,1t}^{(I,1)}\right]$ provides the effects of the load applied on the first segment of the first crack, normal to crack surface, referred to Mode I (superior index), over the traction in the same segment, referred Mode I. $\left[cQ_{I,1t}^{(II,1)}\right]$ provides the effects of the load applied on the first segment of the first crack, tangential to crack surface, referred to Mode II (superior index), over the traction in the same segment. $\left[cQ_{I,1t}^{(I,2)}\right]$ provides the effects of the load applied on the second segment of the first crack, normal to crack surface, referred to Mode I (superior index), over the traction in the first segment of the first crack tip, referred to Mode I, and so forth.

To make it easier to understand the paragraph explained above:

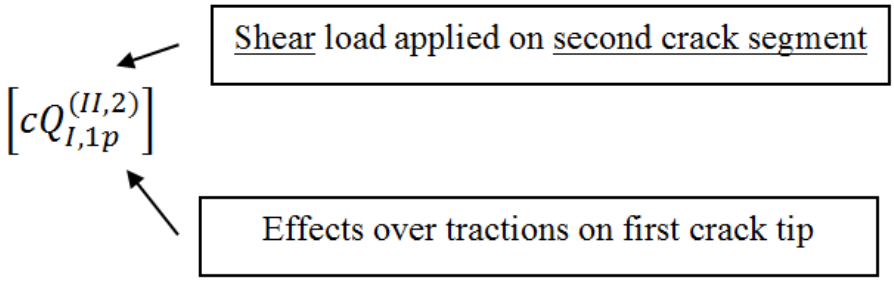

$\left[cQ_{I,1t}^{(I,1)}\right]$ is described in detail below (Equation 3.39):

$$[cQ_{I,1t}^{(I,1)}] = \begin{bmatrix} \int_0^{a_1} (c_{1,1}^{I(1)} \cdot Q_{y,1} + \cdots + c_{1,J}^{I(1)} Q_{y,J}) Q_{y,1} \partial\xi & \int_0^{a_1} (c_{1,1}^{I(2)} \cdot Q_{y,1} + \cdots + c_{1,J}^{I(2)} Q_{y,J}) Q_{y,1} \partial\xi & \cdots & \int_0^{a_1} (c_{1,1}^{I(J)} \cdot Q_{y,1} + \cdots + c_{1,J}^{I(J)} Q_{y,J}) Q_{y,1} \partial\xi \\ \int_0^{a_1} (c_{1,1}^{I(1)} \cdot Q_{y,1} + \cdots + c_{1,J}^{I(1)} Q_{y,J}) Q_{y,2} \partial\xi & \int_0^{a_1} (c_{1,1}^{I(2)} \cdot Q_{y,1} + \cdots + c_{1,J}^{I(2)} Q_{y,J}) Q_{y,2} \partial\xi & \cdots & \int_0^{a_1} (c_{1,1}^{I(J)} \cdot Q_{y,1} + \cdots + c_{1,J}^{I(J)} Q_{y,J}) Q_{y,2} \partial\xi \\ \vdots & \vdots & \ddots & \vdots \\ \int_0^{a_1} (c_{1,1}^{I(1)} \cdot Q_{y,1} + \cdots + c_{1,J}^{I(1)} Q_{y,J}) Q_{y,J} \partial\xi & \int_0^{a_1} (c_{1,1}^{I(2)} \cdot Q_{y,1} + \cdots + c_{1,J}^{I(2)} Q_{y,J}) Q_{y,J} \partial\xi & \cdots & \int_0^{a_1} (c_{1,1}^{I(J)} \cdot Q_{y,1} + \cdots + c_{1,J}^{I(J)} Q_{y,J}) Q_{y,J} \partial\xi \end{bmatrix}$$

(3.39)

The others sub-matrices are shown in Appendix C. $[GI]_G$ is detailed in the sequel (Equation 3.40).

$$[GI]_G = \begin{bmatrix} [cQ_{I,1t}^{(I,1)}] & [cQ_{I,1t}^{(II,1)}] & [cQ_{I,1t}^{(I,2)}] & [cQ_{I,1t}^{(II,2)}] & [cQ_{I,1t}^{(I,3)}] & [cQ_{I,1t}^{(II,3)}] & \cdots & [cQ_{I,1t}^{(II,2I)}] \\ [cQ_{II,1t}^{(I,1)}] & [cQ_{II,1t}^{(II,1)}] & [cQ_{II,1t}^{(I,2)}] & [cQ_{II,1t}^{(II,2)}] & [cQ_{II,1t}^{(I,3)}] & [cQ_{II,1t}^{(II,3)}] & \cdots & [cQ_{II,1t}^{(II,2I)}] \\ [cQ_{I,2t}^{(I,1)}] & [cQ_{I,2t}^{(II,1)}] & [cQ_{I,2t}^{(I,2)}] & [cQ_{I,2t}^{(II,2)}] & [cQ_{I,2t}^{(I,3)}] & [cQ_{I,2t}^{(II,3)}] & \cdots & [cQ_{I,2t}^{(II,2I)}] \\ [cQ_{II,2t}^{(I,1)}] & [cQ_{II,2t}^{(II,1)}] & [cQ_{II,2t}^{(I,2)}] & [cQ_{II,2t}^{(II,2)}] & [cQ_{II,2t}^{(I,3)}] & [cQ_{II,2t}^{(II,3)}] & \cdots & [cQ_{II,2t}^{(II,2I)}] \\ [cQ_{I,3t}^{(I,1)}] & [cQ_{I,3t}^{(II,1)}] & [cQ_{I,3t}^{(I,2)}] & [cQ_{I,3t}^{(II,2)}] & [cQ_{I,3t}^{(I,3)}] & [cQ_{I,3t}^{(II,3)}] & \cdots & [cQ_{I,3t}^{(II,2I)}] \\ [cQ_{II,3t}^{(I,1)}] & [cQ_{II,3t}^{(II,1)}] & [cQ_{II,3t}^{(I,2)}] & [cQ_{II,3t}^{(II,2)}] & [cQ_{II,3t}^{(I,3)}] & [cQ_{II,3t}^{(II,3)}] & \cdots & [cQ_{II,3t}^{(II,2I)}] \\ \vdots & \vdots & \vdots & \vdots & \vdots & \vdots & \ddots & \vdots \\ [cQ_{II,2It}^{(I,1)}] & [cQ_{II,2It}^{(II,1)}] & [cQ_{II,2It}^{(I,2)}] & [cQ_{II,2It}^{(II,1)}] & [cQ_{II,2It}^{(I,3)}] & [cQ_{II,2It}^{(II,3)}] & \cdots & [cQ_{II,2It}^{(II,2I)}] \end{bmatrix}$$

(3.40)

The assemblage of the $\{r\}$ vector is more direct as indicated in Equation (3.41). Therefore, more details about it will be omitted.

$$\{r\} = \begin{Bmatrix} \int_0^{a_1} \left(b_{1,1}^{I} \cdot Q_{y,1} + \cdots + b_{1,J}^{I} Q_{y,J}\right) Q_{y,1} \partial\xi \\ \int_0^{a_1} \left(b_{1,1}^{I} \cdot Q_{y,1} + \cdots + b_{1,J}^{I} Q_{y,J}\right) Q_{y,2} \partial\xi \\ \vdots \\ \int_0^{a_1} \left(b_{1,1}^{II} \cdot Q_{x,1} + \cdots + b_{1,J}^{II} Q_{x,J}\right) Q_{x,J} \partial\xi \\ \int_0^{a_1} \left(b_{1,1}^{II} \cdot Q_{x,1} + \cdots + b_{1,J}^{II} Q_{x,J}\right) Q_{x,2} \partial\xi \\ \vdots \\ \int_0^{a_1} \left(b_{1,1}^{II} \cdot Q_{x,1} + \cdots + b_{1,J}^{II} Q_{x,J}\right) Q_{x,J} \partial\xi \\ \int_0^{a_1} \left(b_{2,1}^{I} \cdot Q_{y,1} + \cdots + b_{2,J}^{I} Q_{y,J}\right) Q_{y,1} \partial\xi \\ \int_0^{a_1} \left(b_{2,1}^{I} \cdot Q_{y,1} + \cdots + b_{2,J}^{I} Q_{y,J}\right) Q_{y,2} \partial\xi \\ \vdots \\ \int_0^{a_1} \left(b_{2,1}^{I} \cdot Q_{y,1} + \cdots + b_{2,J}^{I} Q_{y,J}\right) Q_{y,J} \partial\xi \\ \vdots \\ \int_0^{a_I} \left(b_{2I,1}^{II} \cdot Q_{x,1} + \cdots + b_{2I,J}^{II} Q_{x,J}\right) Q_{x,1} \partial\xi \\ \int_0^{a_I} \left(b_{2I,1}^{II} \cdot Q_{x,1} + \cdots + b_{2I,J}^{II} Q_{x,J}\right) Q_{x,2} \partial\xi \\ \vdots \\ \int_0^{a_I} \left(b_{2I,1}^{II} \cdot Q_{x,1} + \cdots + b_{2I,J}^{II} Q_{x,J}\right) Q_{x,J} \partial\xi \end{Bmatrix} \tag{3.41}$$

Chapter 4: Computational aspects

In order to construct a computational framework to test the combination of the Splitting Method with the GFEM/XFEM, a complete code needed to be created including the mesh generation to the solution of the linear system of equations providing the "α" coefficients of the Splitting Method. The main idealized and implemented procedures are described in this chapter.

There are some computational procedures specifically devoted to each specific sub-problem: $P_G^{(0)}$, $P_L^{(k)}$ or $P_G^{(k)}$. However, there are some other procedures as the mesh generation that are common to more than one type of sub-problem. Such procedures will be explained in the section dedicated to the more convenient sub-problem, according to the author's criterion.

4.1 Procedures associated to $P_G^{(0)}$

This is the simplest among the problems concerning the Splitting Method. However, two idealized procedures are related to it.

The first one aims to generate an unstructured mesh composed by triangular elements. For this mesh generation, the available package for Python® named MeshPy® was used. This package allows an efficient triangular or tetrahedral mesh generation. However, only a triangular mesh generation was used in this work. To better explore the MeshPy®, some restrictions must be provided to the program before starting the analysis and the mesh generation. The most important ones are:

1. Maximum area of each triangle in the mesh. It is not necessary that the area of all triangles in the mesh be the same. A function was defined in this work to allow the calculus of the area of each triangle, depending on, for example, the distance of it to a certain region, edge or hole border. Particularly, a small area was prescribed to the triangles close to the hole border;

2. Minimum internal angle of each triangle: a convenient minimum angle should be set to generate each triangle as indicated in the Figure 4.1. Small minimum internal angles can result in a distorted mesh. On the other hand, higher values for the minimum internal angle can lead to blocking of the mesh generation, owing to the

restrictions of the MeshPy®. Therefore, a range of minimal values for α, β, γ, can be defined, as shown in Figure 4.1:

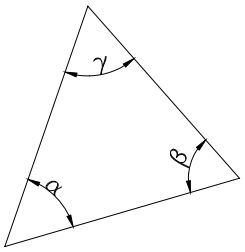

$$25^0 \leq \alpha_{min}, \beta_{min}, \gamma_{min} \leq 35^0$$

Figure 4.1 Restriction to the internal angles of the triangles

3. Additional nodes: it may be necessary to indicate the regions where additional nodes must be concentrated, especially at the boundary of the plate or at the edges of the holes. It is important to mention that, sometimes, it is necessary to refine the mesh close to the crack lines S_{ci}, especially when the stress distribution is irregular.

In the developed program, optionally it is also possible to define the mesh manually when global problems $P_G^{(0)}$ are considered. This option is advisable when there are no holes in the problem and the geometry is relatively simple and, therefore, the adopted mesh is also simple.

It is very important to stress that the MeshPy® generates a mesh with Constant Stress Triangle (*CST*), therefore with only 3 nodes. However, in the developed program, the created *CST* can also be transformed in the Linear Stress Triangle (*LST*) by adding intermediate nodes at the sides of the triangle. In this paper, the *LST* is optimally indicated for global sub-problems $P_G^{(0)}$ and $P_G^{(k)}$. Considering the local sub-problems $P_L^{(k)}$, only *CST* must be used due to the use of enrichment strategies of the Generalized Finite Element Method, as explained in Chapter 5.

The second idealized procedure aims to approximate the traction vector taking local values as reference computed at some points placed along the crack line S_{ci}, as explained in Section 3.5. In fact, this procedure consists of a collection of simple functionalities. The most important among them is responsible for finding out to which element the point belongs. This functionality is described in Appendix B with more details.

In short, after determining the element in which the point is contained, the next step is to recover the stress tensor components (σ_x, σ_y, τ_{xy}) associated to the reference Cartesian

axis. The Figure 4.2 depicts a small region of the mesh where the crack is inserted, as well as points distributed on the crack line.

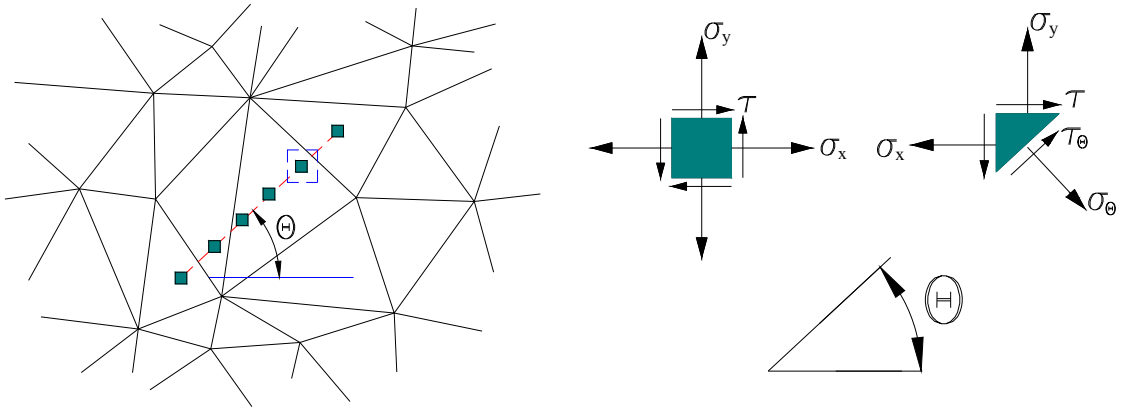

Figure 4.2 Evaluation of the stress tensor in a given point of the mesh

The squares on the crack line depicted in Figure 4.2 are points where the stress tensor will be evaluated. The stress components σ_θ and τ_θ, respectively normal and tangential to the crack line at the point, are easily evaluated using the well-known relation:

$$\begin{Bmatrix}\sigma_\theta \\ \tau_\theta\end{Bmatrix} = \begin{bmatrix}\sigma_x & \tau_{xy} \\ \tau_{xy} & \sigma_y\end{bmatrix}\begin{Bmatrix}n_x \\ n_y\end{Bmatrix} \tag{4.1}$$

It is clear that angle θ refers to the crack angle as shown in Figure 4.2.

For each point placed in the crack line S_{ci} this process is repeated computing the two stress components to each point. Finally, by using the Least Square Method, an approximation function for σ_θ and another for τ_θ is determined. Each approximation function is expressed as a linear combination of monomials of order m.

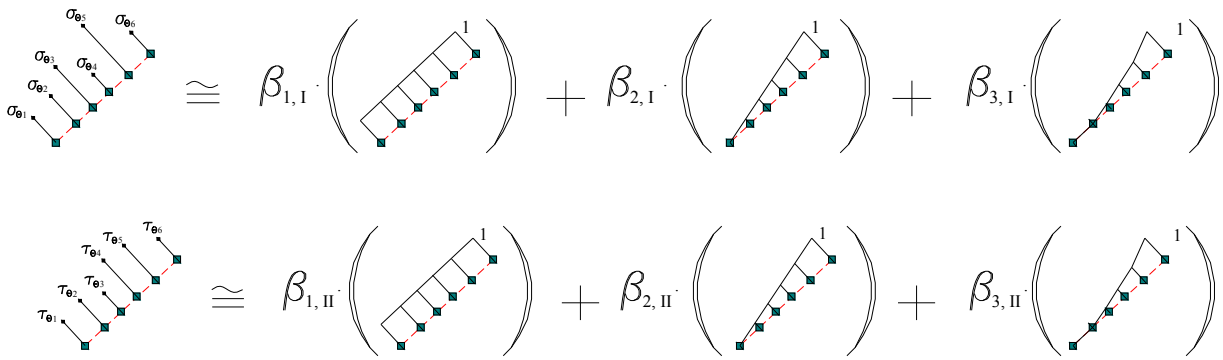

Figure 4.3 Approximation of the components σ_θ and τ_θ along the crack by means of a polynomial function

In Figure 4.3, the crack in Figure 4.2 and its values of components σ_θ and τ_θ in 6 points are reproduced. As also exemplified in the same figure, the approximation functions are constructed by using a polynomial basis of order 2, for example. The coefficients $\beta_{1,I}$, $\beta_{2,I}$, $\beta_{3,I}$, $\beta_{1,II}$, $\beta_{2,II}$ and $\beta_{3,II}$ are obtained by means of the Least Square Method.

This method is also used in global sub-problems $P_G^{(k)}$.

4.2 Procedures associated to local sub-problem $P_L^{(k)}$

Fracture mechanics concepts are involved in this sub-problem. Therefore, all the most important procedures hereby idealized are related to modeling the crack and calculating the *J Integral* according to the concepts described in Section 2.4. In particular, it is important to note that the *J Integral* includes the crack surfaces in its paths.

4.2.1 Mesh generation to local problems $P_L^{(k)}$

The mesh generation in the $P_L^{(k)}$ problems includes the creation of nodes at the external boundary, as well as at the Γ contour and along the crack faces. In addition to the creation of the nodes, the procedure includes routines for mesh refinement close to the crack tips and close to the Γ contour. Such refinements are necessary to better account for the concepts discussed in Sections 3.5 – 3.9.

The shapes of the internal Γ contour and external boundary of the problem can be chosen arbitrarily. However, in order to make the computational development simpler, the rectangular geometry was chosen, as shown in Figure 4.4. As discussed before, the Γ contour must enclose the crack totally and, once existent, the hole with the crack as well. Nevertheless, the respective lengths are arbitrary. In the developed procedure, the length of the contour can be defined a priori on the basis of the length of the crack.

It is important to stress that the crack position and its length are the same as proposed in the original problem, but the external boundary and Γ contour are defined by the code during the analysis.

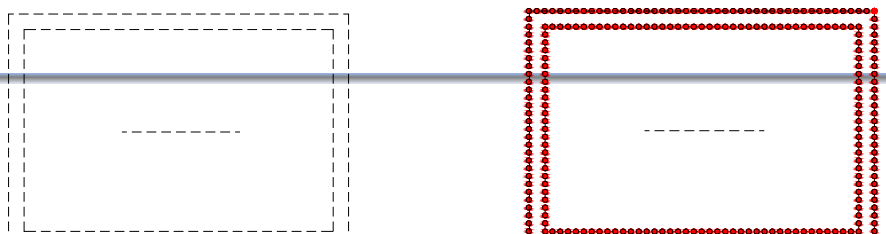

Figure 4.4 Automatic generation of the nodes at the boundary and Γ contour

Particularly at the Γ contour, there must be a sufficient number of nodes in order to ensure that the results are accurate for the vector stress and displacement fields (as already mentioned, these results will be prescribed in the $P_G^{(k)}$ problems as jumps in stress and displacements, respectively).

To distribute the nodes at the crack faces, the process may be more complex, considering that the geometry of the crack can be polygonal. Figure 4.5 illustrates the main steps for the creation of the nodes in a crack with 3 segments, for instance.

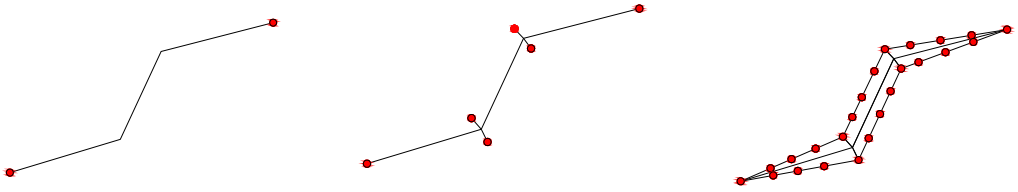

Step 1: Initial and final nodes | Step 2: Nodes at intersections of the incision lines | Step 3: Intermediary nodes

Figure 4.5 Automatic generation of the nodes at crack surfaces

In the first step, two nodes are inserted at the ends of the crack. In the second step, pairs of nodes are created at the ends of the line segments defined by the bisectors of the corner angles formed by two consecutives crack lines. Finally, in the third step the additional nodes are distributed along the crack faces described by joining the nodes defined in the previous steps.

To create the set of nodes at crack faces, each face should be subdivided according to the subdivision rate defined a priori by the user. The subdivision rate can be different for each crack and even for each pair of crack faces.

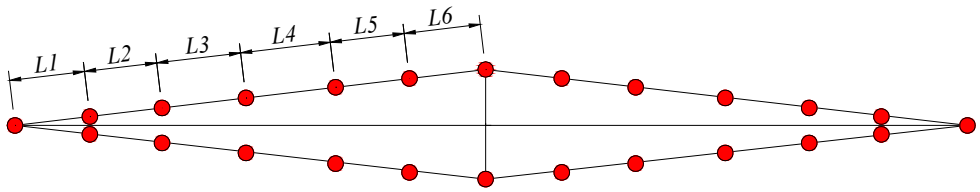

Figure 4.6 Subdivision of the first segment of a crack

In the subdivision process hereby adopted, the nodes distribution along a segment of a crack face follows a geometric rate. For instance, let's consider the first segment of the crack depicted in Figure 4.6. It is possible to note that it was divided into 6 parts. If we define the rate between 2 adjacent subdivisions equal to α, it follows that:

$$L_1 = \alpha \cdot L_2; \qquad L_2 = \alpha \cdot L_3; \ldots; L_5 = \alpha \cdot L_6 \tag{4.2}$$

On the other hand, the total length (L_T) of the first segment is given by:

$$L_T = L_1 + L_2 + L_3 + L_4 + L_5 + L_6 \tag{4.3}$$

Taking in account the equalities 4.2, it follows that:

$$L_T = \alpha^5 \cdot L_6 + \alpha^4 \cdot L_6 + \alpha^3 \cdot L_6 + \alpha^2 \cdot L_6 + \alpha \cdot L_6 + L_6 \tag{4.4a}$$

$$L_T = L_6 \cdot (\alpha^5 + \alpha^4 + \alpha^3 + \alpha^2 + \alpha + 1) \tag{4.4b}$$

Finally:

$$L_6 = \frac{L_T}{(\alpha^6 - 1)}(\alpha - 1) \tag{4.5}$$

The generalization of the equation 4.5 for n subdivisions is immediate. The length of each segment considering n subdivisions is given by:

$$L_j = L_n \alpha^{n-j} \qquad for\ j = 1..n-1 \tag{4.6a}$$

$$L_n = \frac{L_T}{(1-\alpha^n)}(1 - \alpha) \tag{4.6b}$$

In order to refine the mesh around the crack tip, it is necessary to set $0 \leq \alpha < 1$.

After creating the nodes at the crack surface, the refinement around the crack tip is made by inserting nodes along circumferences centered at the crack tip. The number of nodes in the circumference and the number of levels (or circumferences) of refinement can be chosen. However, the radii of the levels are attached to the distance between a node at the crack face and the crack tip, as shown in Figure 4.7.

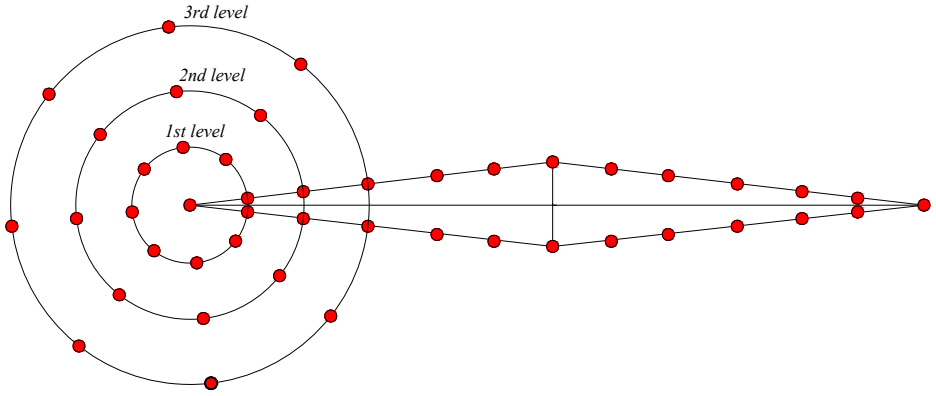

Figure 4.7 Refinement at the crack tip

The exemplified refinement at the left crack tip is shown in Figure 4.7. It can be observed that in each level of refinement, 9 nodes were created, including the ones already positioned at the crack faces. However, as already mentioned, the number of nodes and levels are arbitrary.

The final result of the node generation is depicted in Figure 4.8.

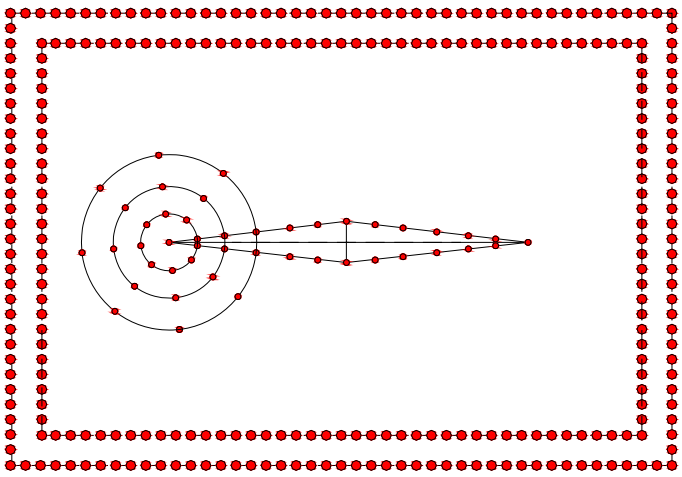

Figure 4.8 Final result after generating initial nodes

It should be mentioned that the procedure is also valid to create nodes around the right crack tip, but these nodes were not shown in Figure 4.8.

The remaining nodes needed to generate the mesh are automatically created by the MeshPy®.

Remark: the GFEM makes possible to perform the analysis without remeshing by means of the Heaviside function taken as enrichment. However, the necessity of prescribing loads at the crack faces made the computational development for exploring the Heaviside function not feasible.

It is also important to address some comments about the creation of nodes when holes associated to cracks are considered. Although the cracks do not appear in the global problems, the holes associated to them must be modeled in these problems. It is well known that the stress fields experience perturbation at the edges of the holes. To exemplify, consider a plate containing a centered hole, shown in Figure 4.9.

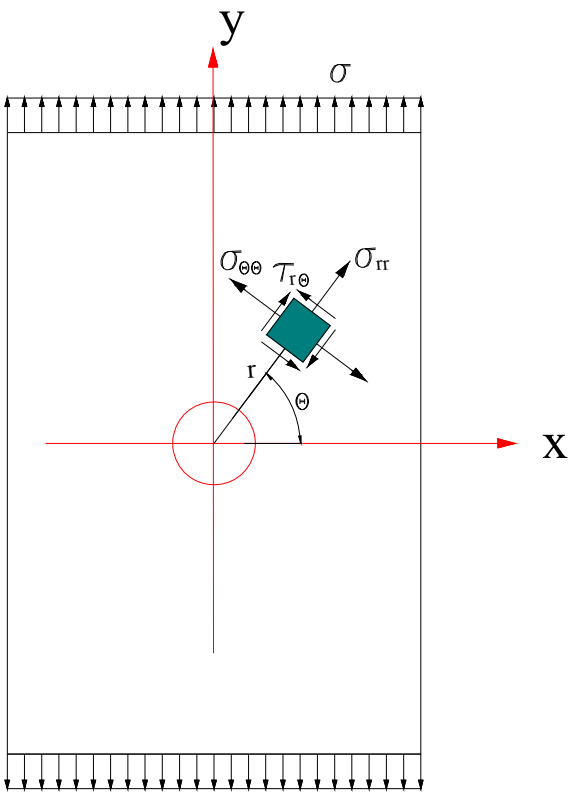

Figure 4.9 **Plate containing a centered hole. Stress state represented in polar coordinates**

In Figure 4.9 the stress state at a point is represented in polar coordinates. The stress components are given by the Equations (4.7a) to (4.7c) below, (see, *e.g.*, Mohammadi (2008)).

$$\sigma_{rr} = \frac{\sigma}{2}\left(1 - \frac{a^2}{r^2}\right)\left[1 - \left(1 - 3\frac{a^2}{r^2}\right)\cos 2\theta\right] \quad (4.7a)$$

$$\sigma_{\theta\theta} = \frac{\sigma}{2}\left[\left(1 + \frac{a^2}{r^2}\right) + \left(1 + 3\frac{a^4}{r^4}\right)\cos 2\theta\right] \quad (4.7b)$$

$$\sigma_{r\theta} = \frac{\sigma}{2}\left[\left(1 - \frac{a^2}{r^2}\right)\left(1 + 3\frac{a^2}{r^2}\right)\sin 2\theta\right] \quad (4.7c)$$

The components σ_{rr} and $\sigma_{\theta\theta}$, for $\theta = 0$, are presented in Figure 4.10. There is a visible perturbation in the stress values when r approaches the edge of the hole. It is also important to note that, in this case, $\sigma_{\theta\theta} = \sigma_{yy}$.

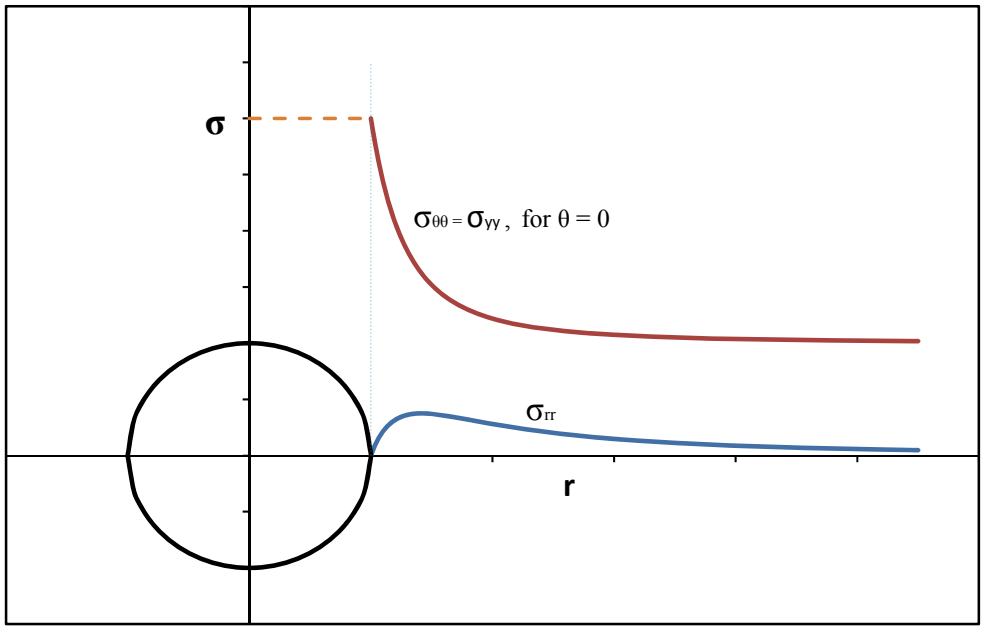

Figure 4.10 Stress components close to the edge of the hole.

To capture the referred perturabion, shown in Figure 4.10, the cracks associated to the holes are modeled using at least two "incision lines" or segments S_{ci}. To exemplify, consider the crack associated to a hole shown in Figure 4.11-a. The hole is centered at the initial point of the first segment, and its radius is smaller than the length of the referred segment, as shown in Figure 4.11-b. It is important to note that the second segment can be dealt with as a segment belonging to a crack without associated holes.

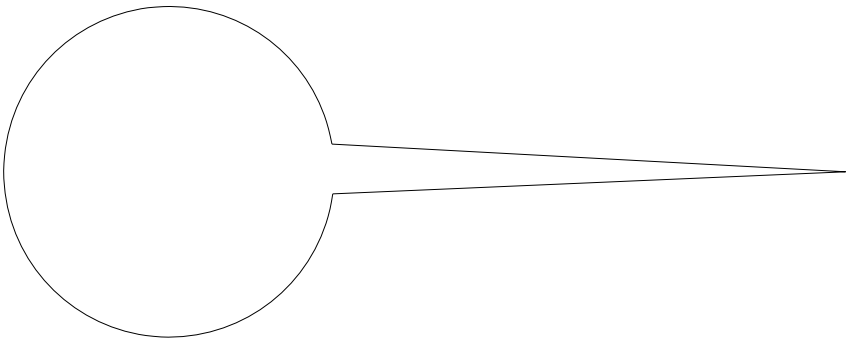

a. Crack associated to a hole to be modeled

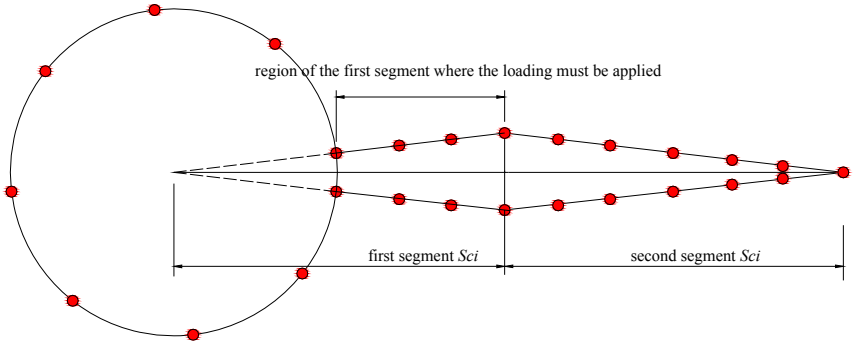

b. Modeling and generated nodes of the crack and the associated hole

Figure 4.11 Modeled crack and associated hole

Remark: to make it easier to understand, the opening of the crack has been amplified in Figure 4.11-b. In the developed code, the opening is very small and thus, the discrepancy between the crack and the adopted model is not so significant.

The length of the first segment is greater than the radius of the associated hole. It is also important to stress that the load in this segment must be applied only at the region that corresponds to the crack surface, as indicated in Figure 4.11-b.

It seems clear that the Stress Intensity Factors must be calculated only at the tip of the second segment.

4.2.2 Enrichment of the nodes close to the crack tip and internal Γ contour

Essentially, this procedure selects some nodes close to the crack tip in order to perform the enrichment. In Figure 4.12, the enrichment procedure to be described in what follows is illustrated.

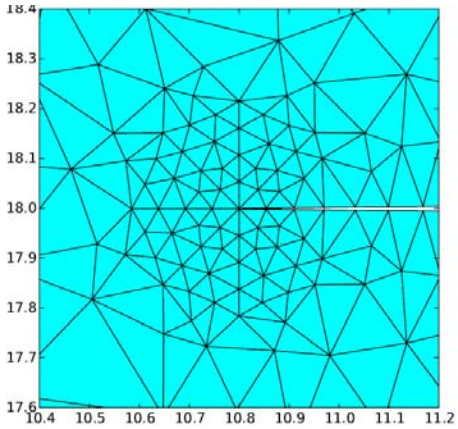

a. Mesh close to the crack tip

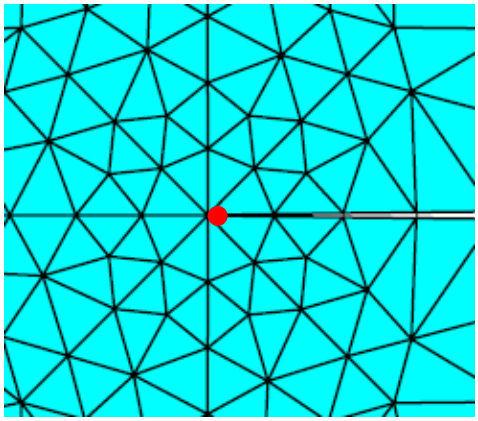

b. Level 0: enrichment in the node of the crack tip

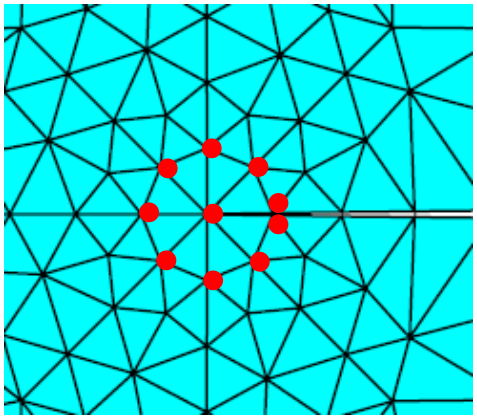

c. Level 1: enrichment in the nodes of the cloud with vertex at the crack tip

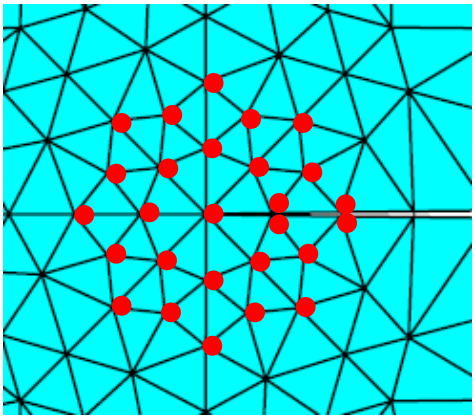

d. Level 2 of the enrichment

Figure 4.12 Enrichment of the nodes close to the crack tip

The nodes to be enriched composing the level node set are chosen by a topological process. At first, the node at the crack tip is selected. Such node is referenced as level node 0, see Figure 4.12b. The level node 1 is defined by the nodes of the elements belonging to the cloud with vertex at the node 0 (Figure 4.12c). As shown in Figure 4.12d, the next level node set is defined by the nodes belonging to the clouds centered at the nodes introduced in the level 1. The whole set of nodes must be enriched with stress functions, presented in Section 2.2.

In order to minimize the effects of the blending elements, *i.e.*, the elements that contain enriched nodes and nodes that are not enriched, more than 2 levels were hereby adopted in the numerical analyses.

Nevertheless, the set of nodes enriched with stress functions can also be enriched with polynomials.

It is worth to stress that the effects of the enrichment using stress functions are restricted to a neighborhood very close to the crack tip, as shown in the works of Rice (1973) and Larsson and Carlsson (1973). Thus, it is advisable to enrich only the first and second levels using stress functions and to restrict the enrichment to polynomial functions in the subsequent levels.

Furthermore, it is advisable to enrich with polynomials as well, the whole set of nodes along the Γ contour. The basic aim is to improve the accuracy of the stress and displacement fields, since such results will be extracted and used in the global problems.

4.2.3 Crack face loading

The last procedure refers to the loading at the cracks surfaces of the local sub-problems. For an explanation of this procedure, let us consider Figure 4.13.

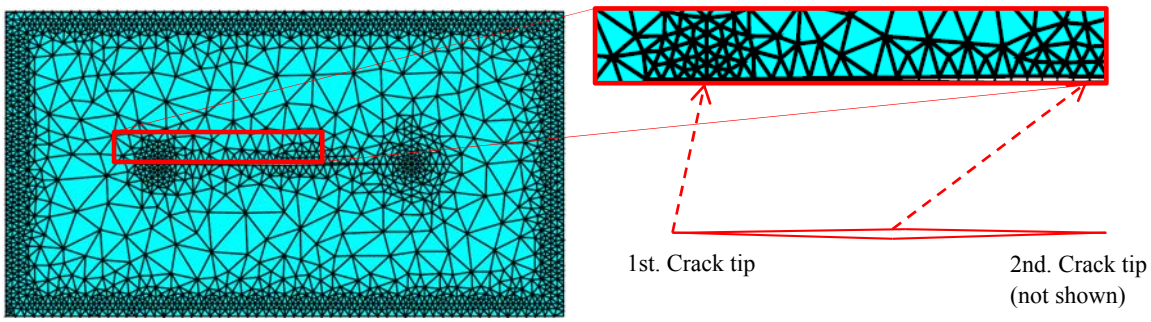

a. Generated Mesh

b. Amplified region around the upper crack surface of the first segment

Figure 4.13 General aspects of the procedure to apply the loads at the crack surface

In Figure 4.13-a, the unstructured generated mesh is shown. It is worth noting that the resulting mesh refinement around the left and right crack tips can have different results.

The procedure for applying the loads to the crack faces consists of the following steps:

1. Selecting the nodes positioned at the crack faces, in the segment referred to the crack line where the load must be applied. In the Figure 4.13-b, only the upper

crack surface of the first segment, is shown. It is clear that the process is analogous on the opposite surface (see also Figure 3.6);

2. For each pair of subsequent nodes that are on the same side of the crack face, the element containing these nodes must be identified, as exemplified in Figure 4.14-a. Obviously, only one element in the mesh contains the referred nodes, since these node are at the crack face;

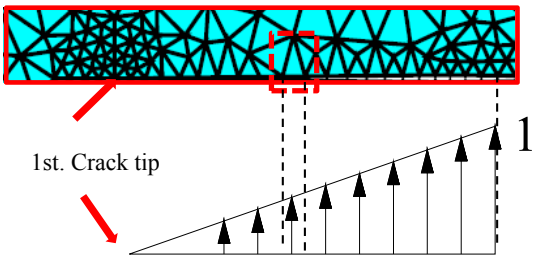

a. Load applied in the first segment of the upper crack surface

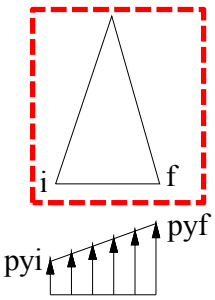

b. Detail of the applied pressure load in the element highlighted in Figure 4.11-a

Figure 4.14 Details of the procedure to apply the loads to the crack surface

3. A distributed load must be applied. In the Figure 4.14-b, the element triangle highlighted in Figure 4.11-a is depicted. The values of p_{yi} and p_{yf} are defined considering the proportion of the node distances to the crack tips as follows:

$$pyi = \left(\frac{l_i}{l_T}\right)^j; \qquad pyf = \left(\frac{l_f}{l_T}\right)^j$$

where:

i. l_i: distance between the initial node (i) up to the first crack tip;
ii. l_f: distance between the final node (f) up to the first crack tip;
iii. l_T: total length of the first segment;
iv. j: degree of polynomial. In the developed program, j can assume the values 0, 1 or 2.

4.3 Procedures associated to global sub-problem $P_G^{(k)}$: imposition of the boundary conditions.

Related to the global sub-problem $P_G^{(k)}$ there are two important procedures idealized in the computational framework. The first one is the same cited in Section 4.1 and Appendix B, aiming to evaluate the stress field in the points placed along the crack line prescribed in the original problem.

The second procedure is related to the imposition of the "jumps" in displacements and tractions in the Γ contour.

In order to do that, first of all, the option hereby adopted was to set node pairs as close as possible following the whole Γ contour. Each pair of nodes must be very close to each other, in order to ensure the accuracy of the results. This means that the distance δ depicted in Figure 4.15 must be as small as possible. However, if such a relative distance δ is set excessively small, MeshPy® cannot identify the strip between the two contours and, therefore, does not generate a "void" inside that region. Therefore, for each problem to be solved, the distance δ must be set. As a rule of thumb a reasonable value for δ must be of the order 10^{-1} of the displacements to be prescribed as "jumps".

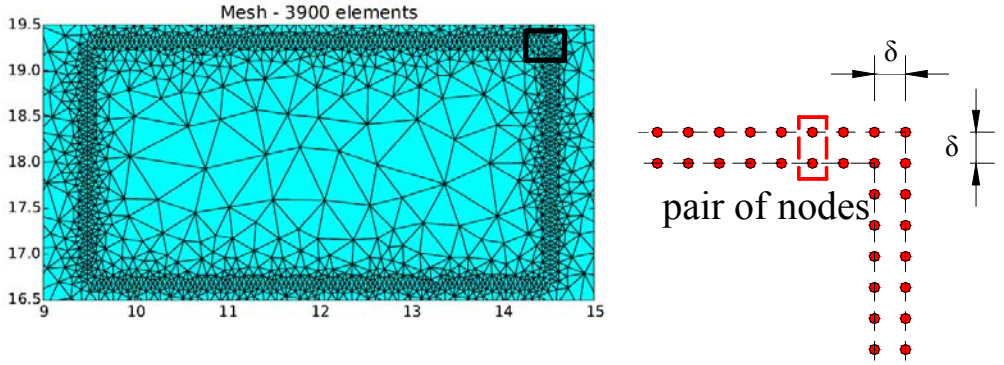

a. Γ contour in the $P_G^{(k)}$ b. Pair of nodes and δ distance

Figure 4.15 Region close to the Γ contour in the $P_G^{(k)}$

Once the pairs of nodes are defined along the Γ contour, the traction vector must be imposed only in one line of nodes of each pair. In the analysis hereby performed it was chosen to impose this condition in the internal node, but this is arbitrary. To impose the jump in displacements, the penalty method can be used.

4.4 Parallel Processing

In this section, the parallel processing hereby explored in the Splitting Method is addressed. Such procedure was implemented in the SCIEnCE code using Python® language. In order to elucidate concepts, a class of the Python® language and one of its methods are cited and explained.

An important advantage of the Splitting Method is its compatibility for exploring parallel processing. In the Python® language such tool is available by the Multiprocessing package.

The parallel processing adopted in this work is described in Piedade Neto *et al* (2011). In short, the computation in parallel was performed using a Multiprocessing Pool. According to Piedade Neto *et al* (2011), "a pool is a collection of processes kept ready to be used depending on the demand of their 'service' ". In the following, the adopted procedure to create those processes is discussed.

First of all, it is important to stress that it was used the *Pool* class, that belongs to the *Multiprocessing* module. Using the referred class, one can create a pool which will carry out tasks submitted to it. Thus, an object of this class is declared: *pool = Pool( )*. Next, the *apply_async( )* method is used to create and control all the worker process that will be solved. This method has the following syntax:

Pool.apply_async(*func, args[, kwds[, callback]]]*)

where:

1. *func* is a function previously created;
2. args are the arguments of *func*.

kwds and *callback* were not used in this work.

Two functions were created to be used as *func*: "*create_PLKs"* and "*create_PGKs"*.

The simplified algorithm of "*create_PLKs*" is described in the following:

For each "incision line" of the crack do
For each mode (I and II) do
For each component of the approximation basis do
Construct external boundary
Construct Γ contour
Construct mesh
Create nodes and elements
Insert material
Insert boundary conditions
Assemble clouds
Apply enrichments
Solve linear system
Update points attributes
Plot results

Remark: it is not necessary to present the arguments for understanding of this section.

It is possible to note in the algorithm above that the procedure "*create_PLKs*" assembles and solves all the local problems related to a crack. Once the procedures are defined, a process is created for each crack:

for each crack
pool.apply_async(func = create_PLK, args = (...))

This means that each crack corresponds to a process.

1 Crack ⟷ *1 Process*

By using the method "join", the processes start to be solved by an available processor. If the number of cracks, and consequently the number of processes, is greater than the number of processors, then the remaining processes must "wait" in the pool of processes. The first processor that concludes the calculus, in other words, that finish to solve all the local (or global) problems referred to a given crack, starts to solve the next process in the pool, as exemplified in Figure 4.16.

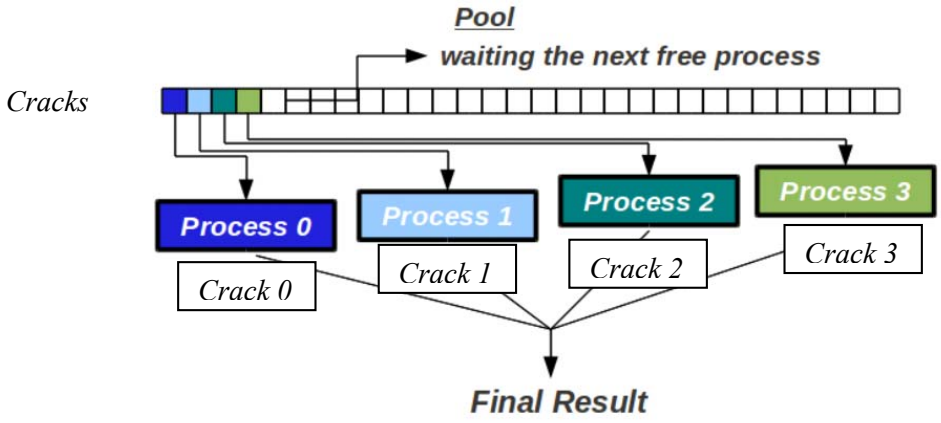

Figure 4.16 Relation between process and cracks (Adapted from Piedade Neto *et al*, 2011*)*

We choose to create a process for each crack of the analyzed problem, because each one can be assessed independently of the other cracks. However, the local (or global) problems referred to a given crack cannot be analyzed independently, *i.e.*, they need to share some information, as the mesh generation, for example. Still according to Piedade Neto *et al*, "it is usually better to avoid using shared state as far as possible". Each process, related to a single crack, will solve many local (or global) sub-problems.

The number of these sub-problems will depend on: i) the number of the "incision lines" or segment lines of the crack (See Section 3.8); ii) the number of terms of the approximation. In the first local (or global) sub-problem of each crack, the mesh will be created. In the other sub-problems, the same mesh can be used, reducing the computational effort.

Remark: regarding the Splitting Method, the parallel processing can be used for analyzing local sub-problems $P_L^{(k)}$ as well as global sub-problems $P_G^{(k)}$. It is possible to restrict the use of the parallel processing only to the local problems, or only to the global problems, or either to both of them. It seems to be more advantageous to use it in both of them.

Chapter 5: Considerations about Generalized Finite Element Method

5.1 Historical preliminary: the HP-Cloud Method

The HP-Cloud Method is a meshless method originally proposed by Duarte (1996) and Duarte and Oden (1996). From this method the GFEM has lent the enrichment strategy of the approximation to the solution.

Let R^n be a vector space and let Ω be a subset of R^n. A covering to Ω is formed by open circular regions called *clouds*, such that its radii R_j are arbitrary (see Fig.5.1). In other words, each cloud ω_j is defined as:

$$\omega_j = \{x \in \Omega; |x - x_j| \leq R_j\} \tag{5.1}$$

where x_j is a point in the interior or Ω and defines the center of the cloud. Being x an arbitrary point in Ω, it must be covered by a number n > 1of clouds ω_j.

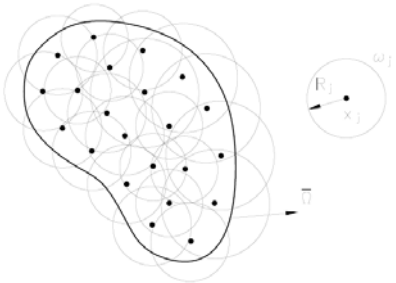

Figure 5.1 Clouds ω_j in R^2 (Extracted of Barros, 2002)

Each cloud ω_j is a support of a single shape function $\phi_j(x)$. The set of $\phi_i(x)$ functions constitutes a *Partition of Unit* (PU) if the following conditions are fulfilled:

1. $\phi_i(x) \in C_0^\infty(\omega_i)$: this means that each shape function $\phi_i(x)$, as well its partial derivatives of any order, are continuous on ω_i and have compact support in ω_i;

2. $\sum_{i=1}^{n} \phi_i(x) = 1$: this condition is necessary to assure that the shape functions be able to reproduce a constant value;
3. $\phi_i(x) \geq 0$ em ω_i.

It is worthwhile to mention that the second condition is the most important among all cited conditions, because it ensures the reproducibility property of the enrichment functions and the compatibility for the global approximation constructed by the linear combination of the shape functions.

Remark: the last condition can be met, especially in the local problems, by using the shape functions of the Constant Strain Triangle (*CST*).

In the HP-Cloud Method, the enrichment of the shape functions of an arbitrary cloud implies the addition of new nodal parameters.

Let us then consider that the local approximation function be generated from a basis $P_K=\{p_i\}_{i=1}^{m}$ of m monomials, that spans the polynomial space whose maximum degree is equal to k. It is possible to increase the degree of approximation function up to $p>k$, by using the set of functions that provide the family of HP-Clouds $\Im_N^{k,p}$, as follows:

$$\Im_N^{k,p} = \left\{ \{\emptyset_j(x)\}_{j=1}^{N} \cup \{\emptyset_j(x)p_i(x)\}_{j=1}^{N}; i = m+1, \dots, q(p); p_i \in P_p - P_k; p \geq k \right\} \quad (5.2)$$

where:

1. P_p is the polynomial space of maximum degree equal to p, generated by the basis $P_p = \{p_i\}_{i=1}^{q(p)}$, formed by $q(p)$ monomials.

The global approximation function can be constructed by a linear combination of the local approximations, according to Equation (5.3):

$$u(x) \approx \tilde{u}(x) = \sum_{j=1}^{n(x)} \emptyset_j(x) u_j \quad (5.3)$$

Substituting the Equation (5.2) in (5.3), the following expression by the approximation function is obtained:

$$\tilde{u}(x) = \sum_{j=1}^{N} \emptyset_j(x) \left(u_j + \sum_{i=k+1}^{p} x^i b_{j(i-k)} \right) \quad (5.4)$$

where:

1. u_j are the initial nodal parameters;
2. $b_{j(i-k)}$ are the added parameters.

5.2 Generalized Finite Element Method (GFEM)

According to the hereby presented foundations of the HP-Cloud Method, it is possible to use the set of nodes and meshes, or else, the finite element mesh, to define the clouds. Thus, the cloud is defined as the set of finite elements sharing a common node.

The strategy used in GFEM (MELENK, 1995; DUARTE *et al*, 2000) is very simple and consists of employing the shape functions of the Finite Element Method (FEM) as Partition of Unity. For example, as already mentioned, the shape functions of the Constant Strain Triangle (CST) and bi-linear functions of the four nodes quadrilateral elements can be used in two-dimensional analysis.

Obviously, the dimension of the FE approximation space is increased when the enrichment is explored.

The possibility of adding hierarchic refinements to the set of shape functions is another characteristic of GFEM worth of mention.

The main features of the GFEM can be summarized as:

1. It can be interpreted as a meshless method;
2. It provides an efficient manner to obtain an accurate local approximation function;
3. It is a method whose boundary conditions can be easily imposed, like FEM;
4. It presents good robustness, even under strong distortion of the mesh, since the enrichment is performed over the spatial coordinates.

5.3 Formulation of GFEM

As mentioned above, in this method the shape functions of FEM can be interpreted as a PU and the clouds are formed by a set of elements sharing a node x_j. For example, considering the Lagrange functions depicted in Figure 5.2, the cloud or support ω_j of the function $N_j(x)$ is defined by the union of the elements β - *1* and β, sharing the node j.

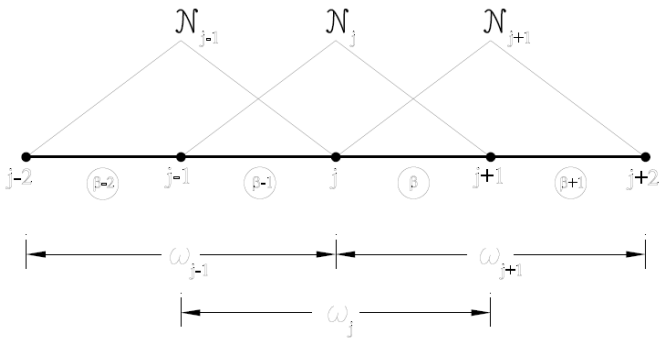

Figure 5.2 Partition of Unit from FE in R^1 (Extracted of Barros, 2002)

In the interior of the element β, for example, the initial approximation function belongs to the vector space spanned by the shape functions related to the nodes x_j and x_{j+1}, or else:

$$\tilde{u}(x) \in \langle N_j, N_{j+1} \rangle \tag{5.5}$$

The enrichment allows that the approximation basis can be increased by multiplying the shape function N_j attached to each node x_j of the element β, by a new set of linearly independent functions $\Im_j = \{1, L_{j1}, L_{j2}, \ldots, L_{jq_j}\}$. Thus, we have:

$$\tilde{u}(x) \in \langle \cup_{i=1}^{q_j} N_j L_{ji}, \cup_{i=1}^{q_j} N_{j+1} L_{j+1i} \rangle = \langle S_\beta \rangle \tag{5.6}$$

where S_β represents the resulting functions from the multiplication of the $\Im_j$ by the PU in the element β.

In principle, the functions L_{ji} are arbitrary. They can be monomials or even be defined once *a priori* knowledge of the solution is available. In this case, the local approximation function may represent the exact solution in the associated cloud. In the Splitting Method, for example, the functions L_{ji} are described in Section 1.2.

The generalization of the GFEM for R^2 can be illustrated in the Figure 5.3. It is shown the PU (bi-linear function, that generates an approximation function that belongs to C^0), the special arbitrary enrichment function, and the product of both. It must be noted that the product function presents compact support as the PU.

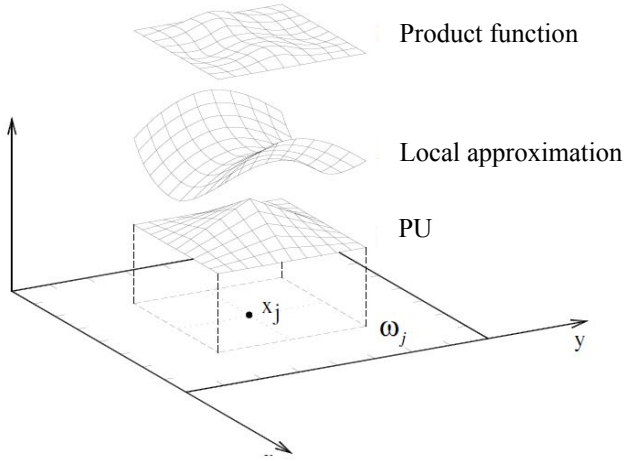

Figure 5.3 Enrichment of the PUM (Extracted from Barros, 2002)

In short, the family of shape functions for GFEM can be defined as:

$$\Im_N^{k,p} = \left\{\{N_j(x)\}_{j=1}^N \cup \{N_j(x)L_{ji}(x)\}_{j=1}^N | i \in \Im_j\right\} \tag{5.7}$$

Finally, the approximation function $\tilde{u}(x)$, for instance, can be represented as:

$$\tilde{u}(x) = \sum_{j=1}^N N_j(x)\left\{u_j + \sum_{i=1}^{q_j(p)} p_{ji}(x)b_{ji}\right\} \tag{5.8}$$

If the functions L_{ji} are taken as polynomials functions, the relation (5.7) defines the family indicated as $\Im_N^{k=1,p}$.

When polynomials are considered, a possible problem of the enrichment strategy is the linear dependence introduced by the family $\Im_N^{k=1,p}$ (DUARTE, BABUSKA, ODEN, 2000). However, such problem can be easily avoided by using numerical strategies as the ones suggested by Strouboulis, Babuska and Copps (2000).

Chapter 6: Numerical examples

In this chapter, some examples are shown in order to validate the developed computational framework constructed combining the Splitting Method and GFEM.

The first example is more detailed aiming to elucidate some of the main aspects of the Splitting Method, the employment of the GFEM and, consequently, the developed computational framework. Furthermore, the analysis of the fatigue and propagation is performed, therefore exemplifying the simple method proposed in Chapter 2 to assess fatigue crack growth. In the remaining examples, various aspects of interest of the process are explored.

6.1 Example 1: An Embedded Through-Thickness Crack

This first example was solved by Huang, Sukumar and Prévost (2003) using XFEM, as well as by Dong and Atluri (2013) using Symmetric Galerking Boundary Element Method, or SGBEM, both aiming to calculate the Stress Intensity Factors. In fact, it is a benchmark problem consisting of a plate with measures of ($2b$ =) 24 width and ($2h$ =) *36* height, subjected to a unit constant tensile load σ, applied on the upper and lower edges, as shown in Figure 6.1a. A crack of length ($2a$ =) *2.4* is located at the center of the plate. The thickness of the plate is equal to 1.0.

Constant, linear and quadratic approximation basis were considered when describing stress distribution at crack faces in the Splitting Method. Therefore, for each component of the approximation basis, the number of problems to be solved is given in Table 6.1:

Table 6.1 Example 1 – Number of assembled problems to solve example 1 using Splitting Method

Type of approximation	Number of problems of the type:			Total
	$\boldsymbol{P_G^{(0)}}$	$\boldsymbol{P_L^{(k)}}$	$\boldsymbol{P_G^{(k)}}$	
Constant	1	4	4	9
Linear	1	8	8	17
Quadratic	1	12	12	25

To exemplify the calculus of the number of problems, let be considered the number of $\boldsymbol{P_L^{(k)}}$**'s** for constant approximation**.** It is important to stress that, for any analysis, each crack is formed by, at least, 2 incision lines. Particularly in this example, the crack is formed by 2 incision lines (see Section 3.8, Figure 3.5). Therefore, the number of problems (*nop*) is equal to:

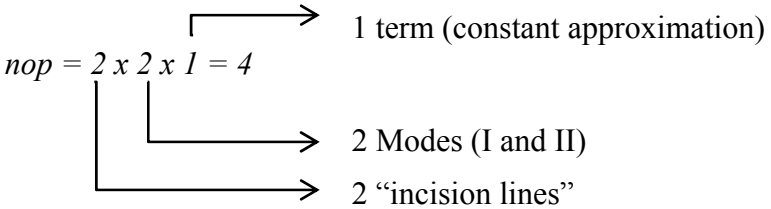

Remark: this example can be solved considering only the Mode I crack opening. However, in order to validate the implemented computational procedure as a whole, the terms related to Mode II were also considered.

The use of the high order components of the approximation basis demands more computational effort and, consequently, processing time. Nevertheless, such components can be necessary when the stress field in the neighborhood of the real problem is not so smooth. Despite the fact that in this particular example, the obtained results using constant, linear and quadratic were very close, the results related to the quadratic approximation basis are presented from now on.

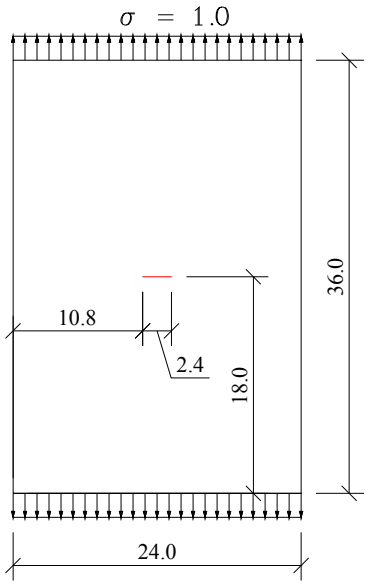

a. Geometry of the plate

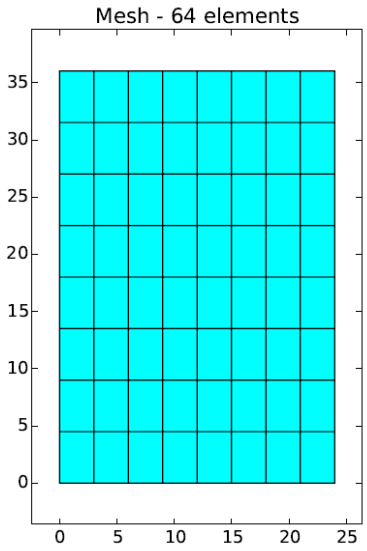

b. Problem 1: mesh used for solving $P_G^{(0)}$

Figure 6.1 Example 1 – Geometry and mesh used in $\boldsymbol{P_G^{(0)}}$

6.1.1 Global Problem $P_G^{(0)}$

To solve the global problem $P_G^{(0)}$, some features were assumed:

i. Mesh: it was defined as a structured mesh modeled with 64 quadrilateral elements, as depicted in Figure 6.1b. It is important to remind that there are no cracks in this global problem. Therefore, it was possible to use a simpler mesh to solve it;

ii. Material properties: the Young modulus of the adopted material is *1000* (dimensionless), and the Poisson coefficient is equal to *0.3*. Actually, Dong and Atluri (2013) omitted these values, since their goal was to compare only the obtained *SIFs* by SGBEM and GFEM/XFEM. However, as in this work the main aim is to validate the hereby developed method, the above indicated values are adopted;

iii. Boundary conditions: fixed grips are prescribed only to avoid rigid body movement. Unit constant tensile load is applied on the upper and lower edges.

Another important aspect to stress is the fact that the $P_G^{(0)}$ will not change, independent of the number of components of the adopted approximation basis for the local and global problems. Some results for the problem are depicted in the Figure 6.2:

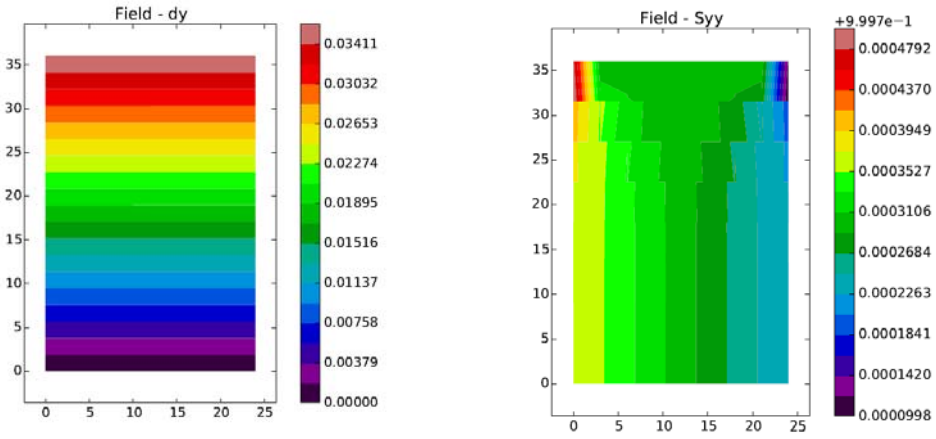

a. Displacement field: *dy* b. Stress field: σ_{yy}

Figure 6.2 Example 1 – Fields of interest of the $P_G^{(0)}$

The obtained results, especially the stress field distribution, confirm some of the drawbacks of FEM, mainly the less accurate approximation in the stress fields near the boundaries. However, to the practical use of the $P_G^{(0)}$, the obtained accuracy in the central region of the plate is sufficient.

The next step in this global problem consists in the construction of an approximation to the obtained stress field in the line where the crack is placed, in the original problem. This can be done, for instance, by using the Least Square Method (LSM).

6.1.2 Local Problem $P_L^{(k)}$

The next step consists of solving the local problems. It is important to highlight some features of these problems:

i. Mesh: it was generated by the MeshPy® and complemented by other methods for refinement of the mesh around the crack tip and for creating the Γ contour. Moreover, the mesh generator must take in account the discretization of the crack and the associated hole, if there is. It is possible to note in Figure 6.3 that the refinement can result in different discretization around each crack tip;

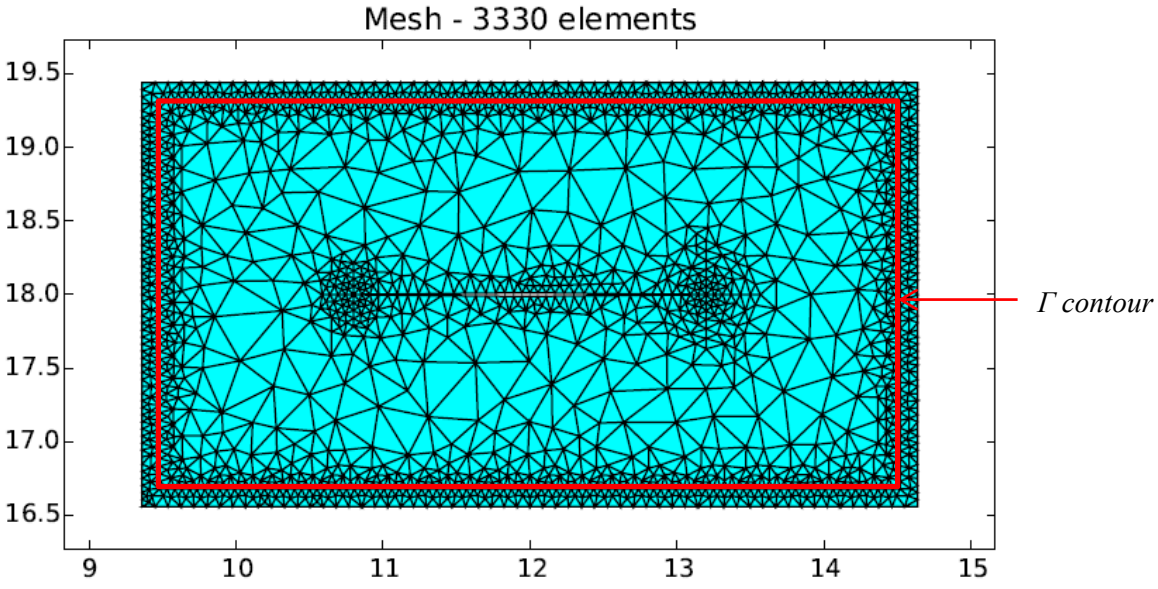

Figure 6.3 Example 1 - Local problem $P_L^{(k)}$ and the generated mesh

ii. Material properties: same values as adopted in the *Global Problem*;

iii. Boundary conditions: restrictions to the displacements in both directions, x and y, were imposed in the whole boundary.

An advantage of using this kind of restriction and to define a Γ contour close to the boundary, is that the displacements, that must be prescribed as "jumps" in the correspondents Global Problems $P_G^{(k)}$, will be almost null, therefore becoming easier their imposition.

In relation to the traction vector involved in this local problem, it must be imposed to the crack surfaces just as described in the Section 3.8.

The obtained fields of interest for $\boldsymbol{P_L^{(k)}}$, $k = 0$, are depicted in Figure 6.4.

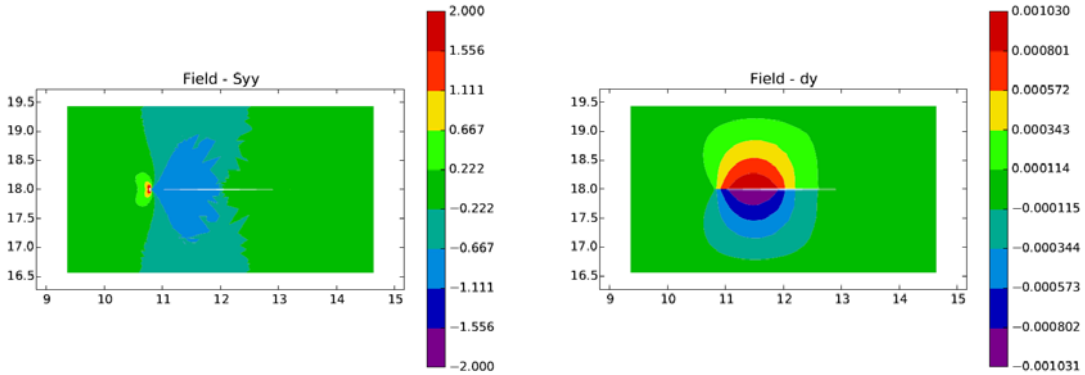

a. Stress field: S_{yy} b. Displacement field: dy

Figure 6.4 Example 1 - Stress and displacements fields in the Local problem $\boldsymbol{P_L^{(k)}}$

Remark: In the local problem presented in Figure 6.4a, the stress components are more concentrated at the left crack tip because the load was applied in the first segment of the crack surfaces. A symmetric result must be found when the load is applied in the second segment. The same conclusion is valid for the displacement field.

In order to illustrate the good effects of the enrichment, since the main goal of the enrichment in the local problems is to provide more accuracy in the values of *SIFs*, a zoom of the stress field S_{yy} ahead the crack tip is shown in Figure 6.5.

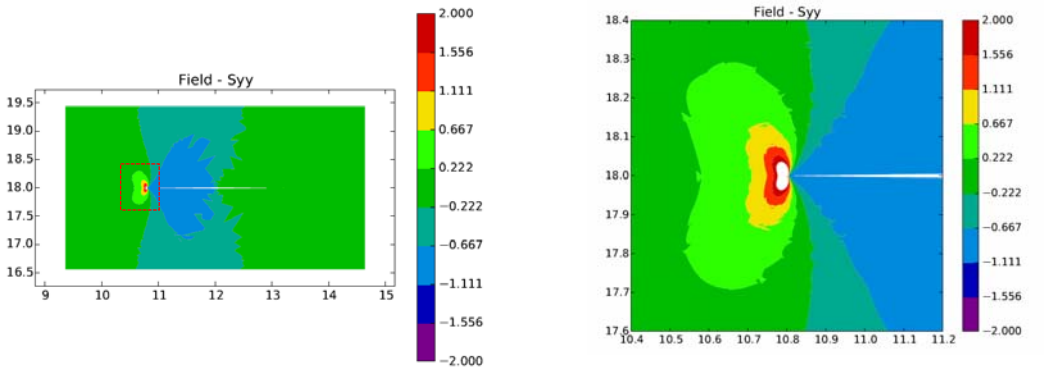

a. Stress field (<u>with</u> enrichment): S_{yy} b. Amplified region, close to the crack tip

Figure 6.5 Example 1 – Effects of the enrichment ahead the crack tip

In the Figure 6.6, the same stress component is depicted, but without exploring the enrichment. The mesh used in both cases was the same.

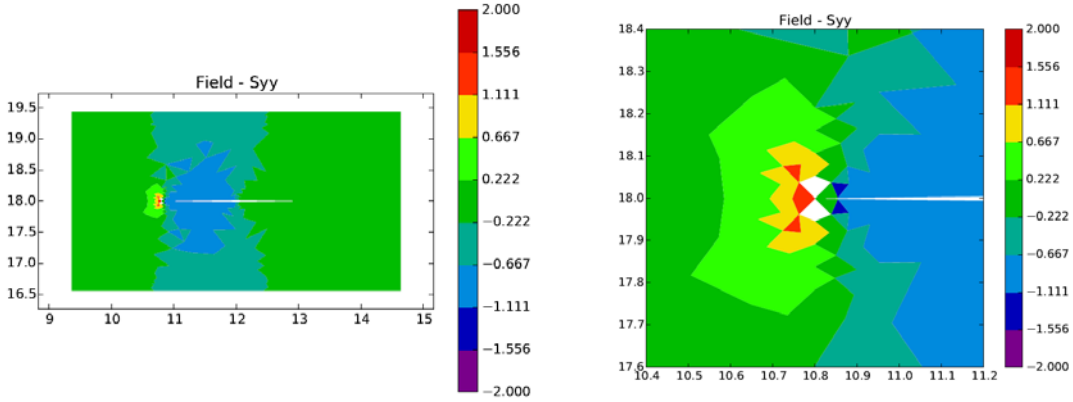

a. Stress field (<u>without</u> enrichment): S_{yy} b. Amplified region, close to the crack tip

Figure 6.6 Example 1 – Stress component ahead the crack tip, without the enrichment

As depicted in the Figures 6.5b and 6.6b, the stress field close to the crack tip is out of scale, since it is very high (white color at crack tip). This feature of the stress field in problems containing cracks cannot be precisely recovered at low cost by using only standard FEM. However, it is easily recovered using GFEM.

By comparing the results with the analytic isostress graph presented in Figure 6.7b, it is possible to note that the stress distribution obtained with GFEM is, apparently, similar to the theoretical ones.

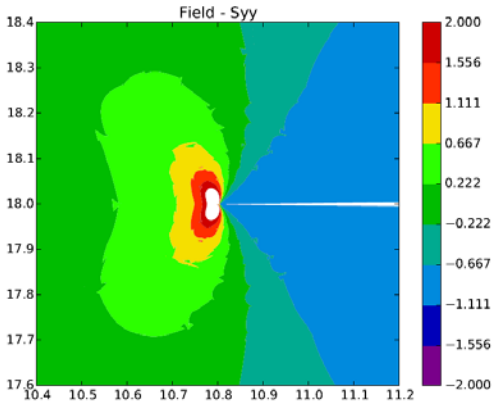

a. Amplified region, close to the crack tip (repeated – Figure 6.5b)

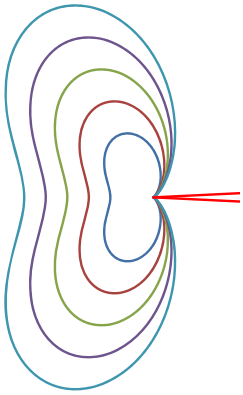

b. Analytic isostress curves

Figure 6.7 Example 1 - Effects of the enrichment x analytic curves

6.1.3 The *J* Integral

On what follows, the computed values for *SIFs* are presented. These values were compared with the ones obtained by the Franc-2D® program. The mesh of Linear Strain Triangle (*LST*) used in Franc-2D and some stress components of interest are depicted in Figure 6.8.

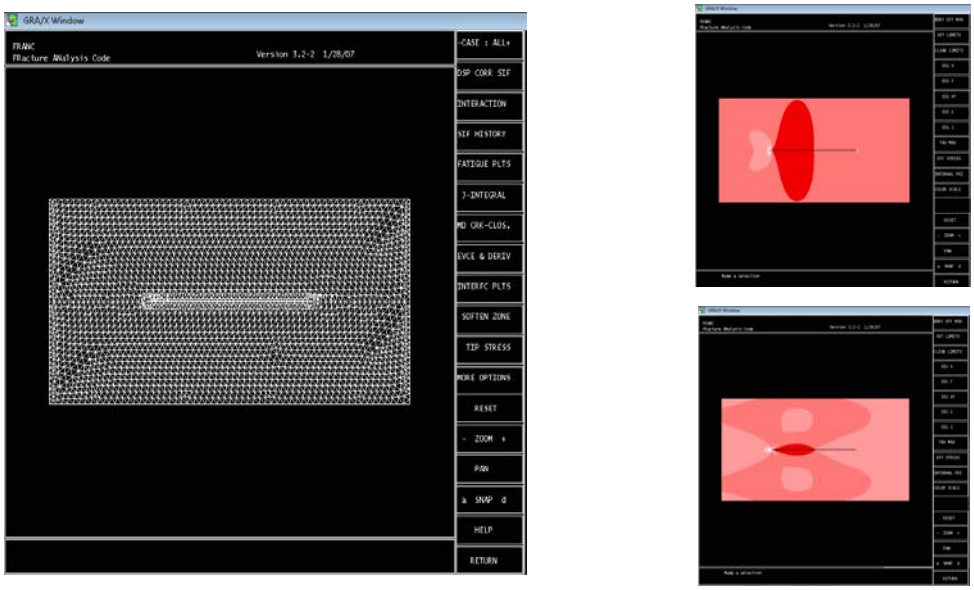

Figure 6.8 Example 1 - Analysis of the local problem using Franc-2D®

In the Table 6.2 the values for *SIFs* are presented. Since only normal loads are imposed at the crack surfaces in these local problems, we expect values for K_{II} close to zero.

Table 6.2 Example 1 - *SIFs* obtained from *SCIEnCE* (GFEM) and Franc-2D® (FEM)

$P_L^{(k)}$	*SCIEnCE*				Franc-2D®			
	Left crack tip		Right crack tip		Left crack tip		Right crack tip	
	K_I	K_{II}	K_I	K_{II}	K_I	K_{II}	K_I	K_{II}
0	1.068	0.0110	0.0210	0.0000	1.134	0.002	0.0267	0.000
1	0.2356	0.0030	0.0190	0.0000	0.2337	0.0003	0.0197	0.000
2	0.1111	0.0030	0.0167	0.0000	0.1059	0.0001	0.0170	0.000
6	0.0232	-0.002	1.060	-0.0030	0.0269	0.0000	1.133	0.000
7	0.0030	-0.001	0.8208	0.0056	0.0030	0.0000	0.8993	0.000
8	0.0010	0.0000	0.6934	-0.0010	0.0004	0.0000	0.7713	0.000

The problems 3 up 5 and 9 up 11 were omitted because they are related to shear loads, *i.e.*, the Mode II opening.

It is possible to note maximum relative discrepancies (*redi*) in the results of about 10%, as shown in Table 6.3.

Table 6.3 Example 1 - Error between *SIFs* obtained from *SCIEnCE* and Franc-2D® (left crack tip)

$P_L^{(k)}$	Left crack tip			Right crack tip		
	SCIEnCE	Franc-2D®	*redi* (%)	SCIEnCE	Franc-2D®	*redi* (%)
0	1.0680	1.1340	-5.82%	0.0210	0.0267	***
1	0.2356	0.2337	0.81%	0.0190	0.0197	***
2	0.1111	0.1059	4.91%	0.0167	0.0170	***
6	0.0232	0.0269	***	1.0600	1.1330	-6.44%
7	0.0030	0.0030	***	0.8208	0.8993	-8.73%
8	0.0010	0.0004	***	0.6934	0.7713	-10.1%

Even if some other aspects as differences in the mesh, use or not of the enrichment and type of finite element may have influence, an explanation for the discrepancies is that the extraction methods used by *SCIEnCE* and Franc-2D® are quite different in each other. Actually, *SCIEnCE* performs a line integral while Franc-2D® performs an area integral.

Moreover, the program Franc-2D® provides several methods to provide the *SIFs*. Among them are the Modified Crack Opening Displacement, *J Integral* and Crack Opening Displacement. The results for *SIFs* using these methods are presented in the Table 6.4, and relative discrepancies above 10% can be observed.

Therefore, to the sake of practical interest, it is possible to accept the values obtained by *SCIEnCE* as accurate enough in order to carry on the analysis.

Table 6.4 Example 1 - *SIFs* obtained from Franc-2D® using different methods

$P_L^{(k)}$	Left Crack tip			Right Crack tip		
	J Integral	COD	M-COD	*J Integral*	COD	M-COD
0	1.1340	1.1420	0.9893	0.0227	0.0201	0.0224
1	0.2337	0.2172	0.2330	0.0197	0.0178	0.0195
2	0.1059	0.0995	0.1057	0.0170	0.0155	0.0168
6	0.0227	0.0201	0.0224	1.1330	1.1410	0.9897
7	0.0030	0.0023	0.0029	0.8993	0.9241	0.7573
8	0.00044	-0.000066	0.000051	0.7713	0.8065	0.6306

6.1.4 Global Problem $P_G^{(k)}$

The last problem to be solved consists of Global Problems $P_G^{(k)}$. The main features of these problems are:

i. Mesh: it was generated by MeshPy®, with the aid of routines created in order to insert the Γ contour. Pairs of nodes were used in this contour in order to apply the discontinuities in displacements (see Section 4.3);

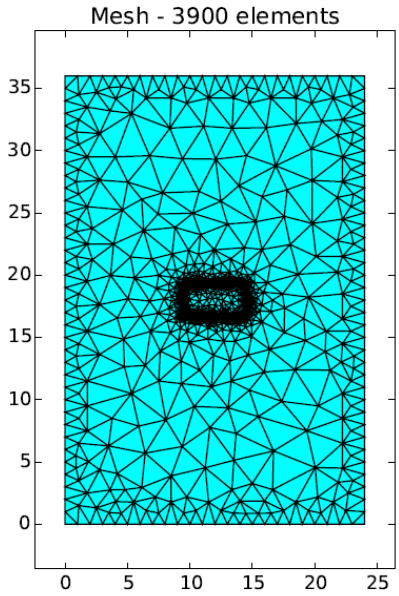

Figure 6.9 Example 1 - Mesh of $P_G^{(k)}$ generated by *SCIEnCE*

It can be seen in Figure 6.9 that a very refined mesh was generated in the neighborhood of Γ contour, and a refined one next to the boundaries, while a coarse mesh was created in the remaining regions of the domain. The Linear Strain Triangle (LST) was adopted in this problem; however the nodes are not depicted in Figure 6.9, to facilitate the mesh visualization.

ii. Boundary conditions: the same as the ones imposed in the Global Problem $P_G^{(0)}$.

The results obtained in $P_G^{(k)}$, $k = 0$, are depicted in Figure 6.10.

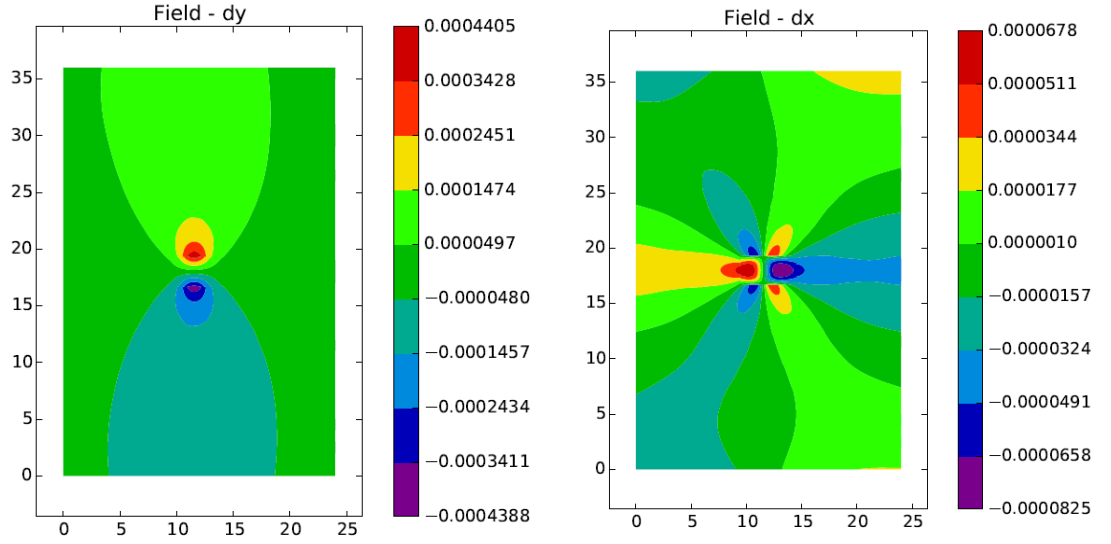

a. Displacement field: *dy* b. Displacement field: *dx*

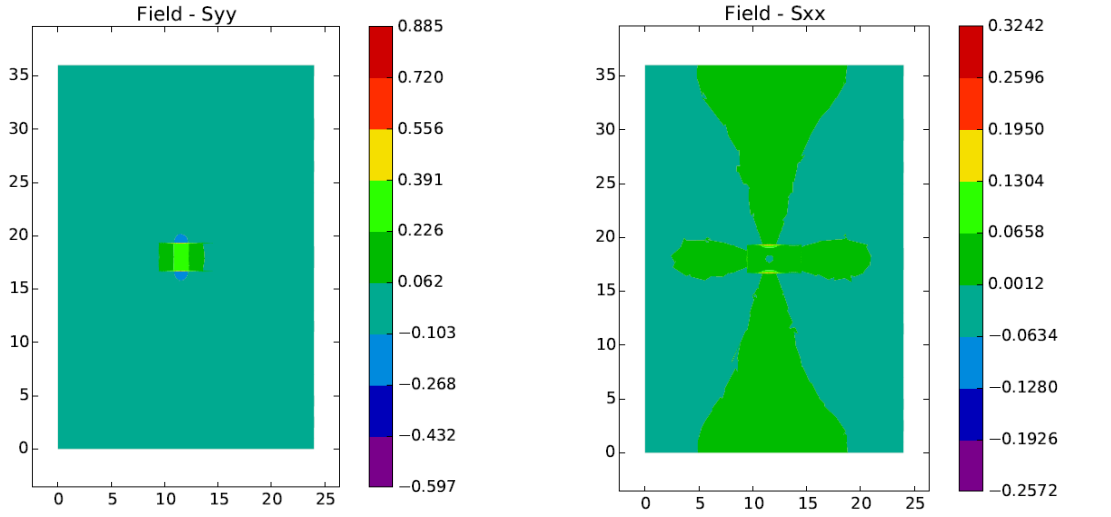

c. Stress field: σ_{yy} d. Stress field: σ_{xx}

Figure 6.10 Example 1 - Fields of interest of $P_G^{(k)}$

It is possible to note the "jumps" in displacements and tractions, especially in the Figures 6.10a and 6.10c.

After solving the global problem $P_G^{(k)}$'s, the system presented in Section 3.7 can be assembled and solved. It was considered not necessary to add any further comments about this procedure.

6.1.5 Solution of the problem

In the Table 6.5, the values of *SIFs* are presented, and compared with the ones obtained by Huang, Sukumar and Prévost (2003). The analytic value of the K_I can be calculated by the following expression:

$$K_I = C\sigma\sqrt{\pi a} \tag{6.1}$$

According to Feddersen:

$$C = \sqrt{\sec(\frac{\pi a}{W})} \therefore \mathrm{C} = \frac{K_I}{\sigma\sqrt{\pi a}} = \sqrt{\sec\left(\frac{\pi 1.2}{24}\right)} = 1.006 \tag{6.2}$$

where *W* is the width of the plate and *a* is the half-length of the crack.

Table 6.5 Example 1 - Comparison with analytic solution

XFEM:[Huang, Sukumar and Prévost (2006)]			**SCIEnCE**	
r_d	$\frac{K_I}{\sigma\sqrt{\pi a}}$	Error (%)	$\frac{K_I}{\sigma\sqrt{\pi a}}$	Mean Error (%)
0.424	1.0230	1.69	0.9559	-4.98
0.573	1.0000	-0.60		
0.716	0.9920	-1.40		
0.859	0.9940	-1.20		

In Table 6.5, r_d means the adopted radius of the circumference used for computing the stress intensity factors. SCIEnCE takes into account a mean value among the results obtained with the several radii adopted. Particularly, 10 different radii were considered.

Some complementary comments must be done. First of all, the computed error using *SCIEnCE* is of the same order as the error calculated for *J Integral* (as presented in section referred to *J Integral*). Secondly, the Splitting Method result is obtained from a composition of 25 different problems. In each one of them, there is a certain loss of accuracy. Thus, to the practical ends, the result can be considered satisfactory.

6.1.6 Fatigue problem

On what follows, the analysis of fatigue is presented. In order to proceed to this analysis the Splitting Method was used in the following manner: after the calculus of both SIFs and the propagation angle, the crack was increased of an incremental length, and the analysis repeated for computing the new *SIFs*. After a few steps, it was possible to establish a function relating the length of the crack and the *SIFs* variation.

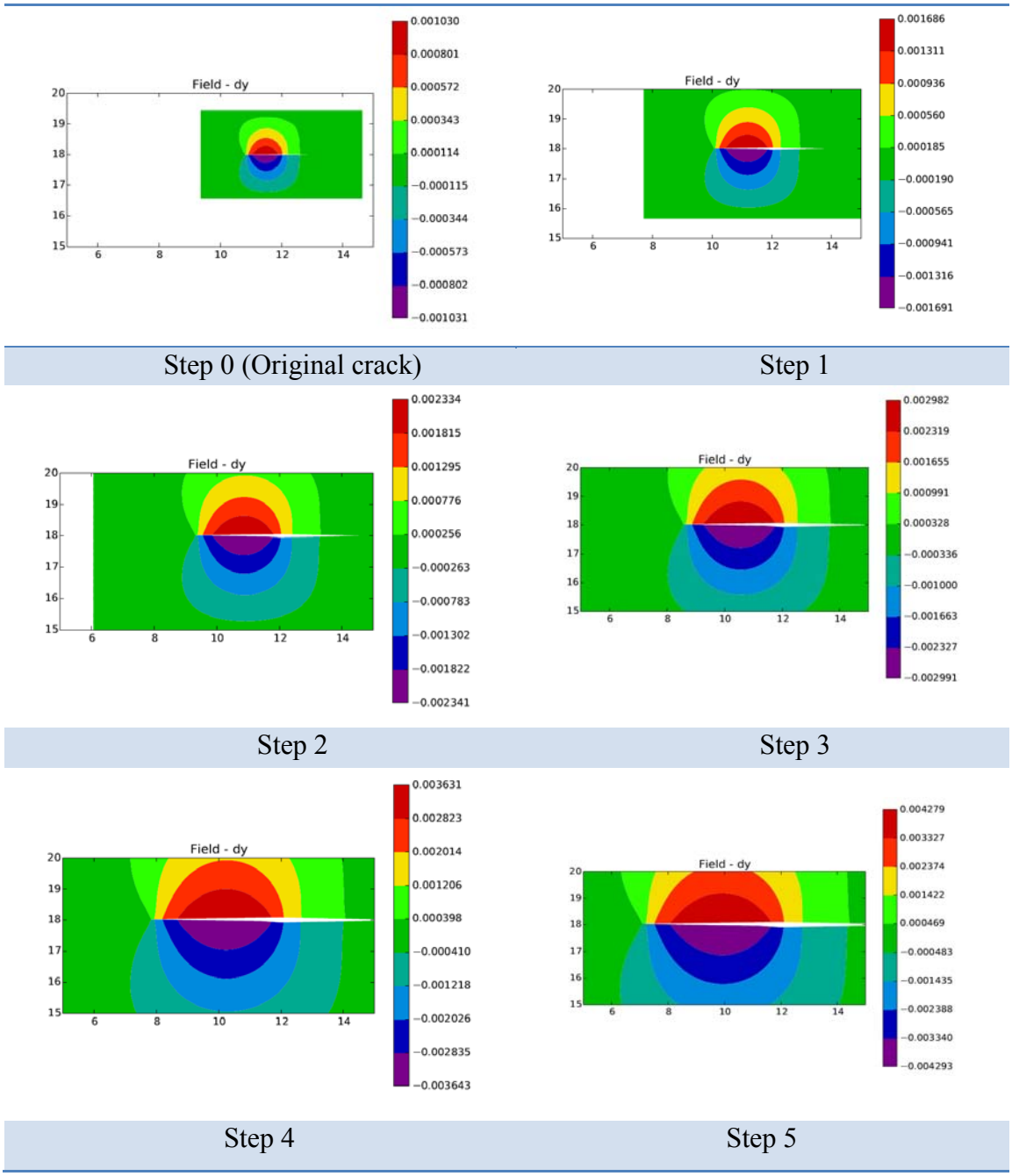

Figure 6.11 Example 1 - Propagation of the crack

Remark: in Figure 6.11, the displacement component *dy* referred to the first local problem is presented. In each step of analysis, there is a first local problem, *i.e.*, $\boldsymbol{P}_{\boldsymbol{L}}^{(\boldsymbol{k})}$, for $k = 0$. The author expects that these mapping of the displacement component, aid the visualization of the crack propagation in the figures.

An important aspect to be mentioned is the redefinition of the Γ contour, since it must enclose the crack. Some care must be taken for avoiding interception either with another crack, a hole or the external boundary of the problem. If the external boundary is involved in the Γ definition, the boundary condition of the real problem must be applied to the local problem as well.

In order to compute the ΔK_I and ΔK_{II} values, it is necessary to consider in $P_G^{(0)}$ the maximum and minimal values of the applied load, respectively σ_{max} and σ_{min}. However, since only linear elastic conditions have been considered, it is possible to assess the global problem $P_G^{(0)}$ using only $\sigma_{max} = \sigma$. In addition, considering that the adopted σ_{min} is equal to 0 ($\sigma_{min} = 0$), this implies that $K_{I,\,min} = K_{II,\,min} = 0$, and therefore the relation between the minimal and maximum values of the *SIFs* becomes also equal to zero, i.e. $R = K_{I,\,min}/\,K_{I,\,max} = K_{II\,min}/\,K_{II\,max} = 0$. Thus:

$$\Delta K_I = K_I \tag{6.3a}$$

$$\Delta K_{II} = K_{II} \tag{6.3b}$$

Remark: the angle of propagation can be arbitrary, although, particularly in this problem, the value of K_{II} is well-known and null.

After some steps of incremental growths and analysis using Splitting Method, it is possible to establish a function between *da/dn* and *a*.

However, as already mentioned before, it is necessary to establish a relation between $K_{I,eq}$ and *a*. Since, in this problem, $K_{II} = 0$, then $K_{I,eq} = K_I$. In Table 6.6, the obtained values are presented:

Table 6.6 Example 1 - Values of K_I for a sequence of "half-lengths"

Step	Half-length (a)	K_I	
		Left crack tip	Right crack tip
0	1.20	1.856	1.841
1	1.95	2.506	2.504
2	2.70	2.999	3.012
3	3.45	3.479	3.473
4	4.20	3.937	3.921
5	4.95	4.430	4.413

Remark: the adopted value for Δa is equal to 0.75. Sometimes, it can be necessary to perform a second analysis to correct the adopted crack length increment since it is arbitrary, a priori.

First of all, it can be stated that (see Section 2.6):

$$\Delta K_I = K_I = f(a) \tag{6.4}$$

Using a polynomial as approximation function, we have:

$$K_I = \beta_0 + \beta_1 a + \beta_2 a^2 + \cdots + \beta_2 a^n \tag{6.5}$$

Particularly, in this problem, since we are using only 6 steps of growth of the crack, and assuming that constant and linear polynomials will not provide a good approximation, the maximum polynomial degrees n = 2...5 were considered to obtain 4 different approximation functions, as depicted in Figure 6.12.

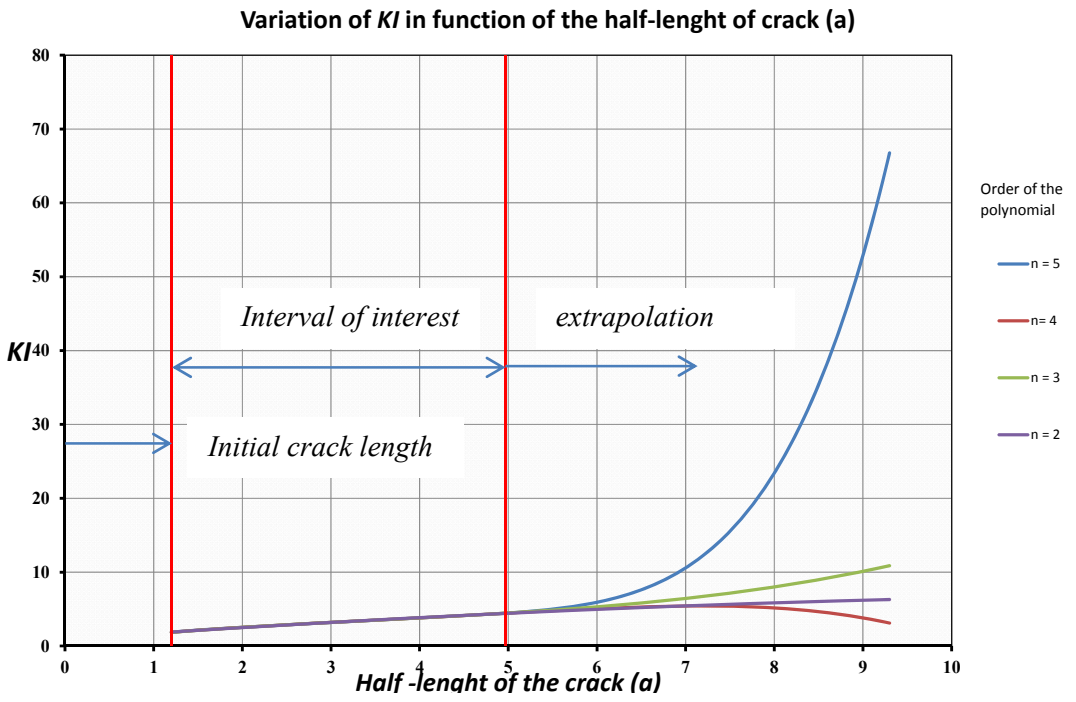

Figure 6.12 Example 1 - Variation of K_I x half-length (a) of crack

It is possible to note in the graph of the Figure 6.12, that the approximation functions are relatively close in the interval of interest, *i.e*, until the half-length (a) equal

to 4.95. We choose $n = 3$, since it appears to be more coherent at the points outside of the interval of interest, *i.e*, for points $a > 4.95$. Thus, according to Section 2.6, and using the Least Square Method:

$$\Delta K_I = 0.488 + 1.375a + (-0.218)a^2 + (0.0205)a^3 \quad (6.6)$$

Now, using the Paris law:

$$\frac{da}{dn} = C.\Delta K^m \quad (6.7)$$

In this example, we have considered the values adopted by Dong and Atluri for other examples presented in the same paper (Dong and Atluri, 2013): $C = 6.9x10^{-12}$ and $m = 3$.

Substituting the (6.6) into (6.7), one obtain:

$$\frac{da}{dn} = C.(0.488 + 1.375a + (-0.218)a^2 + (0.0205)a^3)^m \quad (6.8)$$

Therefore, after substituting the values of C and m, the integration follows as:

$$\int_{a_0}^{a_f} \frac{da}{(0.488+1.375a+(-0.218)a^2+(0.0205)a^3)^3} = 6.9x10^{-12}.\int_{n_0}^{n_f} dn \quad (6.9)$$

Obviously:

$$\int_{n_0}^{n_f} dn = \Delta n \quad (6.10)$$

For example, if we take a_f= 4.95, we find Δn = 2,295x 10^{10} cycles.

Repeating the calculus above for each half-lengths of the Table 6.6, in other words, if we assume that a_f in the Equation (6.9) is equal to each half-length a of the Table 6.6, it is possible to recovery the Fatigue crack growth curve. It is possible to observe in Figure 6.12 that the numerical solution is close to the analytical solution.

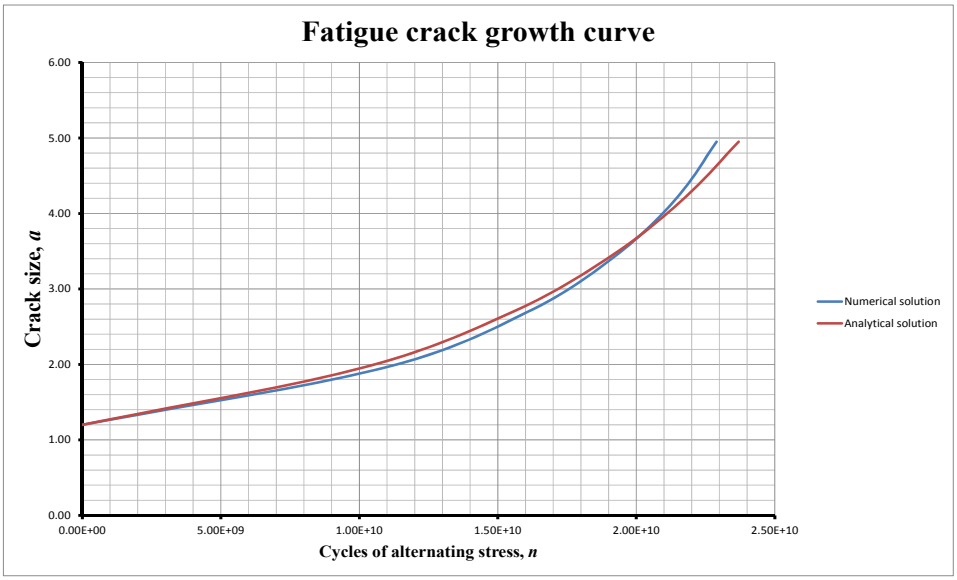

Figure 6.13 Example 1 - Fatigue crack growth curve

The presented procedure provides a first estimative of the fatigue crack curve. It is clear that the accuracy will depend on the adopted crack length increment.

6.2 Example 2: Three Embedded Parallel Cracks

The main goal of this example is to assess the efficacy of Splitting Method for solving problems with two or more cracks. Moreover, the propagation of the cracks is simulated. This example was also presented by Dong and Atluri (2013), and consists of a plate with three parallel cracks, which are orthogonal to the loading direction. The plate problem, with boundary conditions and applied loads, as well the dimensions and material properties are depicted in Figure 6.14.

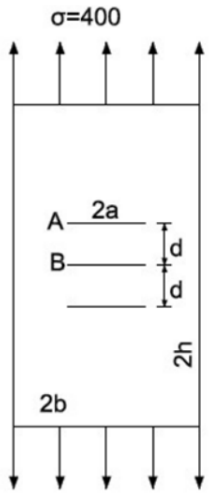

Data of the geometry:	
2a	2.540
2b	40
d	3.175
2h	80
Material properties (non dimensionless)	
Young modulus (E):	1000
Poisson's ratio (v)	0.3

Figure 6.14 Example 2 - Three parallel cracks (extracted from Dong and Atluri, 2013)

The mesh for the $P_G^{(0)}$ problem is very simple and is shown in Figure 6.15, together with the computed displacement fields *dy* and *dx*. It is important to stress that the plate is depicted in the deformed shape.

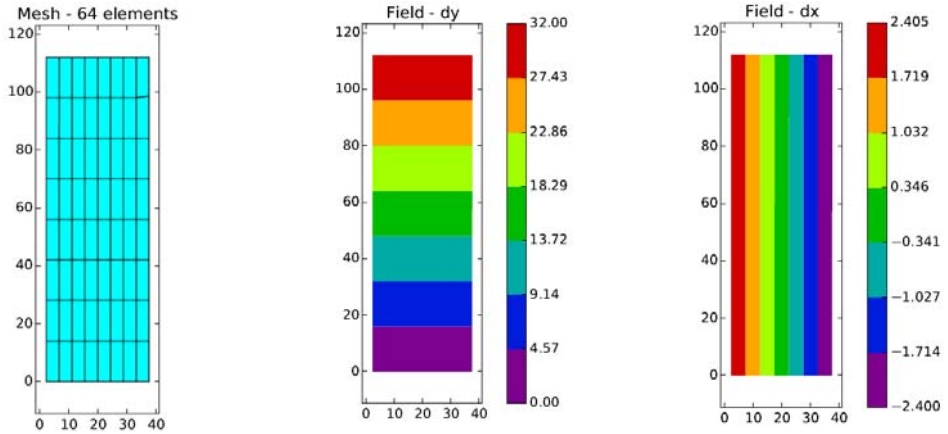

a. Used mesh b. Displacement *dy* c. Displacement *dx*

Figure 6.15 Example 2 - Used mesh and displacement fields

The constant and linear components of the approximation basis for the stresses at the crack lines were to analyze this problem (see Section 3.8). Thus, 24 local problems were performed. The calculus of the number of problems (*nop*) is similar to indicated below:

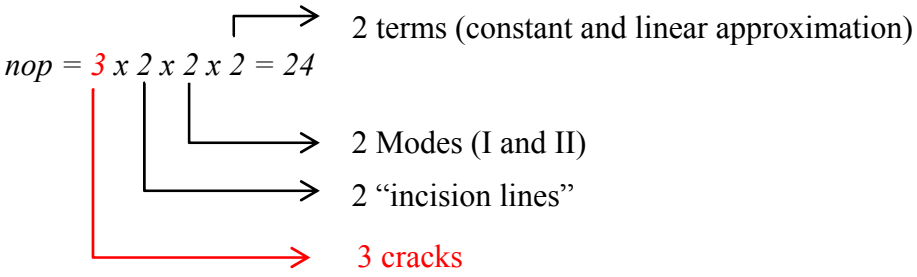

It is clear that the number of global problems $\boldsymbol{P_G^{(k)}}'s$ is also equal to 24.

The adopted mesh for solving the local problems at the beginning of the analysis and the computed stress component σ_{yy} are shown in Figure 6.16. The displacement fields are restricted at the external boundary.

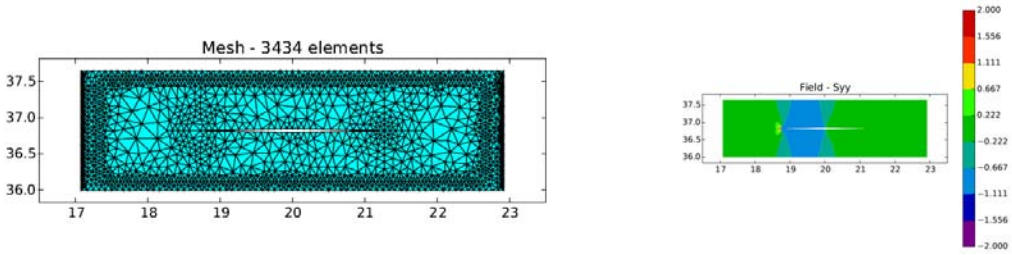

Figure 6.16 Example 2 - Adopted mesh and stress component σ_{yy}

Some comments must be done about the Figure 6.16. The crack shown in this figure is the non-labeled crack of the Figure 6.14. However, at the beginning of the analysis the meshes are the same for the three cracks, since the features of the cracks and the geometry of local problems are also identical.

The patterns of the local problems in steps 0 and 9 are depicted in Figure 6.17.

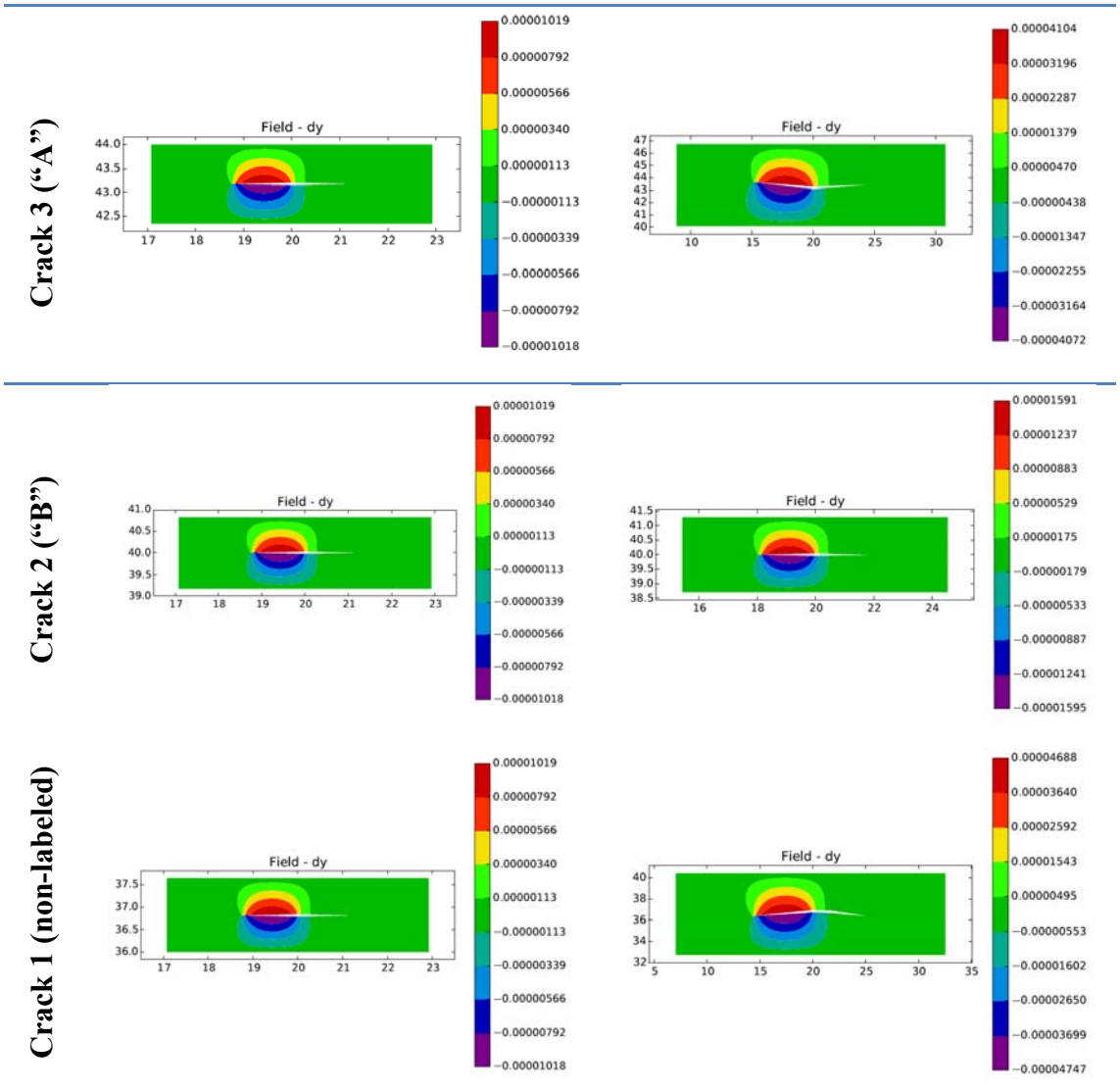

Figure 6.17 Example 2 - Propagation of the three parallel cracks in 9 steps

In order to promote the visual comparison between the results obtained by Dong and Atluri (2013) and the Splitting Method, all the pattern cracks are depicted simultaneously in the Figure 6.18. It is possible to note that the propagation path is similar.

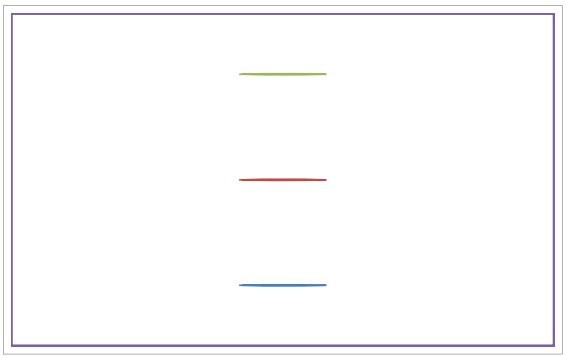

a. Original pattern

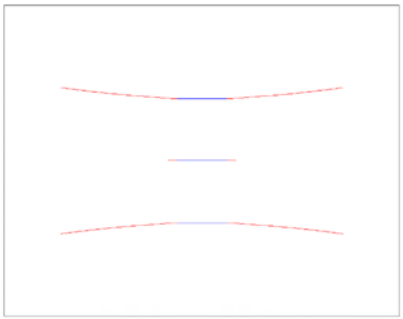

b. Dong and Atluri (2013)

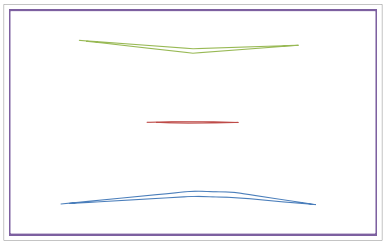

c. Splitting Method in the SCIEnCE

Figure 6.18 Example 2 - Propagation of the three parallel cracks after 9 steps

This example is interesting because the three cracks are identical in its original patterns. Thus, it is possible to use an unique local problem in order to get the jumps in displacement fields and traction fields in the Γ contour. Particularly in *step 0*, the problems are distinct only in the coordinates in which they are generated. Obviously, once the propagation process starts, the paths may become considerably different, but still a similar propagation can occur. In this case, it would be possible to reduce the number of local problems in the analysis.

The Fatigue crack growth curves for cracks A and B (analogous to Figure 6.13) are presented in the Figure 6.19. The growth of the crack B tends to a constant value when the number of cycles is greater than 10^6.

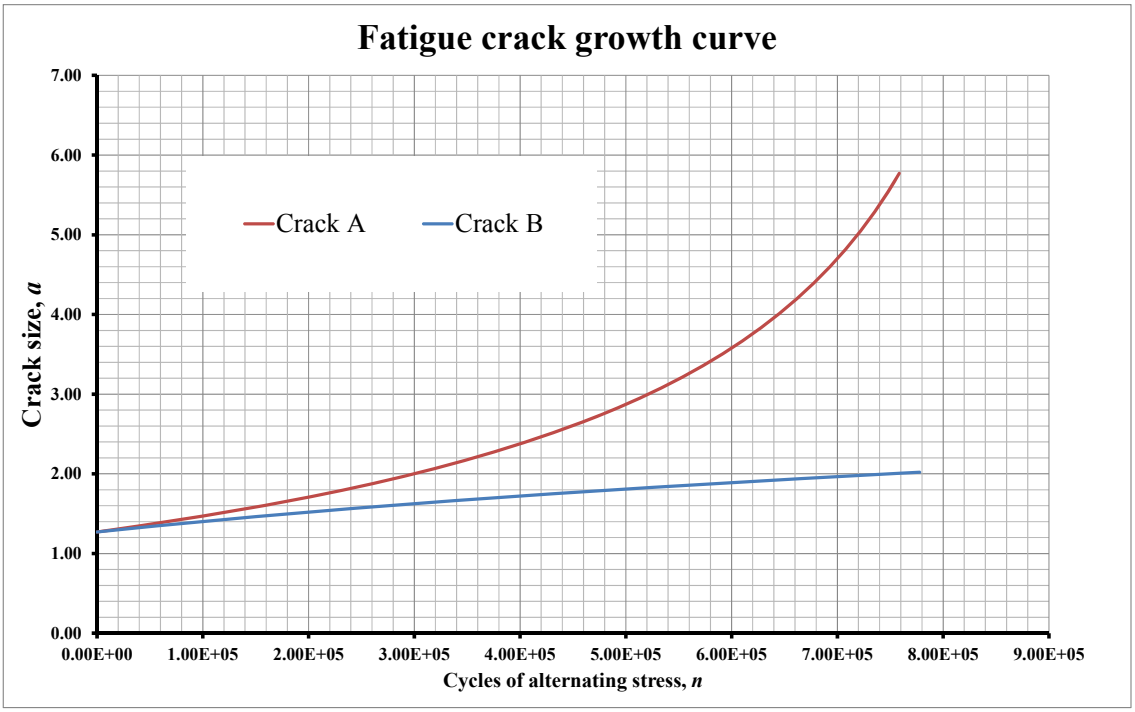

Figure 6.19 Example 2 - Propagation of the three parallel cracks after 9 steps

Finally, it is important to stress that the Splitting Method was capable to recover the phenomenon in which one crack growth shields a second crack tip, therefore reducing its crack growth. See also Figure 6.18.

6.3 Example 3: An Embedded Slanted Crack

This example was studied by Stazi, Budyn, Chessa and Belystschko (2003), using XFEM, and assessed by Dong and Atluri (2013) with SGBEM. In the present work, we have chosen it to extend the application of the Splitting Method to a problem with slanted crack.

The geometry of the problem is depicted in Figure 6.20a. By the Splitting Method, this problem was analyzed by using a very coarse mesh in the global problem $P_G^{(0)}$, as depicted in Figure 6.20b.

It is important to mention that it is possible to use different types of finite elements in the local or global problems. Particularly, in the $P_G^{(0)}$, quadrilateral elements were used.

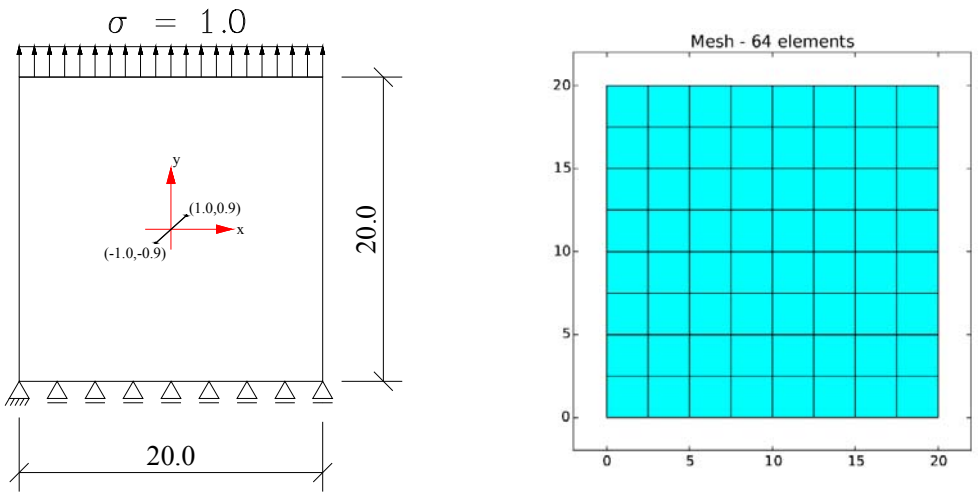

a. Geometry b. Mesh used in Splitting Method

Figure 6.20 Example 3 - An Embedded Slanted Crack

Regarding to the local problem, the mesh adopted is depicted in Figure 6.21a. Some other fields of interest obtained in the analysis of the local problems are also shown in Figure 6.21.

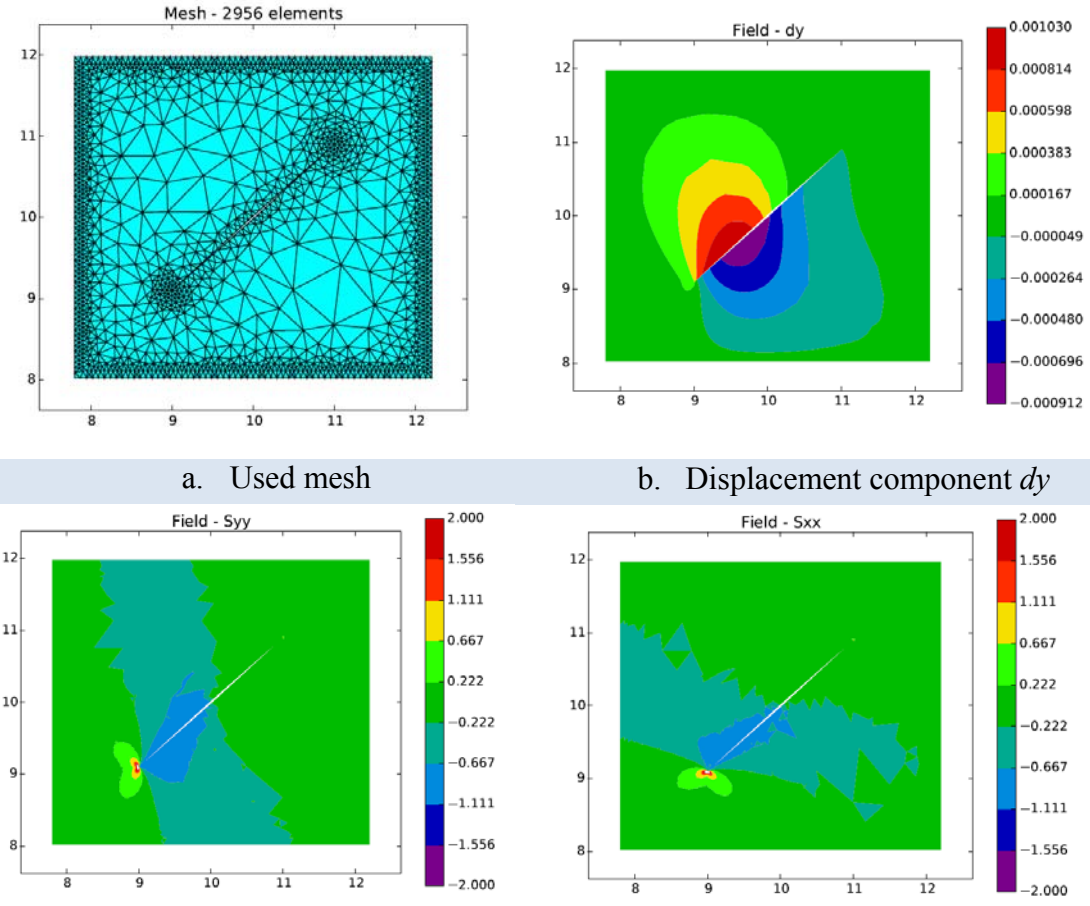

a. Used mesh b. Displacement component *dy*

c. Stress component σ_{yy} d. Stress component σ_{xx}

Figure 6.21 Example 3 - Used mesh and some fields of interest

A quadratic approximation was used for analyzing the local problems $P_L^{(k)}$'s (and also the global problems $P_G^{(k)}$'s). Thus, the number of problems (*nop*) is:

nop = 2 x 2 x 3 = 12

- 3 terms (quadratic approximation)
- 2 Modes (I and II)
- 2 "incision lines"

In relation to the boundary conditions of the local problems, all the displacements components (*dx* and *dy*) were prescribed equal to zero at the whole external boundary. In fact, for example, the displacement component *dy* is null at the external boundary, as shown in the Figure 6.21b. Another important feature that can be highlighted is the irregular distribution of the stress components far away of the crack, since the enrichment was not used in such region. Instead, the good effect of the enrichment close to the crack tip is evident, as already shown in the Example 1.

Particularly for the first local problem $P_L^{(k)}$ (*i.e.*, k = 0), in which the first segment S_{ci} of the crack is subjected to a constant normal stress component, the displacement component *dy* is shown in Figure 6.21-b and repeated in the Figure 6.22-a. Furthermore, the displacement component *dy* is shown after each one of the 5 steps of propagation.

Obviously, the constant and linear terms were applied in other local problems, not shown in the text.

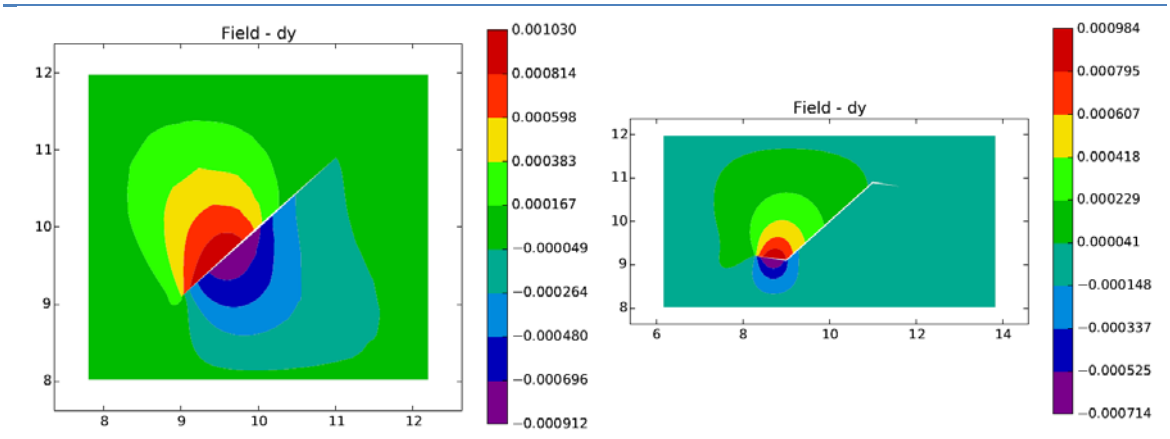

Step 0 (Original crack) Step 1

Figure 6.22 Example 3 - Propagation of the crack in 5 steps

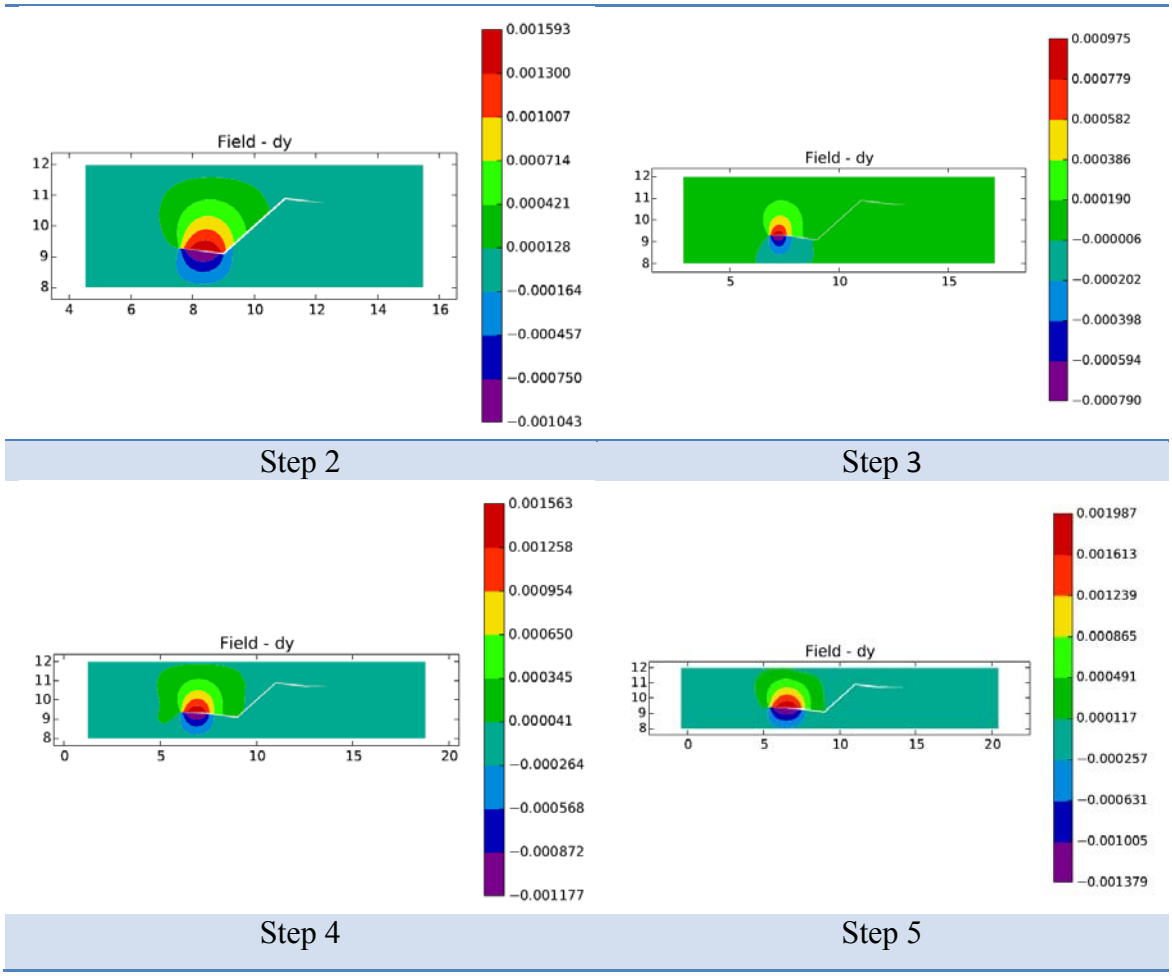

Figure 6.22 (continued) Example 3 - Propagation of the crack in 5 steps

At each step, the boundary of the local problem involves completely the propagated crack. It is possible to see that the advancement of the propagation line tends to the horizontal direction, since the critical mode of rupture is Mode I.

Referred to crack in its initial pattern (step 0), the analytical *SIFs* together with the more accurate values encountered by Stazy *et al* and Splitting Method are presented in Table 6.7 and compared to the theoretical values.

Table 6.7 Example 3 - K_I : Stazi *et al* x SCIEnCE (Splitting Method)

K_I	Stazi *et al*		SCIEnCE		K_{II}	Stazi *et al*		SCIEnCE	
	K_I	Error (%)	K_I	Error (%)		K_{II}	Error (%)	K_{II}	Error (%)
1,136	1,164	-2,51	1,137	-0,088	1,022	1,075	-5,15	0,965	5,58

The GFEM has provided a very accurate result for K_I in the Splitting Method. In relation to K_{II}, the absolute value of the error was very close to obtained by XFEM in the

work of Stazy *et al,* see Table 6.10. In the Splitting Method, it was used exactly 1633 nodes in each local problem, against 5293 used in XFEM.

6.4 Example 4: Plate subjected to a tensile load with a slanted crack and a crack associated to a hole

This example aims to demonstrate the ability of the developed framework to account for mixed opening mode and cracks associated to holes.

The geometry of the problem is depicted in Figure 6.23a. The tips of the cracks are labeled with the capital letters A, B and C. The reference values were obtained by using the Franc2D® program, and the mesh adopted to assess the reference solution is shown in Figure 23b.

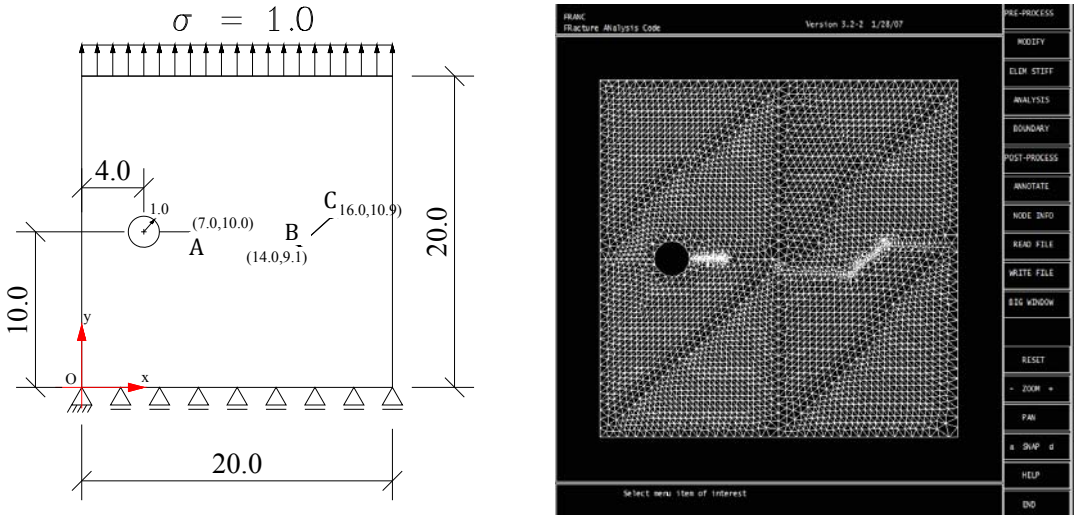

a. Geometry b. Mesh used in Franc2D®

Figure 6.23 Example 4: Domain with embedded slanted crack and hole with crack

Regarding to the local problems, the meshes adopted are depicted in Figures 6.24a and 24b. Some stress fields of interest obtained in the analysis of the local problems are also shown in Figures 6.24c and 6.24d.

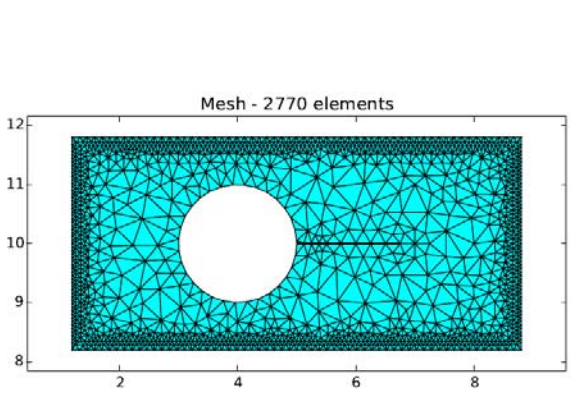

a. Used mesh for analyzing the crack attached to a hole

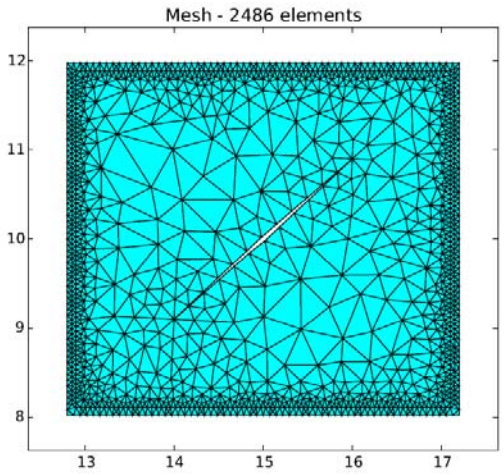

b. Used mesh for analyzing the slanted crack

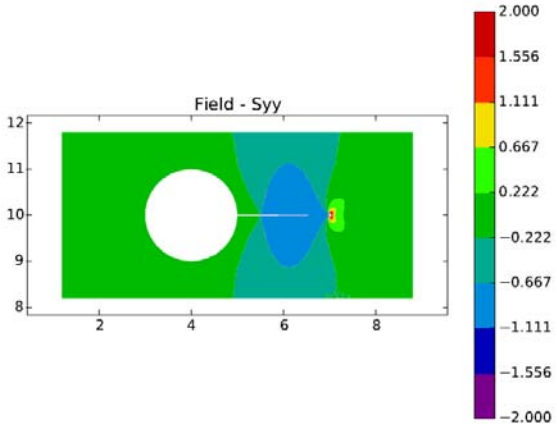

c. Stress component σ_{yy}

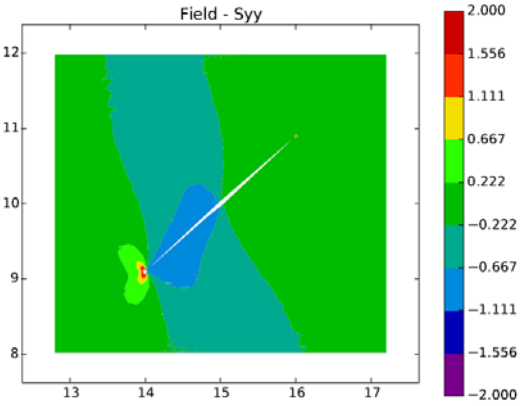

d. Stress component σ_{yy}

Figure 6.24 Example 4:Adopted meshes and stress fields of interest

A polynomial basis up to quadratic approximation was used to analyze the local problems $P_L^{(k)}$'s (as well as to recover the stress vector at the crack lines of the global sub-problems $P_G^{(k)}$'s). Thus, the number of problems (*nop*) is:

nop = 4 x 2 x 3 = 24

- 3 terms (quadratic approximation)
- 2 Modes (I and II)
- 4 "incision lines", 2 for each crack.

In relation to the boundary conditions of the local problems, the displacements components (*dx* and *dy*) were prescribed equal to zero at the whole external boundary.

Particularly for the sixtieth local problem $P_L^{(k)}$ (i.e., k = 6), in which the second segment S_{ci} of the crack is subjected to a constant normal stress component, the stress component σ_{yy} is shown in Figure 6.24c. The same component stress for the second crack and local problem k = 12, in which its first segment is subjected to a constant normal stress component, is depicted in Figure 6.24d.

The *SIFs* obtained using Franc2D® (for both *J Integral* and Displacement Correlation Technique, *DCT*) and with SCIEnCE code are presented in Table 6.8.

Table 6.8 *SIFs* obtained using Franc2D® *et al* x SCIEnCE (Splitting Method)

	Crack tip A		Crack tip B		Crack tip C	
	K_I	K_{II}	K_I	K_{II}	K_I	K_{II}
SCIEnCE	2.820	0.0280	1.264	0.968	1.248	0.973
Franc2D (DCT)	2.815	-0.0219	1.248	1.013	1.201	1.018
Franc2D (J Integral)	2.815	-0.0241	1.255	0.967	1.208	0.978

It can be observed that the results obtained using SCIEnCE are very close to those obtained with Franc2D®. It should be noted from Table 6.28 that even using Franc2D® there are some discrepancies when using the *J Integral* and Displacement Correlation Technique, especially in K_{II} values. Obviously, since both results were computed numerically, it is reasonable to expect some differences among them. This difference can be observed in Figure 6.25.

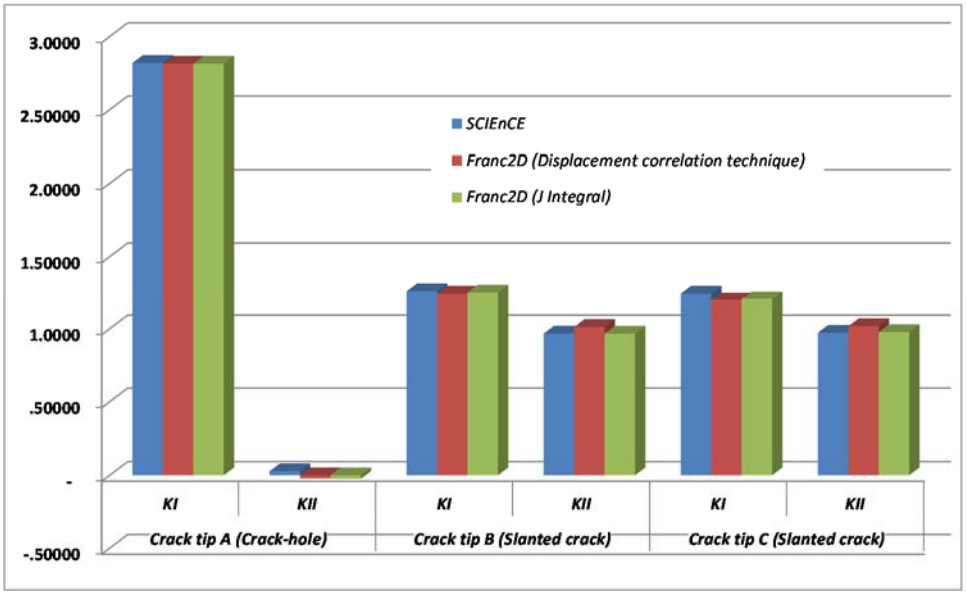

Figure 6.25 Example 4: SIFs obtained using Franc2D x SCIEnCE (Splitting Method)

6.5 Example 5: Plate subjected to a tensile load with several cracks attached to holes

The main goal of this example is to assess the efficacy of the Splitting Method for solving problems with cracks associated to holes. After the analysis, the values of *SIFs* related to all possible patterns of cracks could be computed by using the General Influence Matrix. This will be better explained at the final of the example.

This example was presented in Andersson & Babuska (2005), consisting of a plate with 36 holes and subjected to a tensile load. There is an initial distribution of cracks attached to some holes, as depicted in the Figure 6.26.

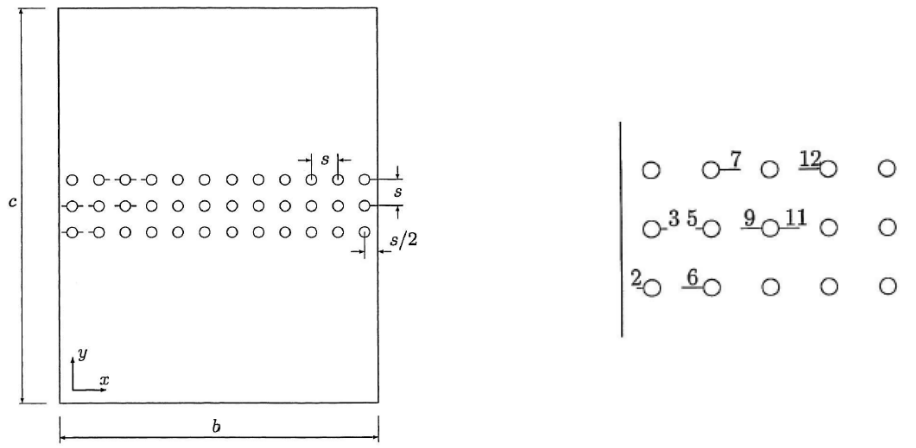

a. Geometry b. Pattern of cracks

Figure 6.26 Example 4 - Plate subjected to a tensile load, with 36 holes, and a given pattern of cracks (Andersson & Babuska, 2005)

The set of data to this example is given in Table 6.9.

Table 6.9 Example 4 - Data for analysis

Plate dimensions				
b = 216mm	c = 600 mm	t = 1 mm	ϕ_{hole} = 5 mm	s = 18 mm
Material characteristics				
Modulus of elasticity (E) = 71000 *MPa*			Poisson's ratio (v) = 0.3	
Applied load				
σ_{yy} = 100 *MPa* on the plate borders $y = 0$ and $y = c$				

In the problem $P_G^{(0)}$ and, as already mentioned, only the holes were modeled. The mesh was automatically generated by *SCIEnCE*. The generated model, as well the values for stress field σ_{yy} are depicted in Figure 6.27.

The stress concentration effect of the holes can be observed in Figure 6.27-b. This fact demands the utilization of additional terms of the polynomial basis used to approximate the stress distribution at the crack lines S_{ci}. Therefore, a quadratic approximation was adopted.

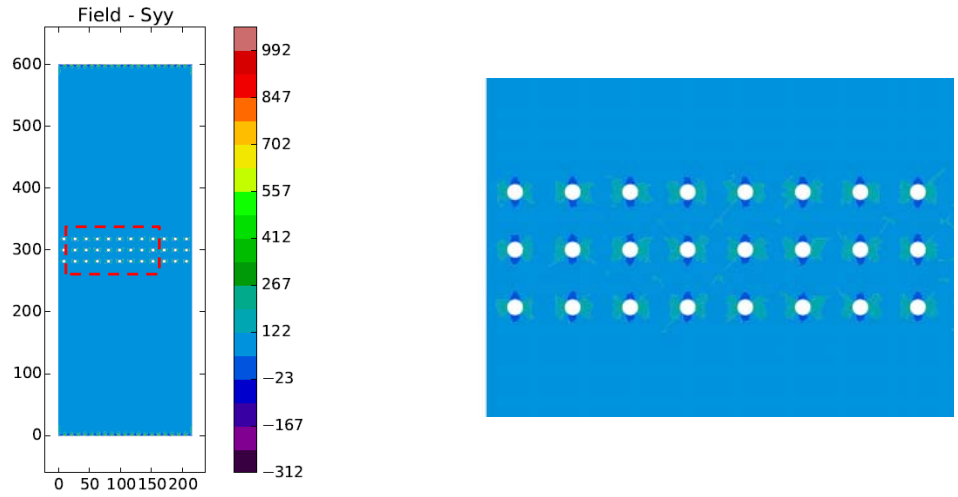

a. Plate with 36 holes: σ_{yy} in $P_G^{(0)}$

b. Stress concentration on holes borders

Figure 6.27 Example 4 - Model of $P_G^{(0)}$

A quadratic approximation was used for this example. Therefore, the number of problems (*nop*) is:

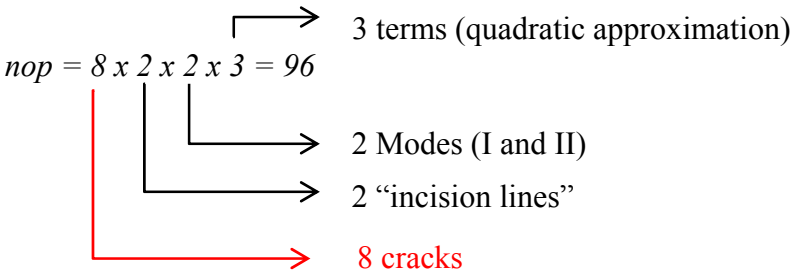

Figure 6.28 depicts the stress field for $P_L^{(k)}$, $k = 0$. This local problem is referred to crack 2, shown in the Figure 6.26-b. However, since all the cracks have the same length, and all the holes have the same radius, it is possible to use a single local problem for all cracks.

In order to improve the accuracy, enrichment was applied around the crack tip.

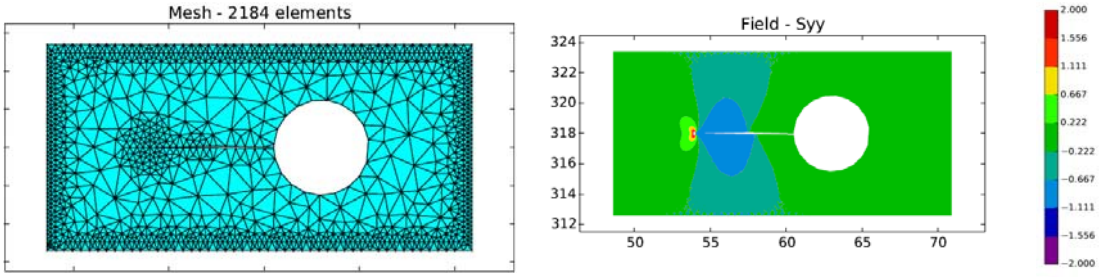

Figure 6.28 Example 4 - $P_L^{(k)}$ (cracks 2, 6, 5, 9, 12)

The results of the analysis are shown in Table 6.10. The crack numbered as "9" is the one considered the most critical in the pattern that contains all the cracks, since it presents the maximum K_I value. It can be noted that the results obtained using *SCIEnCE*, particularly for K_{II} are more accurate than that obtained by Andersson & Babuska (2005). This improved accuracy is provided by combining the refinement of the mesh with the enrichment strategy.

Table 6.10 Example 4 - Values obtained by Andersson & Babuska (2005) x *SCIEnCE*

Crack	Reference		Andersson & Babuska				*SCIEnCE*			
	K_I	K_{II}	K_I	K_{II}	error (%)		K_I	K_{II}	error (%)	
					K_I	K_{II}			K_I	K_{II}
2	492	-8.6	519	-43.4	5.49	-405	469	-6.3	4.76	-27.23
3	449	5.2	463	34	3.12	554	420	3.7	6.38	29.64
5	402	-23.3	417	-26.6	3.73	-14	397	-21.4	1.17	-8.22
6	559	-10.1	528	-24.8	5.55	-146	550	-5.3	1.55	-47.69
7	499	40.4	468	59.7	6.21	48	465	41.2	6.73	1.97
9	680	0.3	635	-11.2	6.62	3833	682	-0.9	0.36	390
11	669	-19.7	622	2.3	7.03	-112	631	-19.9	5.67	-1.10
12	510	-71.2	477	-84.2	6.47	-18	485	-67.7	4.83	-4.89

Another feature that deserves to be highlighted is the magnitude of the relative errors in values of K_{II}. Nevertheless, the K_{II} values are very small in comparison with their respective K_I values and thus this difference causes no impact in the analysis. According to Table 6.10, the relative error tends to increase, whenever reference K_{II} approaches to zero.

Besides the original pattern containing all the possible cracks, shown in Figure 6.26-b, the Splitting Method makes easier to repeat the analysis considering several

possible patterns of cracks. Particularly in this example, considering a combination of 8 possible cracks, there are $2^8 - 1 = 255$ different patterns that can be analyzed by the Splitting Method when looking for the worst scenario.

The *SIFs* referred to the complete set of possible patterns of cracks above indicated, were calculated. A resume of the maximum K_I value for each crack and its respective pattern is shown in Table 6.11.

Table 6.11 Example 4 - $K_{I,max}$ and the respective pattern of cracks

Crack	$K_{I,\,max}$	Pattern
2	473	2-6-5-9-11-7-12
3	427	6-3-5-9-11-7-12
5	467	2-3-5-9-11-12
6	568	2-6-9-11-12
7	502	2-3-11-7-12
9	702	2-6-3-5-9-11-12
11	650	2-6-3-5-9-11-7
12	515	2-6-3-5-9-7-12

An important aspect that deserves to be commented is the fact that the pattern that contains 8 cracks is not, in general, the most critical pattern. Particularly in this example, the most critical patterns were composed from 5 to 7 cracks. This kind of analyses, otherwise extremely expensive, evidences one of the main advantages of using Splitting Method.

Chapter 7: Results and discussion

The Splitting Method was originally proposed by Andersson & Babuska (2005) and has proved to be an efficient method to analyze multi-site damage problems. In these problems, where each individual crack can be harmless, the combined effects of multiple growing of several cracks can be disastrous. Aiming to further explore the potentialities of the method, some natural improvements for the Splitting Method were hereby investigated, therefore enabling the extension of its application to analyze mixed mode fracture and fatigue problems.

On the other hand, it could be very expensive to analyze such problems using numerical methods as FEM owing to the difficulties for discretizing complex geometries and patterns of the several cracks. Thus, enrichment strategies of the approximation, as the one provided by the Generalized Finite Element Method, can be interesting, furthermore avoiding costly mesh refinements. In this work, the ability of the stress functions to reproduce in the GFEM the stress fields close to the crack tips with more accuracy was confirmed.

In order to test the proposed improvements to the Splitting Method a computational code was conceived involving, since generation and analysis of each sub-problem up to linear system solution.

The main achievements and/or contributions of this work are summarized below.

Splitting Method programming: the resulting code for generating each sub-problem, as well for assembling the linear system of the unknown weights is a very important tool for future developments. Moreover, the code contains special procedures as, for instance, the creation of nodes for supporting refinement around the crack tips. Another example is the procedure dedicated to automatically apply loading at the crack surfaces. The development of this code was a very hard task, but necessary to conduce the analysis of fatigue crack growth.

FEM x GFEM: it was possible to confirm the good effects of the enrichment for improvement of the results as compared to the standard FEM. Indeed the enrichment provided better accuracy, especially in the calculus of the Stress Intensity Factors. It was clear that such a good precision is necessary to evaluate the critical angle of propagation, widely used in the Fatigue Crack Growth problems, particularly considered in this work.

Analysis of Fracture Mechanics problems considering cracks with arbitrary shapes and mixed crack opening modes: another important contribution of this work consisted in the extension of the Splitting Method to the analysis of problems containing cracks with arbitrary shapes, as explained in Chapter 2. Obviously, when cracks with arbitrary shapes are considered, mixed crack opening modes must be also taken into account. When such modeling is available, complex real-life problems can be analyzed, with emphasis on multisite damage problems. For instance, it was possible to find out the most critical pattern of cracks attached to holes in a rivet connection.

Looking for the worst scenario of multiple cracks using the Splitting Method: the developed code allows to compare several scenarios of multiple cracks and looking for the worst one, by taking the maximum value of Stress Intensity Factors (*SIFs*) as the main criterion. Using a small number of problems, it is possible to evaluate a great number of scenarios and pick the worst to continue the analysis considering the fatigue aspects.

It was also possible to note that some features of the problem in analysis can make easier the use of Splitting Method. For example, if many cracks are similar, except maybe for a rotation, the local problems related to a few cracks can be employed for many other cracks.

Analysis of fatigue problems: to analyze fatigue problems, the adopted strategy consisted of imposing an increment of length for each crack and to compute the patch of propagation in the sequence. The fatigue crack growth curve could be constructed, taking into account, for example, the Paris Law. With the aid of the computational code, it was possible to use very small increments and to perform a reasonable number of propagation steps. Doing so, it was possible to obtain more accurate results in the analysis.

Regarding suggestions for future studies, some options can be enumerated in what follows:

Extension for 3D domain: the developed computational framework can be used to analyze 3D problems. However, some aspects must be taken into account carefully as, for instance, the variation of the Stress Intensity Factors along the crack front.

Additional aspects to be modeled: In this work, the plastic zone size was assumed very small in comparison with the length of the crack. In future developments it can be possible to taking in account the effects of plasticity. Regarding the fatigue analysis, crack closure can be taken into account by contact modeling.

Furthermore, since the Dirichlet boundary conditions in global sub-problems $P_G^{(k)}$ are homogeneous, it is possible to study dynamic problems just changing the global problem $P_G^{(0)}$.

Use of other numerical methods combined with the Splitting Method: in order to improve the accuracy in the extraction of SIFs, for example, the hybrid-mixed formulation can be used. In this formulation, the SIFs can be extracted directly as an enrichment parameter. We have laid in evidence in Chapter 6 the very expressive variation among the results by using different extraction methods, which prove the importance of implementing more efficient methods. It is important to mention that the local sub-problem $P_L^{(k)}$ is the only one where the crack is modeled. Therefore, any method developed in order to improve the accuracy in the parameters related to Fracture Mechanics must be focused in this sub-problem.

References and Bibliography

ALIABADI, M.H.; ROOKE, D.P. Numerical Fracture Mechanics. Computational Mechanics Publications: Kluwer Academic Publishers, 1991.

ALVES, M.M. **Método da partição na análise de múltiplas fissuras**. Tese (Doutorado em Engenharia de Estruturas)- Escola de Engenharia de São Carlos, Universidade de São Paulo, São Carlos, 2010.

ANDERSSON, B.; BABUSKA, I.; STEHLIN, P. Reliable analysis of 3D multiple-site fatigue crack growth, Flygtekniska Forsoksanstalten, the Aeronautical Research Institute of Sweden, 1999.

BABUSKA, I.; ANDERSSON, B. The splitting method as a tool for multiple damage analysis. **Siam J. SCI comput,** v. 26, n.4, p. 1114-1145, 2005.

BABUSKA, I.; BANERJEE, U. Stable Generalized Finite Element Method (SGFEM). **Comput. Methods Appl. Mech. Engrg**, p. 91-111, 2012.

BUCHHOLZ, F-G.; CHERGUI, A.; RICHARD, H.A. Computational fracture analyses by means of virtual crack closure integral methods. MECOM99. 1999.

BARROS, F.B. **Métodos sem malha e método dos elementos finitos generalizados em análise não-linear de estruturas.** Tese (Doutoramento em Engenharia de Estruturas)- Escola de Engenharia de São Carlos, Universidade de São Paulo, São Carlos, 2002.

BAZANT, Z. P.; CHEN, E-P. Scaling of structural failure. **Americam Society of Mechanical Engineers**, v.50, n.10, 1997.

BÉCHET, E.; MINNEBO, H.; MOËS, M.; BURGARDT, B. Improved implementation and robustness study of the X-FEM for stress analysis around cracks. **International Journal for Numerical Methods in Engineering,** 2005.

BISHOP, N. W. M.; SHERRATT, F. **Finite Element Based Fatigue Calculations.** RLD Ltd. Farnham, UK. 2000.

BLOCHWITZ, C.; TIRSCHLER, W.; WEIDNER, A. Crack opening displacement and propagation rate of microstructurally short cracks. **Materials Science and Engineering,** A357, p. 264 – 269. 2003.

BROEK, D. Artificial slow crack growth under constant stress. The *R*-Curve concept in plane stress. **Engineering Fracture Mechanics,** v. 5, p. 45 -53, 1973.

_____. **Elementary Engineering Fracture Mechanics.** Kluwer Academic Publishers. Dordrecht, 1986.

BUECKNER, H. The propagation of cracks and the energy of elastic deformation. **Transactions of the American Society of Mechanical Engineers,** n.80, p. 1225-1230, 1958.

CARPINTERI, A.; PAGGI, M. Asymptotic analysis in linear elasticity: from the pioneering studies by Wieghardt and Irwin until today. **Engineering Fracture Mechanics,** 76, p. 1771-1784, 2009.

CHESSA, J. WANG, H. BELYTSCHKO, T. On the constructions of blending elements for local partition of unity enriched finite elements. **Int. J. Numer. Methods Eng.** 57, p. 1015-1038, 2003.

DECREUSE, P.Y.; POMMIER, S.; GENTOT, L.; PATTOFATTO, S. History effect in fatigue crack growth under mixed-mode loading conditions. **International Journal of Fatigue,** 31, p. 1733- 1741, 2009.

DONG, L.; ATLURI, S. N. Fracture & Fatigue Analyses: SGBEM-FEM or XFEM? **CMES**, v. 90, n. 2, p. 91-146, 2013.

DUARTE, C.A. The hp-cloud method. Tese de doutoramento. The University of Texas at Austin, 1996.

DUARTE, C.A.; BABUSKA, I.; ODEN, J.T. Generalized Finite Element Methods for three-dimensional structural mechanics problems. **Computers & Structures.** v.77, n.2, p. 215-232, 2000.

DUARTE, C.A.; KIM, D-J.; BABUSKA, I. A Global-Local Approach for the Construction of Enrichment Functions for the Generalized FEM and Its Application to Three-Dimensional Cracks. **Advances in Meshfree Techniques.** Springer, p. 1-26, 2007.

DUARTE, C.A.; KIM, D-J. Analysis and applications of a generalized finite element method with global-local enrichment functions. **Computer Methods in Applied Mechanics and Engineering,** 197, p. 487-504, 2008.

DUARTE, C.A.; ODEN, J.T. H-p Clouds – an *h-p* meshless method. **Numerical methods for Partial Differential Equations,** John Wiley & Sons, n. 12, p. 673 -705, 1996.

ELGUEDJ, T.; GRAVOUIL, A.; COMBESCURE, A. Appropriate extended functions for X-FEM simulation of plastic fracture mechanics. **Comput. Methods Appl. Mech. Engrg,** 195, p. 501-515, 2006.

FEDDERSEN, C.E. Discussion. ASTM STP 410, p. 77-79, 1967.

FETT, T.; MATTHECK, C.; MUNZ, D. On the calculation of crack opening displacement from the stress intensity factor. **Engineering Fracture Mechanics,** v. 27, n. 6, p. 697 -715, 1987.

FRIES, T.P. A corrected XFEM approximation without problems in blending elements. **Int. Journal Numerical Methods Eng,** n. 75, p. 503-532. 2008.

GRACIE, R. WANG, H. BELYTSCHKO, T. Blending in the extended finite element method by discontinuous Galerkin and assumed strain methods. **Int. J. Numer. Methods Eng,** 74, p. 1645-1669. 2008.

HUANG, R.; SUKUMAR, N.; PRÉVOST, J.H. Modeling quasi-static crack growth with the extended finite element method Part II: Numerical applications. **International Journal of Solids and Structures.** Vol.40. issue 26, pp. 7539-7552. 2003;

HUGHES, T.J.R. **The Finite Element Method –** Linear Static and Dynamic Finite Element Analysis. Dover Publications, INC. Mineola, New York. 2000.

HUTCHINSON, J.W. Singular behavior at the end of a tensile crack in a hardening material. **Journal Mech. Phys. Solids,** v.16, p. 13-31, 1968.

ISHIKAWA, H.; KITAGAWA, H.; OKAMURA, H.. J-Integral of mixed mode crack and application. **Proc. 3rd. Int. Conf. on Mechanical Behavior of Material.** Pergamon Press. Oxford, v.3, p. 447-455, 1980.

JANSSEN, M.; ZUIDEMA, J.; WANHILL, R.J.H. Fracture Mechanics. VSSD. 2006.

KACHANOV, M. Elastic solids with many cracks: a simple method of analysis. **Int. J. Solids Structures,** v. 23, n.1, p. 23-43, 1987.

KARLSSON, A.; BÄCKLUND, J. J-Integral at Loaded Crack Surfaces. **Int. Journal of Fracture,** 14, 1978.

KIM, D.J. Development, analysis and applications of the generalized finite element method with global-local enrichment functions.

KIM, J-H.; DUARTE, C.A.; PEREIRA, J.P. Analysis of interacting cracks using the generalized finite element method with global-local enrichment functions. **Journal of applied mechanics**, v.75, set. 2008.

KIM, J-H.; PAULINO, G.H. On Fracture Criteria for Mixed-Mode Crack Propagation in Functionally Graded Materials. **Mechanics of Advanced Materials and Structures**, 14, p. 227-244, 2007.

KRUEGER, R. Virtual crack closure technique: History, approach, and applications. **Appl. Mech. Rev.** v. 57, n. 2, 2004.

KZAM, A. K. L. **Formulação dual em Mecânica da Fratura Utilizando Elementos de Contorno Curvos de Ordem Qualquer.** Dissertação (Mestrado em Engenharia de Estruturas)- Escola de Engenharia de São Carlos, Universidade de São Paulo, São Carlos, 2009.

LACHENBRUCH, A.H. Depth and spacing of tension cracks. **Journal of Geophysical Research**. Vol. 66. pp 171-190. 1961.

LAN, M.; WAISMAN, H.; HARARI, I. A direct analytical method to extract mixed-mode components of strain energy release rate from Irwin's integral using extended finite element method. **International Journal for Numerical Methods in Engineering 95,** p. 1033- 1052, 2013.

LARSSON, S.G.; CARLSOON, A.J. Influence of non-singular stress terms and specimen geometry on small-scale yielding at crack tips in elastic-plastic materials. **Journal Mech. Phys. Solids,** v.21, p. 263-277, 1973.

LEONEL, E.D. Notas de aula da disciplina SET5926. Introdução à Mecânica da Fratura. Escola de Engenharia de São Carlos. Universidade de São Paulo. 2010.

LI, H.; YUAN, H.; LI, X. Assessment of low cycle fatigue crack growth under mixed-mode loading conditions by using a cohesive zone model. **International Journal of Fatigue 75,** p. 39-50, 2015.

MELENK, J.M. **On Generalized Finite Element Methods.** Tese de Doutoramento. University of Maryland, College Park. 1995.

MOËS, N.; DOLBOW, J.; BELYTSCHKO, T. A finite element method for crack growth without remeshing. **International Journal for Numerical Methods in Engineering,** 46, p. 131- 150, 1999.

MOHAMMADI, S. **Extended Finite Element Method.** Blackwell Publishing Ltd. Tehran, 2008.

NATARAJAN, S.; SONG, C. Representation of singular fields without asymptotic enrichment in the extended finite element method, **Internacional Journal for numerical methods in engineering,** 96, 13, pp. 813-841, 2013.

NIKISHKOV, G.P.; ATLURI, S.N. Calculation of fracture mechanics parameters for an arbitrary three-dimensional crack, by the "equivalent domain integral" method.

NISHIOKA, T.; ATLURI, S.N. Analytical solution for embedded elliptical cracks, and finite element alternating method for elliptical surface cracks, subject to arbitrary loadings. Engineering Fracture Mechanics, vol. 17. N.3. pp 247-268, 1983.

NUISMER, R.J. An energy release rate criterion for mixed mode fracture. **International Journal of Fracture,** v.11, n.2, p. 245-250, 1975.

ODEN, J.T.; DUARTE, C.A.M.; ZIENKIEWICZ, O.C. A New Cloud-Based *hp* Finite Element Method. **Computer Methods in Applied Mechanics and Engineering,** 153, p. 117-126. 1998.

PALANISWAMY, K. **Crack propagation under general in-plane loading.** Ph.D. Thesis, California Institute of Technology. 1972

PARK, K.; PEREIRA, J.P.; DUARTE, C.A.; PAULINO, G.H. Integration of singular enrichment functions in the generalized/ extended finite element method for three-dimensional problems. **International Journal for Numerical Methods in Engineering.** v.78, p. 1220-1257, 2009.

PEREIRA, J.P. **Extração de fatores de intensidade de tensão utilizando a solução do método dos elementos finitos generalizados.** Dissertação (Mestrado em Engenharia de Estruturas)-Escola de Engenharia de São Carlos, Universidade de São Paulo, São Carlos, 2004.

PEREIRA, J.P.; DUARTE, C.A. Extraction of stress intensity factors from generalized finite element solutions. **Engineering Analysis with Boundary Elements,** 29, p. 397-413, 2005.

PIEDADE NETO, D. **On the Generalized Finite Element Method in Nonlinear Solid Mechanics Analyses.** Escola de Engenharia de São Carlos. Tese (Doutorado em Engenharia de Estruturas). Universidade de São Paulo. São Carlos. 2013.

PIEDADE NETO, D.; FERREIRA, M.D.C.; PROENÇA, S.P.B. Generalized Finite Element Method Computation: Parallelization using Python Multiprocessing Package. **Mecánica Computacional,** Rosário, v. **XXX**, p. 3045-3061, 2011.

PROPPE, C. Probabilistc analysis of multi-site damage in aircraft fuselages. **Computational Mechanics**, v. 30, p. 323-329. 2003.

RICE, J.R. A Path Independent Integral and the Approximate Analysis of Strain Concentration by Notches and Cracks. Journal of Applied Mechanics, v. 35, p. 379-386. 1968.

RICE, J.R.; ROSENGREN, G.F. Plane Strain Deformation Near a Crack Tip in a Power-Law Hardening Material. **J. Mech. Phys. Solids,** v. 16, p. 1-12. 1968.

ROCHA, J.A.de L. Aplicação do método dos elementos finitos a problemas planos da mecânica da fratura. Dissertação de mestrado. COPPE. UFRJ. 1976.

RUBINSTEIN, A.A. Computational Aspects of Crack Path Development Simulation in Materials with Nonlinear Process Zone. **International Journal of Fracture,** v. 119, L15-L20, 2003.

SIH, G.C.; BARTHELEMY, B.M. Mixed Mode Fatigue Crack Growth Predicitions. **Engineering Fracture Mechanics**, v. 13, p. 439-451,1980.

SIH, G.C.; MOYER JR, E.T. Path Dependent Nature of Fatigue Crack Growth. **Engineering Fracture Mechanics,** v. 17, n. 3, p. 269-280, 1983.

SING, I.V.; MISHRA, B.K.; BHATTACHARYA, S.; PATIL, R.U. **The numerical simulation of fatigue crack growth using extended finite element method.** International Journal of Fatigue, v. 36**,** p. 109-119, 2012.

SHI, C.F. Relationships between the J-Integral and the crack opening displacement for stationary and extending cracks. **J. Mech. Phys. Solids,** v. 29, n. 4, p. 305 -326, 1981.

SHI, J.; CHOPP, D.; LUA, J.; SUKUMAR, N.; BELYTSCHKO, T. Abaqus implementation of extended finite element method using a level set representation for three-dimensional fatigue crack growth and life predictions. **Engineering Fracture Mechanics,** v. 77, p. 2840- 2863, 2010.

SHIBANUMA, K. UTSUNOMIYA T. Reformulation of XFEM based on PUFEM for solving problem caused by blending elements. **Finite Elem. Anal Des 45**, p. 806-816, 2009.

SMITH, I.M.; GRIFFITHS, D.V. **Programming the Finite Element Method.** John Wiley & Sons Ltd. England, 2004

STAZI, F.L.; BUDYN, E.; CHESSA, J.; BELYTSCHKO, T. An extended finite element method with higher-order elements for curved cracks. **Computational Mechanics,** v. 31, issue 1-2**,** pp..38-48, 2003.

VARFOLOMEEV, I.; BURDACK, M.; MOROZ, S.; SIEGELE, D.; KADAU, K. Fatigue crack growth rates and paths in two planar specimens under mixed mode loading. **International Journal of Fatigue,** v. 58, p. 12-19, 2014.

VOJTEK, T.; POKLUDA, J.; HORNÍKOVÁ, J.; ŠANDERA, P.; SLÁMECKA, K. Description of fatigue crack growth under modes II, III and II + III in terms of J-integral. **Procedia Materials Science,** v. 3, p. 835-840, 2014.

WANG, C.H. **Introduction to Fracture Mechanics.** DSTO Aeronautical and Maritime Research Laboratory. Melbourne, 1996.

WANG, S.S.; YAU, J.F.; CORTEN, H.T. A mixed-mode crack analysis of rectilinear anisotropic solids using conservation laws of elasticity. **International Journal of Fracture,** v. 16, n. 3, 1980.

WESTERGAARD, H.M. Bearing Pressures and Cracks. **Journal of Applied Mechanics.** v. 61. Pp A49-A53. 1939.

Appendix A: Westergaard Complex Stress Functions

A.1 Introduction to the general complex functions

A complex function *f(z)* is called analytic if its derivative $f'(z)$ does exist. An immediately consequence of this definition is that if the primitive of a function *f(z)* does exist, then this primitive also is an analytic function.

For a given analytic function, the *Cauchy-Riemann* equations can be derived. Defining the complex variable $z = x + i \cdot y$, it is possible to write:

$$\frac{\partial f}{\partial x} = \frac{df}{dz}\frac{\partial z}{\partial x} = \frac{df}{dz} = f'(z) \tag{A.1}$$

$$\frac{\partial f}{\partial y} = \frac{df}{dz}\frac{\partial z}{\partial y} = \frac{df}{dz} \cdot i = f'(z) \cdot i$$

Therefore:

$$\frac{\partial f}{\partial x} = \frac{\partial Ref(z)}{\partial x} + i \cdot \frac{\partial Imf(z)}{\partial x} = f'(z) \tag{A.2}$$

$$\frac{\partial f}{\partial y} = \frac{\partial Ref(z)}{\partial y} + i \cdot \frac{\partial Imf(z)}{\partial x} = f'(z) \cdot i$$

By eliminating the term $f'(z)$ exploring the equality with $f'(z) \cdot i$, one obtains:

$$i \cdot \left(\frac{\partial Ref(z)}{\partial x} + i \cdot \frac{\partial Imf(z)}{\partial x}\right) = \frac{\partial Ref(z)}{\partial y} + i \cdot \frac{\partial Imf(z)}{\partial y} \tag{A.3}$$

Finally, the Cauchy-Riemann equations are present in the following manner:

$$\frac{\partial Ref(z)}{\partial x} = \frac{\partial Imf(z)}{\partial y}, \frac{\partial Ref(z)}{\partial y} = -\frac{\partial Imf(z)}{\partial x} \tag{A.4}$$

The real part (or imaginary part) can be identified, for example, through a second order derivative as follows:

$$\frac{\partial^2 Ref(z)}{\partial x^2} = \frac{\partial^2 Imf(z)}{\partial y \partial x}, \frac{\partial^2 Ref(z)}{\partial y^2} = -\frac{\partial^2 Imf(z)}{\partial x \partial y} \tag{A.5}$$

Consequently:

$$\frac{\partial^2 Ref(z)}{\partial x^2} + \frac{\partial^2 Ref(z)}{\partial y^2} = 0 \tag{A.6}$$

or

$$\nabla^2 Ref(z) = 0 \tag{A.7}$$

An identical relation can be obtained by exploring instead the equality with $f'(z)$ in (A.2). It is clear that the real part of the complex function satisfies the Laplace's equation condition:

$$\frac{\partial^2 Ref(z)}{\partial x^2} + \frac{\partial^2 Ref(z)}{\partial y^2} = 0 \tag{A.8}$$

A.2 Westergaard complex stress functions

Westergaard introduced a specific Airy stress function Φ, using an analytic complex stress function $\phi(z)$, for which is assumed the existence of the first and second orderintegral functions:

$$\Phi = Re\,\bar{\bar{\phi}}(z) + y \cdot Im\,\bar{\phi}(z) \tag{A.9}$$

Where:

i. $\bar{\phi}(z)$ is the first order integral of $\phi(z)$;

ii. $\bar{\bar{\phi}}(z)$ is the second order integral of $\phi(z)$.

In order to be an Airy stress function, Φ must hold the bi-harmonic equation. It is important to verify that the image of function is the real set number. Since the function $\bar{\bar{\phi}}(z)$ is an analytic function, it is clear that the first part of the equation (A.9) is a harmonic function that obeys the Laplace's equation and, therefore, also obeys the bi-harmonic equation. In relation to the second part of the equation, we can consider a function $y \cdot \varphi$, where φ is harmonic. Therefore:

$$\nabla^2(y \cdot \varphi) = \frac{\partial^2(y \cdot \varphi)}{\partial x^2} + \frac{\partial^2(y \cdot \varphi)}{\partial y^2} = \frac{\partial}{\partial x}\left(y \cdot \frac{\partial \varphi}{\partial x}\right) + \frac{\partial}{\partial y}\left(\varphi + y \cdot \frac{\partial \varphi}{\partial y}\right) = y \cdot \frac{\partial^2 \varphi}{\partial x^2} + \frac{\partial \varphi}{\partial y} + \frac{\partial \varphi}{\partial y} + y \cdot \frac{\partial^2 \varphi}{\partial x^2} = 2 \cdot \frac{\partial \varphi}{\partial y} \tag{A.10}$$

Therefore:

$$\nabla^2 \nabla^2 (y \cdot \varphi) = \nabla^2 \left(2 \cdot \frac{\partial \varphi}{\partial y}\right) = 2 \cdot \frac{\partial}{\partial y} \nabla^2 \varphi = 0 \tag{A.11}$$

Therefore, the function Φ defined in terms of the complex stress functions $\phi(z)$, which was introduced by Westergaard, can be characterized as an Airy stress function.

The next step is to represent the stress components σ_{xx}, σ_{yy} and τ_{xy} in terms of complex stress functions $\phi(z)$. Therefore, it is possible to find:

$$\sigma_{xx} = \frac{\partial^2 \Phi}{\partial y^2} = \frac{\partial}{\partial y}\left\{\frac{\partial}{\partial y}\left[Re\,\bar{\bar{\phi}}(z)\right] + \frac{\partial}{\partial y}\left[\,y \cdot Im\,\bar{\phi}(z)\right]\right\}$$

$$= \frac{\partial}{\partial y}\left\{-\frac{\partial}{\partial x}\left[Im\,\bar{\bar{\phi}}(z)\right] + Im\,\bar{\phi}(z) + y \cdot \frac{\partial}{\partial x} Re\,\bar{\phi}(z)\right\}$$

$$= \frac{\partial}{\partial y}\{-Im\,\bar{\phi}(z) + Im\,\bar{\phi}(z) + y \cdot Re\,\phi(z)\}$$

$$= Re\,\phi(z) + y \cdot \frac{\partial}{\partial y} Re\,\phi(z) = Re\,\phi(z) - y \cdot \frac{\partial}{\partial x} Im\,\phi(z)$$

$$= Re\,\phi(z) - y \cdot Im\,\phi'(z) \qquad \text{(A.12a)}$$

Analogously, we have for the other components:

$$\sigma_{yy} = Re\,\phi(z) + y \cdot Im\,\phi'(z) \qquad \text{(A.12b)}$$

$$\tau_{xy} = -y \cdot Re\,\phi'(z) \qquad \text{(A.12c)}$$

The expressions given above provide the stress components for any Westergaard complex stress functions. The solution of the stress field concerned to a bi-dimensional elastic problem is found by choosing a stress function $\phi(z)$ such that all the boundary conditions are fulfilled. However, it is important to note that such aspect limits the use of a Westergaard complex stress function.

A.3 Biaxially loaded plate

Let be an infinite plate containing a crack of length equal to *2a*. The plate is biaxially loaded by a unit traction, as depicted in Figure A.1:

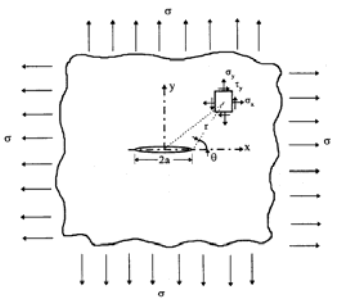

Figure A.1 **Crack of length equal to *2a,* embedded in a remotely loaded plate (Source: Wang, 1996)**

The boundary conditions from this problem are:

i) $\sigma_{yy} = 0$ for $-a < x < a$ and $y = 0$

ii) $\sigma_{xx} \to \sigma$ and $\sigma_{yy} \to \sigma$ for $x \to \pm\infty$ or y $\to \pm\infty$

iii) $\sigma_{yy} \to \infty$ for $x \to \pm a$ and $y = 0$

The first condition arises from the fact that the stress fields are null in the crack faces. The second conditions states that far away of the crack the stress will be equal to applied tension. As already mentioned in Chapter2, the condition (iii) is a characteristic of the fracture mechanics problems and is obtained from the analysis. However, since it is necessary to find out a complex function that encompasses this condition, it can be stated as a boundary condition.

It is necessary to find a function $\phi(z)$ such that the stress components, defined according to equations (A.12) fulfill the boundary conditions. This function should be like:

$$\phi(z)=\frac{\sigma \cdot z}{\sqrt{z^2-a^2}} \qquad \text{(A.13)}$$

It is possible to verify that the boundary conditions are satisfied:

1. If $y = 0$, it follows that $z = x$ and, therefore:

$$\phi(z) = \phi(x)=\frac{\sigma \cdot x}{\sqrt{x^2-a^2}} \qquad \text{(A.14)}$$

Therefore, bearing in mind that $|x| < a$ and, in the crack surface, the function $\phi(z)$ has only the imaginary part, i.e. $Re\ \phi(z) = 0$. Consequently:

$$\sigma_{yy} = Re\ \phi(z) + y \cdot Im\ \phi'(z) = 0$$

2. For $x \to \pm\infty$ or $y \to \pm\infty$, i.e., $|z| \to \infty$, the equation (A.13) becomes $\phi(z)=\sigma$. Therefore, as $Im\ \phi(z) = 0$, it follows that:

$$\sigma_{xx} = \sigma_{yy} = Re\ \phi(z) = \sigma \qquad \text{(A.15)}$$

Moreover, for $z = \pm a$, it is possible to conclude that $\phi(z)=\infty$. Therefore, in the crack tip ($y = 0$ and, thus, $z = x$) the stress component σ_{yy} becomes singular:

$$\sigma_{yy} = Re\ \phi(z) \to \infty \qquad \text{(A.16)}$$

A.4 The Stress Intensity Factor (SIF) referred to Mode I

In this section, it will be convenient to translate the origin of the coordinate system to the crack tip at $z = a$ by introducing the variable $\eta = z - a$. The complex stress function $\phi(z)$ becomes:

$$\phi(\eta)=\frac{\sigma}{\sqrt{1-\frac{a^2}{(a+\eta)^2}}} = \frac{\sigma(a+\eta)}{\sqrt{(a+\eta)^2-a^2}} \qquad \text{(A.17)}$$

Close to the crack tip, or else, $|\eta| \ll a$, the stress function can be approximated by:

$$\phi(\eta) \approx \frac{\sigma a}{\sqrt{2a\eta}} = \sigma\sqrt{\frac{a}{2}} \cdot \eta^{-1/2} \tag{A.18}$$

In polar coordinates, i.e., considering $\eta = re^{i\theta}$, it is possible to write:

$$\phi(\eta) = \sigma\sqrt{\frac{a}{2}} \cdot r^{-1/2} e^{(-1/2)i\theta} = \sigma\frac{\sqrt{\pi a}}{\sqrt{2\pi r}} e^{(-1/2)i\theta} \tag{A.19}$$

In order to assess the stress components by using the equations (A.12), it is necessary to calculate the first derivative of the function $\phi(\eta)$:

$$\phi'^{(\eta)} = \sigma\sqrt{\frac{a}{2}} \cdot (-1/2)\,\eta^{-3/2} = \sigma\sqrt{\frac{a}{2}} \cdot (-1/2)\left(re^{i\theta}\right)^{-3/2} = \frac{\sigma}{2r}\frac{\sqrt{\pi a}}{\sqrt{2\pi r}} - e^{(-3/2)i\theta} \tag{A.20}$$

Considering the identity $re^{i\theta} = r(cos\theta + i \cdot sen\theta)$, the expressions to stress components can be written in the following manner:

$$Re\ \phi(\eta) = \sigma\frac{\sqrt{\pi a}}{\sqrt{2\pi r}} cos\frac{\theta}{2} \tag{A.21a}$$

$$Re\ \phi'(\eta) = -\frac{\sigma}{2r} \cdot \frac{\sqrt{\pi a}}{\sqrt{2\pi r}} cos\frac{3\theta}{2} \tag{A.21b}$$

$$y \cdot Im\ \phi'(\eta) = r \cdot sen\theta\,\frac{\sigma}{2r} \cdot \frac{\sqrt{\pi a}}{\sqrt{2\pi r}} sen\frac{3\theta}{2} = \frac{\sigma\sqrt{\pi a}}{\sqrt{2\pi r}} sen\frac{\theta}{2} cos\frac{\theta}{2} sen\frac{3\theta}{2} \tag{A.22b}$$

After some substitutions and algebraic changes, it is possible to obtain the stress components, that are valid near to the crack tip, in a biaxially loaded plate:

$$\sigma_{xx} = \frac{\sigma\sqrt{\pi a}}{\sqrt{2\pi r}} cos\frac{\theta}{2}\left(1 - sen\frac{\theta}{2} sen\frac{3\theta}{2}\right) \tag{A.23a}$$

$$\sigma_{yy} = \frac{\sigma\sqrt{\pi a}}{\sqrt{2\pi r}} cos\frac{\theta}{2}\left(1 + sen\frac{\theta}{2} sen\frac{3\theta}{2}\right) \tag{A.23b}$$

$$\tau_{xy} = \frac{\sigma\sqrt{\pi a}}{\sqrt{2\pi r}} sen\frac{\theta}{2} cos\frac{\theta}{2} sen\frac{3\theta}{2} \tag{A.23c}$$

The enrichment functions presented in the Chapter 2 arises from the equations (A.23).

Appendix B: Procedure to find the element which the point belongs to

This functionality is relevant because it uses an iterative method in the analysis, what can increase the computation effort.

Let's consider the mesh of a global sub-problem $\boldsymbol{P}_{\boldsymbol{G}}^{(\mathbf{0})}$. In the chapter 3 was stated that there is no cracks in this kind of problem. However, it is necessary to evaluate the traction vector in some points placed in S_{ci}, on the plane of crack surface. Let P be a point among them.

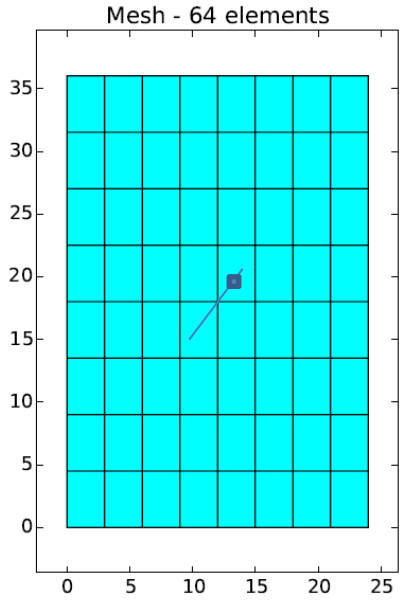

Figure B.1 Point P placed in S_{ci}

It is important to remember the relation of the natural coordinates of the finite elements:

$$\xi_1 = \frac{1}{2A} \cdot [x_2 y_3 - x_3 y_2 + x(y_2 - y_3) + y(x_3 - x_2)] \quad \text{(B.1)}$$

$$\xi_2 = \frac{1}{2A} \cdot [x_3 y_1 - x_1 y_3 + x(y_3 - y_1) + y(x_1 - x_3)] \quad \text{(B.2)}$$

Fixing ξ_1 and ξ_2, it is clear that, for arbitrary coordinates x^* and y^* arises an error:

$$f_1(x, y) = \frac{1}{2A} \cdot [x_2 y_3 - x_3 y_2 + x(y_2 - y_3) + y(x_3 - x_2)] - \xi_1 \quad \text{(B.3)}$$

$$f_1(x, y) = \frac{1}{2A} \cdot [x_3 y_1 - x_1 y_3 + x(y_3 - y_1) + y(x_1 - x_3)] - \xi_2 \quad \text{(B.4)}$$

Using the Newthon-Raphson method, we have:

$$f_1(x,y) + \frac{\partial f_1(x,y)}{\partial x} \cdot \Delta x + \frac{\partial f_1(x,y)}{\partial y} \cdot \Delta y = 0 \tag{B.5}$$

$$f_2(x,y) + \frac{\partial f_2(x,y)}{\partial x} \cdot \Delta x + \frac{\partial f_2(x,y)}{\partial y} \cdot \Delta y = 0 \tag{B.6}$$

In matrix notation:

$$\begin{bmatrix} \frac{\partial f_1(x,y)}{\partial x} & \frac{\partial f_1(x,y)}{\partial y} \\ \frac{\partial f_2(x,y)}{\partial x} & \frac{\partial f_2(x,y)}{\partial y} \end{bmatrix} \begin{Bmatrix} \Delta x \\ \Delta y \end{Bmatrix} = \begin{Bmatrix} f_1(x,y) \\ f_2(x,y) \end{Bmatrix} \tag{B.7}$$

$$\begin{Bmatrix} \Delta x \\ \Delta y \end{Bmatrix} = \begin{bmatrix} \frac{\partial f_1(x,y)}{\partial x} & \frac{\partial f_1(x,y)}{\partial y} \\ \frac{\partial f_2(x,y)}{\partial x} & \frac{\partial f_2(x,y)}{\partial y} \end{bmatrix}^{-1} \begin{Bmatrix} f_1(x,y) \\ f_2(x,y) \end{Bmatrix} \tag{B.8}$$

$$\begin{Bmatrix} \mathrm{x}_{i+1} \\ y_{i+1} \end{Bmatrix} = \begin{Bmatrix} \mathrm{x}_i \\ y_i \end{Bmatrix} + \begin{bmatrix} \left.\frac{\partial f_1(x,y)}{\partial x}\right|_{x_i,y_i} & \left.\frac{\partial f_1(x,y)}{\partial y}\right|_{x_i,y_i} \\ \left.\frac{\partial f_2(x,y)}{\partial x}\right|_{x_i,y_i} & \left.\frac{\partial f_2(x,y)}{\partial y}\right|_{x_i,y_i} \end{bmatrix}^{-1} \begin{Bmatrix} f_1(x_i,y_i) \\ f_2(x_i,y_i) \end{Bmatrix} \tag{B.9}$$

The method must be applied for each element in the mesh. If the point *P* belongs to the referred element, three conditions must be fulfilled:

1. $0 \leq \xi_1 \leq 1$;
2. $0 \leq \xi_2 \leq 1$;
3. $\xi_1 + \xi_2 \leq 1$.

Appendix C: Sub-matrices of the $[GI]_G$

Sub-matrices of the $[GI]_G$ matrix.

$$[GI]_G = \begin{bmatrix} [cQ_{I,1t}^{(I,1)}] & [cQ_{I,1t}^{(II,1)}] & [cQ_{I,1t}^{(I,2)}] & [cQ_{I,1t}^{(II,2)}] & [cQ_{I,1t}^{(I,3)}] & [cQ_{I,1t}^{(II,3)}] & \cdots & [cQ_{I,1t}^{(II,2I)}] \\ [cQ_{II,1t}^{(I,1)}] & [cQ_{II,1t}^{(II,1)}] & [cQ_{II,1t}^{(I,2)}] & [cQ_{II,1t}^{(II,2)}] & [cQ_{II,1t}^{(I,3)}] & [cQ_{II,1t}^{(II,3)}] & \cdots & [cQ_{II,1t}^{(II,2I)}] \\ [cQ_{I,2t}^{(I,1)}] & [cQ_{I,2t}^{(II,1)}] & [cQ_{I,2p}^{(I,2)}] & [cQ_{I,2t}^{(II,2)}] & [cQ_{I,2t}^{(I,3)}] & [cQ_{I,2t}^{(II,3)}] & \cdots & [cQ_{I,2t}^{(II,2I)}] \\ [cQ_{II,2t}^{(I,1)}] & [cQ_{II,2t}^{(II,1)}] & [cQ_{II,2t}^{(I,2)}] & [cQ_{II,2t}^{(II,2)}] & [cQ_{II,2t}^{(I,3)}] & [cQ_{II,2t}^{(II,3)}] & \cdots & [cQ_{II,2t}^{(II,2I)}] \\ [cQ_{I,3t}^{(I,1)}] & [cQ_{I,3t}^{(II,1)}] & [cQ_{I,3t}^{(I,2)}] & [cQ_{I,3t}^{(II,2)}] & [cQ_{I,3t}^{(I,3)}] & [cQ_{I,3t}^{(II,3)}] & \cdots & [cQ_{I,3t}^{(II,2I)}] \\ [cQ_{II,3t}^{(I,1)}] & [cQ_{II,3t}^{(II,1)}] & [cQ_{II,3t}^{(I,2)}] & [cQ_{II,3t}^{(II,2)}] & [cQ_{II,3t}^{(I,3)}] & [cQ_{II,3t}^{(II,3)}] & \cdots & [cQ_{II,3t}^{(II,2I)}] \\ \vdots & \vdots & \vdots & \vdots & \vdots & \vdots & \ddots & \vdots \\ [cQ_{II,2It}^{(I,1)}] & [cQ_{II,2It}^{(II,1)}] & [cQ_{II,2It}^{(I,2)}] & [cQ_{II,2It}^{(II,1)}] & [cQ_{II,2It}^{(I,3)}] & [cQ_{II,2It}^{(II,3)}] & \cdots & [cQ_{II,2It}^{(II,2I)}] \end{bmatrix}$$

1. 1st. line:

$$\left[cQ_{I,1p}^{(I,1)}\right]=\begin{bmatrix}\int_0^{a_1}\left(c_{1,1}^{I(1)}\cdot Q_{y,1}+\cdots+c_{1,J}^{I(1)}Q_{y,J}\right)Q_{y,1}\partial\xi & \int_0^{a_1}\left(c_{1,1}^{I(2)}\cdot Q_{y,1}+\cdots+c_{1,J}^{I(2)}Q_{y,J}\right)Q_{y,1}\partial\xi & \cdots & \int_0^{a_1}\left(c_{1,1}^{I(J)}\cdot Q_{y,1}+\cdots+c_{1,J}^{I(J)}Q_{y,J}\right)Q_{y,1}\partial\xi\\ \int_0^{a_1}\left(c_{1,1}^{I(1)}\cdot Q_{y,1}+\cdots+c_{1,J}^{I(1)}Q_{y,J}\right)Q_{y,2}\partial\xi & \int_0^{a_1}\left(c_{1,1}^{I(2)}\cdot Q_{y,1}+\cdots+c_{1,J}^{I(2)}Q_{y,J}\right)Q_{y,2}\partial\xi & \cdots & \int_0^{a_1}\left(c_{1,1}^{I(J)}\cdot Q_{y,1}+\cdots+c_{1,J}^{I(J)}Q_{y,J}\right)Q_{y,2}\partial\xi\\ \vdots & \vdots & \ddots & \vdots\\ \int_0^{a_1}\left(c_{1,1}^{I(1)}\cdot Q_{y,1}+\cdots+c_{1,J}^{I(1)}Q_{y,J}\right)Q_{y,J}\partial\xi & \int_0^{a_1}\left(c_{1,1}^{I(2)}\cdot Q_{y,1}+\cdots+c_{1,J}^{I(2)}Q_{y,J}\right)Q_{y,J}\partial\xi & \cdots & \int_0^{a_1}\left(c_{1,1}^{I(J)}\cdot Q_{y,1}+\cdots+c_{1,J}^{I(J)}Q_{y,J}\right)Q_{y,J}\partial\xi\end{bmatrix}$$

$$\left[cQ_{I,1p}^{(II,1)}\right]=\begin{bmatrix}\int_0^{a_1}\left(c_{1,1}^{I(J+1)}\cdot Q_{y,1}+\cdots+c_{1,J}^{I(J+1)}Q_{y,J}\right)Q_{y,1}\partial\xi & \int_0^{a_1}\left(c_{1,1}^{I(J+2)}\cdot Q_{y,1}+\cdots+c_{1,J}^{I(J+2)}Q_{y,J}\right)Q_{y,1}\partial\xi & \cdots & \int_0^{a_1}\left(c_{1,1}^{I(2J)}\cdot Q_{y,1}+\cdots+c_{1,J}^{I(2J)}Q_{y,J}\right)Q_{y,1}\partial\xi\\ \int_0^{a_1}\left(c_{1,1}^{I(J+1)}\cdot Q_{y,1}+\cdots+c_{1,J}^{I(J+1)}Q_{y,J}\right)Q_{y,2}\partial\xi & \int_0^{a_1}\left(c_{1,1}^{I(J+2)}\cdot Q_{y,1}+\cdots+c_{1,J}^{I(J+2)}Q_{y,J}\right)Q_{y,2}\partial\xi & \cdots & \int_0^{a_1}\left(c_{1,1}^{I(2J)}\cdot Q_{y,1}+\cdots+c_{1,J}^{I(2J)}Q_{y,J}\right)Q_{y,2}\partial\xi\\ \vdots & \vdots & \ddots & \vdots\\ \int_0^{a_1}\left(c_{1,1}^{I(J+1)}\cdot Q_{y,1}+\cdots+c_{1,J}^{I(J+1)}Q_{y,J}\right)Q_{y,J}\partial\xi & \int_0^{a_1}\left(c_{1,1}^{I(J+2)}\cdot Q_{y,1}+\cdots+c_{1,J}^{I(J+2)}Q_{y,J}\right)Q_{y,J}\partial\xi & \cdots & \int_0^{a_1}\left(c_{1,1}^{I(2J)}\cdot Q_{y,1}+\cdots+c_{1,J}^{I(2J)}Q_{y,J}\right)Q_{y,J}\partial\xi\end{bmatrix}$$

$$\vdots$$

$$\left[cQ_{I,1p}^{(II,2I)}\right]=\begin{bmatrix}\int_0^{a_1}\left(c_{1,1}^{I(4J(I-1)+3J+1)}\cdot Q_{y,1}+\cdots+c_{1,J}^{I(4J(I-1)+3J+1)}Q_{y,J}\right)Q_{y,1}\partial\xi & \int_0^{a_1}\left(c_{1,1}^{I(4J(I-1)+3J+2)}\cdot Q_{y,1}+\cdots+c_{1,J}^{I(4J(I-1)+3J+2)}Q_{y,J}\right)Q_{y,1}\partial\xi & \cdots & \int_0^{a_1}\left(c_{1,1}^{I(4IJ)}\cdot Q_{y,1}+\cdots+c_{1,J}^{I(4IJ)}Q_{y,J}\right)Q_{y,1}\partial\xi\\ \int_0^{a_1}\left(c_{1,1}^{I(4J(I-1)+3J+1)}\cdot Q_{y,1}+\cdots+c_{1,J}^{I(4J(I-1)+3J+1)}Q_{y,J}\right)Q_{y,2}\partial\xi & \int_0^{a_1}\left(c_{1,1}^{I(4J(I-1)+3J+2)}\cdot Q_{y,1}+\cdots+c_{1,J}^{I(4J(I-1)+3J+2)}Q_{y,J}\right)Q_{y,2}\partial\xi & \cdots & \int_0^{a_1}\left(c_{1,1}^{I(4IJ)}\cdot Q_{y,1}+\cdots+c_{1,J}^{I(4IJ)}Q_{y,J}\right)Q_{y,2}\partial\xi\\ \vdots & \vdots & \ddots & \vdots\\ \int_0^{a_1}\left(c_{1,1}^{I(4J(I-1)+3J+1)}\cdot Q_{y,1}+\cdots+c_{1,J}^{I(4J(I-1)+3J+1)}Q_{y,J}\right)Q_{y,J}\partial\xi & \int_0^{a_1}\left(c_{1,1}^{I(4J(I-1)+3J+2)}\cdot Q_{y,1}+\cdots+c_{1,J}^{I(4J(I-1)+3J+2)}Q_{y,J}\right)Q_{y,J}\partial\xi & \cdots & \int_0^{a_1}\left(c_{1,1}^{I(4IJ)}\cdot Q_{y,1}+\cdots+c_{1,J}^{I(4IJ)}Q_{y,J}\right)Q_{y,J}\partial\xi\end{bmatrix}$$

2. 2nd. line:

$$\left[cQ_{II,1p}^{(I,1)}\right]=\begin{bmatrix}\int_0^{a_1}\left(c_{1,1}^{II(1)}\cdot Q_{x,1}+\cdots+c_{1,J}^{II(1)}Q_{x,J}\right)Q_{x,1}\partial\xi & \int_0^{a_1}\left(c_{1,1}^{II(2)}\cdot Q_{x,1}+\cdots+c_{1,J}^{II(2)}Q_{x,J}\right)Q_{x,1}\partial\xi & \cdots & \int_0^{a_1}\left(c_{1,1}^{II(J)}\cdot Q_{x,1}+\cdots+c_{1,J}^{II(J)}Q_{x,J}\right)Q_{x,1}\partial\xi\\ \int_0^{a_1}\left(c_{1,1}^{II(1)}\cdot Q_{x,1}+\cdots+c_{1,J}^{II(1)}Q_{x,J}\right)Q_{x,2}\partial\xi & \int_0^{a_1}\left(c_{1,1}^{II(2)}\cdot Q_{x,1}+\cdots+c_{1,J}^{II(2)}Q_{x,J}\right)Q_{x,2}\partial\xi & \cdots & \int_0^{a_1}\left(c_{1,1}^{II(J)}\cdot Q_{x,1}+\cdots+c_{1,J}^{I(J)}Q_{x,J}\right)Q_{x,2}\partial\xi\\ \vdots & \vdots & \ddots & \vdots\\ \int_0^{a_1}\left(c_{1,1}^{II(1)}\cdot Q_{x,1}+\cdots+c_{1,J}^{II(1)}Q_{x,J}\right)Q_{x,J}\partial\xi & \int_0^{a_1}\left(c_{1,1}^{II(2)}\cdot Q_{x,1}+\cdots+c_{1,J}^{II(2)}Q_{x,J}\right)Q_{x,J}\partial\xi & \cdots & \int_0^{a_1}\left(c_{1,1}^{II(J)}\cdot Q_{x,1}+\cdots+c_{1,J}^{II(J)}Q_{x,J}\right)Q_{x,J}\partial\xi\end{bmatrix}$$

$$\left[cQ_{II,1p}^{(II,1)}\right]=\begin{bmatrix}\int_0^{a_1}\left(c_{1,1}^{II(J+1)}\cdot Q_{x,1}+\cdots+c_{1,J}^{II(J+1)}Q_{x,J}\right)Q_{x,1}\partial\xi & \int_0^{a_1}\left(c_{1,1}^{II(J+2)}\cdot Q_{x,1}+\cdots+c_{1,J}^{II(J+2)}Q_{x,J}\right)Q_{x,1}\partial\xi & \cdots & \int_0^{a_1}\left(c_{1,1}^{II(2J)}\cdot Q_{x,1}+\cdots+c_{1,J}^{II(2J)}Q_{x,J}\right)Q_{x,1}\partial\xi\\ \int_0^{a_1}\left(c_{1,1}^{II(J+1)}\cdot Q_{x,1}+\cdots+c_{1,J}^{II(J+1)}Q_{x,J}\right)Q_{x,2}\partial\xi & \int_0^{a_1}\left(c_{1,1}^{II(J+2)}\cdot Q_{x,1}+\cdots+c_{1,J}^{II(J+2)}Q_{x,J}\right)Q_{x,2}\partial\xi & \cdots & \int_0^{a_1}\left(c_{1,1}^{II(2J)}\cdot Q_{x,1}+\cdots+c_{1,J}^{II(2J)}Q_{x,J}\right)Q_{x,2}\partial\xi\\ \vdots & \vdots & \ddots & \vdots\\ \int_0^{a_1}\left(c_{1,1}^{II(J+1)}\cdot Q_{x,1}+\cdots+c_{1,J}^{II(J+1)}Q_{x,J}\right)Q_{x,J}\partial\xi & \int_0^{a_1}\left(c_{1,1}^{II(J+2)}\cdot Q_{x,1}+\cdots+c_{1,J}^{II(J+2)}Q_{x,J}\right)Q_{x,J}\partial\xi & \cdots & \int_0^{a_1}\left(c_{1,1}^{II(2J)}\cdot Q_{x,1}+\cdots+c_{1,J}^{II(2J)}Q_{x,J}\right)Q_{x,J}\partial\xi\end{bmatrix}$$

$$\left[cQ_{II,1p}^{(II,2I)}\right]=\begin{bmatrix}\int_0^{a_1}\left(c_{1,1}^{II(4J(I-1)+3J+1)}\cdot Q_{x,1}+\cdots+c_{1,J}^{II(4J(I-1)+3J+1)}Q_{x,J}\right)Q_{x,1}\partial\xi & \int_0^{a_1}\left(c_{1,1}^{II(4J(I-1)+3J+2)}\cdot Q_{x,1}+\cdots+c_{1,J}^{II(4J(I-1)+3J+2)}Q_{x,J}\right)Q_{x,1}\partial\xi & \cdots & \int_0^{a_1}\left(c_{1,1}^{II(4IJ)}\cdot Q_{x,1}+\cdots+c_{1,J}^{II(4IJ)}Q_{x,J}\right)Q_{x,1}\partial\xi\\ \int_0^{a_1}\left(c_{1,1}^{II(4J(I-1)+3J+1)}\cdot Q_{x,1}+\cdots+c_{1,J}^{II(4J(I-1)+3J+1)}Q_{x,J}\right)Q_{x,2}\partial\xi & \int_0^{a_1}\left(c_{1,1}^{II(4J(I-1)+3J+2)}\cdot Q_{x,1}+\cdots+c_{1,J}^{II(4J(I-1)+3J+2)}Q_{x,J}\right)Q_{x,2}\partial\xi & \cdots & \int_0^{a_1}\left(c_{1,1}^{II(4IJ)}\cdot Q_{x,1}+\cdots+c_{1,J}^{II(4IJ)}Q_{x,J}\right)Q_{x,2}\partial\xi\\ \vdots & \vdots & \ddots & \vdots\\ \int_0^{a_1}\left(c_{1,1}^{II(4J(I-1)+3J+1)}\cdot Q_{x,1}+\cdots+c_{1,J}^{II(4J(I-1)+3J+1)}Q_{x,J}\right)Q_{x,J}\partial\xi & \int_0^{a_1}\left(c_{1,1}^{II(4J(I-1)+3J+2)}\cdot Q_{x,1}+\cdots+c_{1,J}^{II(4J(I-1)+3J+2)}Q_{x,J}\right)Q_{x,J}\partial\xi & \cdots & \int_0^{a_1}\left(c_{1,1}^{II(4IJ)}\cdot Q_{x,1}+\cdots+c_{1,J}^{II(4IJ)}Q_{x,J}\right)Q_{x,J}\partial\xi\end{bmatrix}$$

3. 3rd. line:

$$\left[cQ_{I,2p}^{(I,1)}\right]=\begin{bmatrix}\int_0^{a_1}\left(c_{2,1}^{I(1)}\cdot Q_{y,1}+\cdots+c_{2,J}^{I(1)}Q_{y,J}\right)Q_{y,1}\partial\xi & \int_0^{a_1}\left(c_{2,1}^{I(2)}\cdot Q_{y,1}+\cdots+c_{2,J}^{I(2)}Q_{y,J}\right)Q_{y,1}\partial\xi & \cdots & \int_0^{a_1}\left(c_{2,1}^{I(J)}\cdot Q_{y,1}+\cdots+c_{2,J}^{I(J)}Q_{y,J}\right)Q_{y,1}\partial\xi\\ \int_0^{a_1}\left(c_{2,1}^{I(1)}\cdot Q_{y,1}+\cdots+c_{2,J}^{I(1)}Q_{y,J}\right)Q_{y,2}\partial\xi & \int_0^{a_1}\left(c_{2,1}^{I(2)}\cdot Q_{y,1}+\cdots+c_{2,J}^{I(2)}Q_{y,J}\right)Q_{y,2}\partial\xi & \cdots & \int_0^{a_1}\left(c_{2,1}^{I(J)}\cdot Q_{y,1}+\cdots+c_{2,J}^{I(J)}Q_{y,J}\right)Q_{y,2}\partial\xi\\ \vdots & \vdots & \ddots & \vdots\\ \int_0^{a_1}\left(c_{2,1}^{I(1)}\cdot Q_{y,1}+\cdots+c_{2,J}^{I(1)}Q_{y,J}\right)Q_{y,J}\partial\xi & \int_0^{a_1}\left(c_{2,1}^{I(2)}\cdot Q_{y,1}+\cdots+c_{2,J}^{I(2)}Q_{y,J}\right)Q_{y,J}\partial\xi & \cdots & \int_0^{a_1}\left(c_{2,1}^{I(J)}\cdot Q_{y,1}+\cdots+c_{2,J}^{I(J)}Q_{y,J}\right)Q_{y,J}\partial\xi\end{bmatrix}$$

$$\left[cQ_{I,2p}^{(II,1)}\right]=\begin{bmatrix}\int_0^{a_1}\left(c_{2,1}^{I(J+1)}\cdot Q_{y,1}+\cdots+c_{2,J}^{I(J+1)}Q_{y,J}\right)Q_{y,1}\partial\xi & \int_0^{a_1}\left(c_{2,1}^{I(J+2)}\cdot Q_{y,1}+\cdots+c_{2,J}^{I(J+2)}Q_{y,J}\right)Q_{y,1}\partial\xi & \cdots & \int_0^{a_1}\left(c_{2,1}^{I(2J)}\cdot Q_{y,1}+\cdots+c_{2,J}^{I(2J)}Q_{y,J}\right)Q_{y,1}\partial\xi\\ \int_0^{a_1}\left(c_{2,1}^{I(J+1)}\cdot Q_{y,1}+\cdots+c_{2,J}^{I(J+1)}Q_{y,J}\right)Q_{y,2}\partial\xi & \int_0^{a_1}\left(c_{2,1}^{I(J+2)}\cdot Q_{y,1}+\cdots+c_{2,J}^{I(J+2)}Q_{y,J}\right)Q_{y,2}\partial\xi & \cdots & \int_0^{a_1}\left(c_{2,1}^{I(2J)}\cdot Q_{y,1}+\cdots+c_{2,J}^{I(2J)}Q_{y,J}\right)Q_{y,2}\partial\xi\\ \vdots & \vdots & \ddots & \vdots\\ \int_0^{a_1}\left(c_{2,1}^{I(J+1)}\cdot Q_{y,1}+\cdots+c_{2,J}^{I(J+1)}Q_{y,J}\right)Q_{y,J}\partial\xi & \int_0^{a_1}\left(c_{2,1}^{I(J+2)}\cdot Q_{y,1}+\cdots+c_{2,J}^{I(J+2)}Q_{y,J}\right)Q_{y,J}\partial\xi & \cdots & \int_0^{a_1}\left(c_{2,1}^{I(2J)}\cdot Q_{y,1}+\cdots+c_{2,J}^{I(2J)}Q_{y,J}\right)Q_{y,J}\partial\xi\end{bmatrix}$$

$$\left[cQ_{I,2p}^{(II,2I)}\right]=\begin{bmatrix}\int_0^{a_1}\left(c_{2,1}^{I(4J(I-1)+3J+1)}\cdot Q_{y,1}+\cdots+c_{2,J}^{I(4J(I-1)+3J+1)}Q_{y,J}\right)Q_{y,1}\partial\xi & \int_0^{a_1}\left(c_{2,1}^{I(4J(I-1)+3J+2)}\cdot Q_{y,1}+\cdots+c_{2,J}^{I(4J(I-1)+3J+2)}Q_{y,J}\right)Q_{y,1}\partial\xi & \cdots & \int_0^{a_1}\left(c_{2,1}^{I(4IJ)}\cdot Q_{y,1}+\cdots+c_{2,J}^{I(4IJ)}Q_{y,J}\right)Q_{y}\\ \int_0^{a_1}\left(c_{2,1}^{I(4J(I-1)+3J+1)}\cdot Q_{y,1}+\cdots+c_{2,J}^{I(4J(I-1)+3J+1)}Q_{y,J}\right)Q_{y,2}\partial\xi & \int_0^{a_1}\left(c_{2,1}^{I(4J(I-1)+3J+2)}\cdot Q_{y,1}+\cdots+c_{2,J}^{I(4J(I-1)+3J+2)}Q_{y,J}\right)Q_{y,2}\partial\xi & \cdots & \int_0^{a_1}\left(c_{2,1}^{I(4IJ)}\cdot Q_{y,1}+\cdots+c_{2,J}^{I(4IJ)}Q_{y,J}\right)Q_{y}\\ \vdots & \vdots & \ddots & \vdots\\ \int_0^{a_1}\left(c_{2,1}^{I(4J(I-1)+3J+1)}\cdot Q_{y,1}+\cdots+c_{2,J}^{I(4J(I-1)+3J+1)}Q_{y,J}\right)Q_{y,J}\partial\xi & \int_0^{a_1}\left(c_{2,1}^{I(4J(I-1)+3J+2)}\cdot Q_{y,1}+\cdots+c_{2,J}^{I(4J(I-1)+3J+2)}Q_{y,J}\right)Q_{y,J}\partial\xi & \cdots & \int_0^{a_1}\left(c_{2,1}^{I(4IJ)}\cdot Q_{y,1}+\cdots+c_{2,J}^{I(4IJ)}Q_{y,J}\right)Q_{y}\end{bmatrix}$$

4. *I*-th line:

$$\left[cQ_{II,2Ip}^{(I,1)}\right]=\begin{bmatrix}\int_0^{a_1}\left(c_{2I,1}^{II(1)}\cdot Q_{x,1}+\cdots+c_{2I,J}^{II(1)}Q_{x,J}\right)Q_{x,1}\partial\xi & \int_0^{a_1}\left(c_{2I,1}^{II(2)}\cdot Q_{x,1}+\cdots+c_{2I,J}^{II(2)}Q_{x,J}\right)Q_{x,1}\partial\xi & \cdots & \int_0^{a_1}\left(c_{2I,1}^{II(J)}\cdot Q_{x,1}+\cdots+c_{2I,J}^{II(J)}Q_{x,J}\right)Q_{x,1}\partial\xi\\ \int_0^{a_1}\left(c_{2I,1}^{II(1)}\cdot Q_{x,1}+\cdots+c_{2I,J}^{II(1)}Q_{x,J}\right)Q_{x,2}\partial\xi & \int_0^{a_1}\left(c_{2I,1}^{II(2)}\cdot Q_{x,1}+\cdots+c_{2I,J}^{II(2)}Q_{x,J}\right)Q_{x,2}\partial\xi & \cdots & \int_0^{a_1}\left(c_{2I,1}^{II(J)}\cdot Q_{x,1}+\cdots+c_{2I,J}^{II(J)}Q_{x,J}\right)Q_{x,2}\partial\xi\\ \vdots & \vdots & \ddots & \vdots\\ \int_0^{a_1}\left(c_{2I,1}^{II(1)}\cdot Q_{x,1}+\cdots+c_{2I,J}^{II(1)}Q_{x,J}\right)Q_{x,J}\partial\xi & \int_0^{a_1}\left(c_{2I,1}^{II(2)}\cdot Q_{x,1}+\cdots+c_{2I,J}^{II(2)}Q_{x,J}\right)Q_{x,J}\partial\xi & \cdots & \int_0^{a_1}\left(c_{2I,1}^{II(J)}\cdot Q_{x,1}+\cdots+c_{2I,J}^{II(J)}Q_{x,J}\right)Q_{x,J}\partial\xi\end{bmatrix}$$

$$\left[cQ_{II,2Ip}^{(II,1)}\right]=\begin{bmatrix}\int_0^{a_1}\left(c_{2I,1}^{II(J+1)}\cdot Q_{x,1}+\cdots+c_{2I,J}^{II(J+1)}Q_{x,J}\right)Q_{x,1}\partial\xi & \int_0^{a_1}\left(c_{2I,1}^{II(J+2)}\cdot Q_{x,1}+\cdots+c_{2I,J}^{II(J+2)}Q_{x,J}\right)Q_{x,1}\partial\xi & \cdots & \int_0^{a_1}\left(c_{2I,1}^{II(2J)}\cdot Q_{x,1}+\cdots+c_{2I,J}^{II(2J)}Q_{x,J}\right)Q_{x,1}\partial\xi\\ \int_0^{a_1}\left(c_{2I,1}^{II(J+1)}\cdot Q_{x,1}+\cdots+c_{2I,J}^{II(J+1)}Q_{x,J}\right)Q_{x,2}\partial\xi & \int_0^{a_1}\left(c_{2I,1}^{II(J+2)}\cdot Q_{x,1}+\cdots+c_{2I,J}^{II(J+2)}Q_{x,J}\right)Q_{x,2}\partial\xi & \cdots & \int_0^{a_1}\left(c_{2I,1}^{II(2J)}\cdot Q_{x,1}+\cdots+c_{2I,J}^{II(2J)}Q_{x,J}\right)Q_{x,2}\partial\xi\\ \vdots & \vdots & \ddots & \vdots\\ \int_0^{a_1}\left(c_{2I,1}^{II(J+1)}\cdot Q_{x,1}+\cdots+c_{2I,J}^{II(J+1)}Q_{x,J}\right)Q_{x,J}\partial\xi & \int_0^{a_1}\left(c_{2I,1}^{II(J+2)}\cdot Q_{x,1}+\cdots+c_{2I,J}^{II(J+2)}Q_{x,J}\right)Q_{x,J}\partial\xi & \cdots & \int_0^{a_1}\left(c_{2I,1}^{II(2J)}\cdot Q_{x,1}+\cdots+c_{2I,J}^{II(2J)}Q_{x,J}\right)Q_{x,J}\partial\xi\end{bmatrix}$$

$$\left[cQ_{II,2Ip}^{(II,2I)}\right]=\begin{bmatrix}\int_0^{a_1}\left(c_{2I,1}^{II(4J(I-1)+3J+1)}\cdot Q_{x,1}+\cdots+c_{2I,J}^{II(4J(I-1)+3J+1)}Q_{x,J}\right)Q_{x,1}\partial\xi & \int_0^{a_1}\left(c_{2I,1}^{II(4J(I-1)+3J+2)}\cdot Q_{x,1}+\cdots+c_{2I,J}^{II(4J(I-1)+3J+2)}Q_{x,J}\right)Q_{x,1}\partial\xi & \cdots & \int_0^{a_1}\left(c_{2I,1}^{II(4IJ)}\cdot Q_{x,1}+\cdots+c_{2I,J}^{II(4IJ)}Q_{x,J}\right)Q_{x,1}\partial\xi\\ \int_0^{a_1}\left(c_{2I,1}^{II(4J(I-1)+3J+1)}\cdot Q_{x,1}+\cdots+c_{2I,J}^{II(4J(I-1)+3J+1)}Q_{x,J}\right)Q_{x,2}\partial\xi & \int_0^{a_1}\left(c_{2I,1}^{II(4J(I-1)+3J+2)}\cdot Q_{x,1}+\cdots+c_{2I,J}^{II(4J(I-1)+3J+2)}Q_{x,J}\right)Q_{x,2}\partial\xi & \cdots & \int_0^{a_1}\left(c_{2I,1}^{II(4IJ)}\cdot Q_{x,1}+\cdots+c_{2I,J}^{II(4IJ)}Q_{x,J}\right)Q_{x,2}\partial\xi\\ \vdots & \vdots & \ddots & \vdots\\ \int_0^{a_1}\left(c_{2I,1}^{II(4J(I-1)+3J+1)}\cdot Q_{x,1}+\cdots+c_{2I,J}^{II(4J(I-1)+3J+1)}Q_{x,J}\right)Q_{x,J}\partial\xi & \int_0^{a_1}\left(c_{2I,1}^{II(4J(I-1)+3J+2)}\cdot Q_{x,1}+\cdots+c_{2I,J}^{II(4J(I-1)+3J+2)}Q_{x,J}\right)Q_{x,J}\partial\xi & \cdots & \int_0^{a_1}\left(c_{2I,1}^{II(4IJ)}\cdot Q_{x,1}+\cdots+c_{2I,J}^{II(4IJ)}Q_{x,J}\right)Q_{x,J}\partial\xi\end{bmatrix}$$